# KINETICS OF β-HAEMATIN FORMATION IN BENZOIC ACID

BY

**MMBONENI GIFTY TSHIVHASE**

A DISSERTATION PRESENTED IN FULFILMENT OF THE

REQUIREMENTS FOR THE DEGREE OF

**MASTERS OF SCIENCE**



IN THE DEPARTMENT OF CHEMISTRY

**UNIVERSITY OF CAPE TOWN**

MARCH 2005

Supervisor: Associate Professor T. J. Egan

# DECLARATION

I declare that KINETICS OF β-HAEMATIN FORMATION IN BENZOIC ACID is my own work and that all the sources that I have used or quoted have been indicated and acknowledged by means of complete references.

signature removed

Mmboneni Gifty Tshivhase

# ACKNOWLEDGEMENTS

Special thanks are deserved by many people. In particular I owe a great debt of gratitude to the following people:

- My supervisor, Associate Professor T. J. Egan, for his continued guidance, encouragement, assistance, stimulating discussions and comments while supervising my work and during the preparation of this thesis.
- My fellow group members, Kanyile, Tebogo and Katherine for their friendship, assistance, advice and willingness to help.
- Professor Linder for teaching me and helping me to operate the XRD machine.
- Miranda Waldron for carrying out scanning electron microscopy analysis on my samples.
- John, Odi, Siya (MaP), Shane and Andre for being good company and for the interesting lunch time discussions.
- Mowbray Presbyterian members for their care, support and prayers.
- All my friends, near and far, and also in the chemistry department for their care, availability and for listening.
- NRF for financial support.
- God Almighty for guiding and giving me the strength during this work.
- My parents Ailwei and Tshenuwani for their loving support, patience, encouragement and contribution to my academic success.
- My brothers Eddy, Ntuwe, Livhu, Mphulu together with their families for their endless care, support and for believing in me.

# CONFERENCE PROCEEDINGS

**2003**: 08-11 July, 11th National Inorganic Chemistry Conference of the South African Chemical Institute, Roode Vallei Country Lodge, Pretoria, South Africa.

**POSTER** – ***Formation of malaria pigment from haem in benzoic acid solution.***

**2004**: 04-09 July, 37th National Convention of the South African Chemical Institute, CSIR International Convention Centre, Pretoria, South Africa.

**POSTER** - ***Kinetics of synthetic malaria pigment formation in benzoic acid solution.***

# ABSTRACT

Haemozoin is a cyclic dimer of ferriprotoporphyrin (IX) that occurs in malaria parasites and some other blood-eating organisms. It is chemically identical to β-haematin. In this work, the kinetics of β-haematin formation were investigated in 0.05 M benzoic acid acid solution using a newly developed pyridine-based assay. The formation of β-haematin in this low concentration of benzoic acid requires just over two hours. By contrast, a concentration of acetate that is 90 times higher results in the reaction reaching completion in just under one hour. The β-haematin product formed was characterised using infrared spectroscopy, x-ray diffraction and scanning electron microscopy and was found to be identical to that formed in acetate solution. XRD also revealed that the formation of β-haematin involves conversion of amorphous haematin to crystalline β-haematin. Diffractograms of wet product at different time intervals provided definitive evidence that the conversion occurs during incubation in benzoic acid medium and not during the drying stage. The reaction is easily monitored using the pyridine assay and gives results essentially identical to those found using infrared spectroscopy. The effects of temperature, stirring rate, seeding, pH and concentration of benzoic acid were investigated. Under all conditions the reaction exhibits sigmoidal kinetics, indicating the involvement of nucleation and crystal growth phases. The kinetics were modelled using the Avrami equation, where the reaction rates were obtained and the Avrami constant *n*, which indicates the dimensionality of crystal growth, was found to be 4 implying spherical growth. The reaction rate is not dependent on stirring (the rate constant is $3.9 \pm 0.1 \times 10^{-8}$ $min^{-4}$ for

the reaction carried out with stirring and $3.6 \pm 0.1 \times 10^{-8}$ $min^{-4}$ for a reaction carried out unstirred at 60°C, pH 4.5) but when the reaction was stirred vigorously Avrami kinetics were no longer observed. Instead the data fitted to the Gompertz equation, with the curve showing prolonged nucleation, suggesting that crystal nuclei are destroyed by excessive stirring. Seeding the reaction with 10% β-haematin showed no significant effect on the reaction rate. The effect of temperature and concentration was investigated for both benzoic acid and 4-nitrobenzoic acid. The effect of temperature on the kinetics in benzoic acid and 4-nitrobenzoic acid confirmed Arrhenius behaviour. There is also a linear dependence of rate constant on the concentration of benzoic and 4-nitrobenzoic acid without a change in the Avrami constant (dimensionality of crystal growth). A bell-shaped curve was obtained when rate constants were plotted as a function of pH in the presence of benzoic acid, 4-aminobenzoic acid or 4-cyanobenzoic acid, indicating that the haematin species in which one propionate is protonated and the other is unprotonated is probably required for forming β-haematin. The kinetics of formation of β-haematin were also investigated in the presence of the following para substituted benzoic acids: 4-cyanobenzoic acid, 4-aminobenzoic acid, 4-carboxybenzenesulfonamide, 4-methylsulfonylbenzoic acid, 4-nitrobenzoic acid, 4-carboxyaldehydebenzene and 4-methoxybenzoic acid. It was found that electron donating groups slow down the rate of formation of β-haematin while electron withdrawing groups promote the faster formation of β-haematin, with the exception of 4-carboxybenzenesulfonamide and 4-methylsulfonylbenzoic acid. It is speculated that the reaction is slower in the presence of these two acids owing to the large sizes of the substituents.

It was concluded that electronic effects have major influence on the activity of benzoic acids in promoting β-haematin formation. It is suggested that the carboxylic acids destabilise π-π interactions and hydrogen bonding in the amorphous haematin solid, facilitating reorganisation to β-haematin.

# TABLE OF CONTENTS



## 1. INTRODUCTION

## 2. MATERIALS AND METHODS

## 4. KINETICS OF β-HAEMATIN FORMATION IN BENZOIC ACID



## 5. KINETICS OF β-HAEMATIN FORMATION IN THE PRESENCE OF SUBSTITUTED BENZOIC ACIDS



## 6. GENERAL CONCLUSIONS AND FUTURE RECOMMENDATIONS

# LIST OF FIGURES

## CHAPTER 1

## CHAPTER 3

## CHAPTER 4

## CHAPTER 5

## CHAPTER 6

# LIST OF TABLES

## CHAPTER 1



## CHAPTER 3





## CHAPTER 4

## CHAPTER 5

# 1. INTRODUCTION AND LITERATURE REVIEW

## 1.1 GENERAL INTRODUCTION

The word malaria literally means bad air and the disease was given that name because of its apparent association with the odorous air of swamps. More than 2.1 billion people are currently at risk and 270 – 400 million cases are reported each year. It is a cause of approximately one million deaths annually [1]. Four species of *Plasmodium* are capable of causing malaria in man: *P. vivax*, *P. malariae*, *P. falciparum* and *P. ovale*. *P. falciparum* causes a much more dangerous disease than the other species [2] and it is responsible for almost all deaths.

Lancisi first noted discoloration of the internal organs of deceased chronic malaria sufferers in 1716 [3]. The discolouration was due to malaria pigment or haemozoin, a highly insoluble microcrystalline material which is produced by *Plasmodium* species in their food vacuoles as a non-toxic end product of haemoglobin digestion. The parasite feeds on amino acids from the globin [4, 5] and the haem that is released is autoxidised to haematin, which is known to be toxic to microorganisms [6], and then converted to haemozoin.

The pigment that is released into the human body is found in parasitized erythrocytes, monocytes and granulocytes [7]. Parasitized erythrocytes containing pigment are either phagocytosed directly by leucocytes, or they burst at schizogony,

releasing the crystals into the bloodstream, turning the liver and spleen black in cases of chronic or repeated infection [8, 9].

The protozoan parasite that causes malaria was discovered in 1880 [10] and in 1898 Ross experimentally proved mosquito transmission of the disease when he found granules of black pigment identical in appearance with the well known and characteristic pigment of malaria in cells outside the stomach of the Anopheles mosquito [11].

Malaria pigment has thus enabled researchers to diagnose malaria, to describe related pathology and to define the life cycle of the malaria parasite. A new generation of automated analysers that incorporate flow-cytometric principles are currently employed in many haematology laboratories for routine full blood counts (FBC) and they may provide a novel way to diagnose malaria by automated detection of haemozoin during FBC analysis [12].



The formation of malaria pigment or haemozoin is a detoxification mechanism for the disposal of haematin and represents the major haem-detoxification pathway. A study carried out by Egan *et al.* [13] demonstrated that at least 95% of haem released from haemoglobin is incorporated into haemozoin in *P. falciparum*, meaning that the non-haemozoin iron can account for at most 5% of the parasite iron. They isolated and analysed the total elemental iron content of unparasitized and parasitized red cells, trophozoites, food vacuoles and haemozoin to determine its distribution among these compartments.

Their results suggest that 81±6% of the iron in the trophozoite is in the form of haemozoin and 91±2% is in the food vacuole. Mössbauer spectroscopy on freeze-dried trophozoites confirmed that the only detectable iron species is haemozoin. Further support for this distribution of iron species came from transmission electron microscopy (TEM) with electron spectroscopic imaging (ESI) which showed that iron distribution in the parasite is coincident with the haemozoin crystals (Figure 1.1) [13].

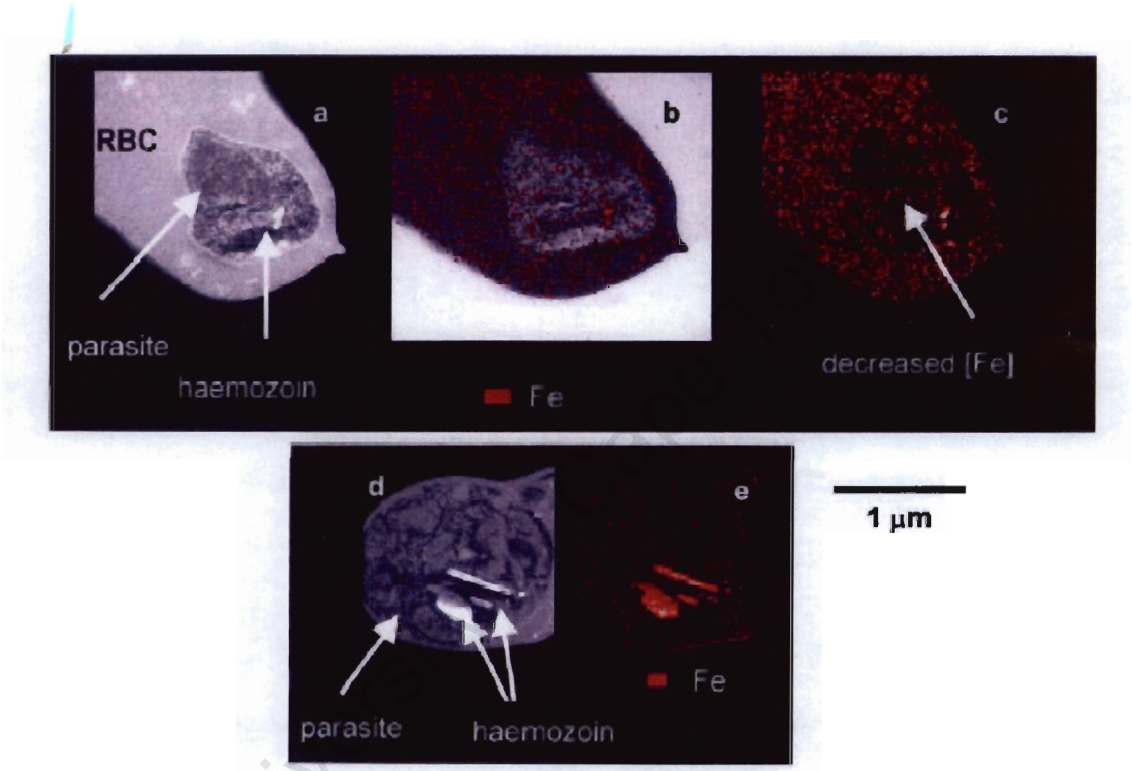


**Figure 1.1** TEM of a trophozoite within the (**a-c**) erythrocyte and (**d-e**) schizont. Very little iron is present in the erythrocyte cytosol of the schizont while haemozoin crystals show up strongly [13].

Fitch *et al.* proposed that haematin is the target of chloroquine and related antimalarials [14]. A number of studies have demonstrated that may antimalarials including 4-aminoquinolines, quinoline methanols, phenanthrenes and hydroxyxanthones inhibit the formation of β-haematin [15-18]. This is now widely hypothesised to be their mechanism of action.

## 1.2 IDENTIFICATION OF HAEMOZOIN

Haemozoin was believed to be melanin until 1911 when Brown [19] first showed that it was constituted of haem. For many decades, it has been known that malaria pigment contains aggregates of ferriprotoporphyrin that are insoluble under physiological conditions [20]. When solubilised it exhibits all the characteristics of haematin [21]. Ashong made observations that suggested that haemozoin was a crystalline complex with a specially synthesized protein [22]. Later Goldie *et al.* found that a haemozoin extract was composed of 65% protein, 16% ferriprotoporphyrin IX (Fe(III)PPIX), 6% carbohydrate and trace amounts of lipid and nucleic acid, where the overwhelmimg majority of the protein component is a mixture of native and denatured human globin non-covalently associated with the metalloporphyrin [23].

Fitch and Kanjananggulpan [24] isolated haemozoin from proteins and suggested that it was identical to β-haematin, a Fe(III)PPIX substance of unknown structure which was already known as a synthetic haematin product first described by Hamsik [25] which contains ferriprotoporphyrin in an insoluble aggregated state [20]. Elemental analysis also confirmed that solubilised haemozoin is identical to haematin and that no protein, only haematin, composes the haemozoin crystals [21].

## 1.3 CHARACTERISATION OF HAEMOZOIN AND β-HAEMATIN

The chemical nature of haemozoin was demonstrated over the period of approximately a decade starting in 1991 using a combination of IR [15], ESR [15, 26],

EXAFS [15], elemental analysis [15, 27, 28] and Mossbauer spectroscopy [26, 13]. It was investigated initially by FTIR spectroscopy and EXAFS by Slater *et al.* in 1991 [15] and later by SEM [27, 29, 30] and Raman spectroscopy [31], and its structure by XRD [27, 32]. It is a crystalline ferriprotoporphyrinIX aggregate in which the haem propionate of one Fe(III)PPIX is coordinated to the Fe(III) centre of another [33].

### *1.3.1 Infrared and Raman spectroscopy*

The IR spectrum obtained from haemozoin is significantly different from that of haematin (Figure 1.2a), although they are clearly from closely related structures.



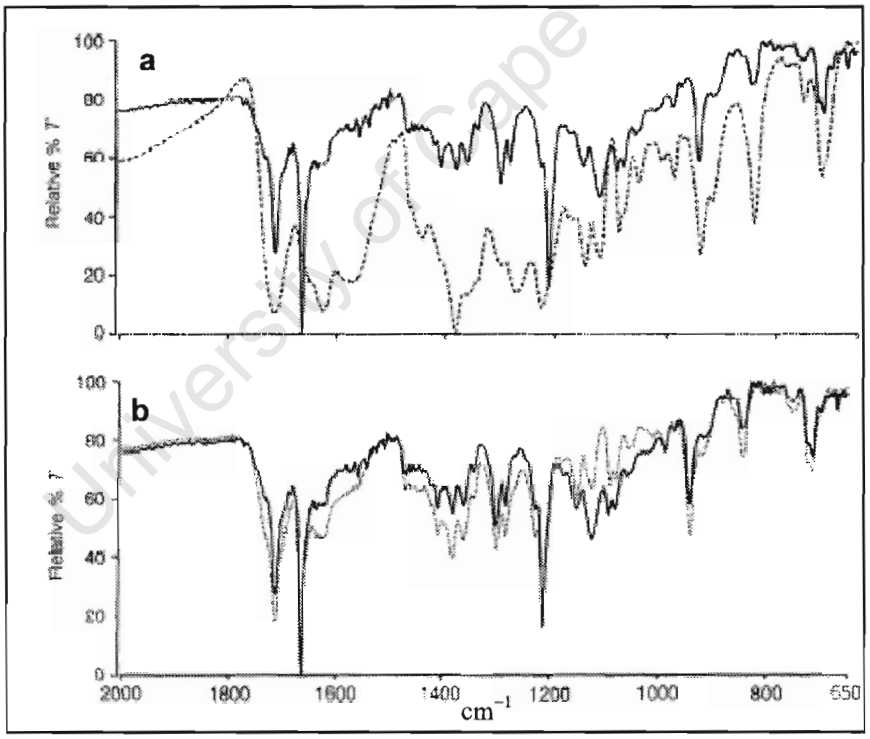


**Figure 1.2** Infrared spectra of (**a**) haemozoin (—) and haematin (·····) and (**b**) haemozoin (—) and β-haematin (·····) [15].

The IR spectrum of haemozoin contains an intense absorbance at 1664 $cm^{-1}$ that is absent in the spectra of either haemin or haematin. The other strong distinguishing IR absorbance in haemozoin is at 1210 $cm^{-1}$. These peaks are characteristic of a carboxylate group coordinated to the iron center of a ferriprotoporphyrin, arising from stretching of the carbon-oxygen double and single bonds, respectively [15]. The peak at 1712 $cm^{-1}$ is due to a hydrogen bonded carboxylic acid group that is thought to link the dimers together in the extended porphyrin array. The characteristic peaks were also observed in β-haematin synthesised in acetic acid (Figure 1.2b).

Wood *et al.* [34] observed a previously unreported peak at 1742 $cm^{-1}$ using FTIR microspectroscopy (Figure 1.3).



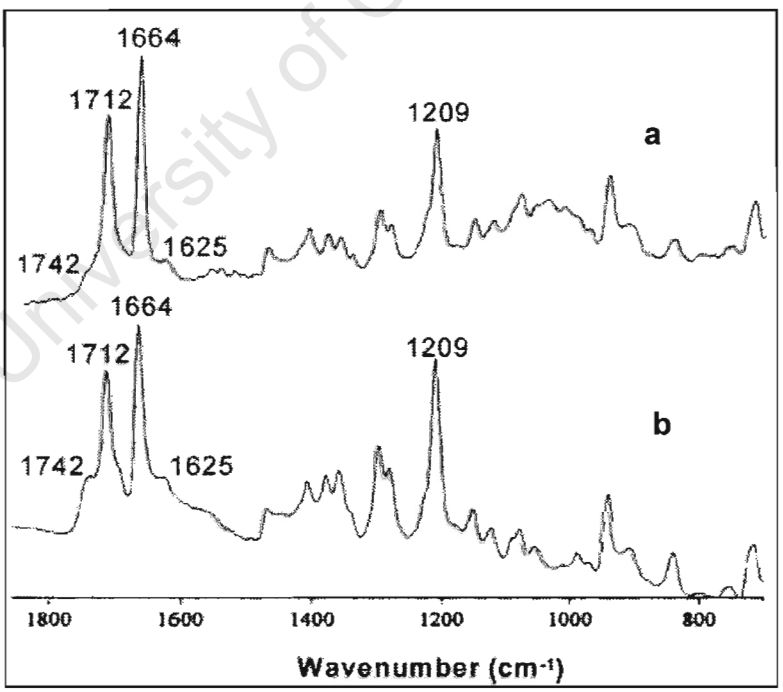


**Figure 1.3** FTIR spectra of (**a**) extracted haemozoin and (**b**) β-haematin [34].

This peak is a very noticeable shoulder in the spectrum of β-haematin and is a weak inflection in haemozoin (Figure 1.3a) and is suggested to arise from a different carbonyl environment. The small size of these bands shows that the carbonyl group is not associated with the bulk of the compound and is probably the result of surface carboxylates at either grain or surface boundaries. Another small band was observed at 1625 $cm^{-1}$ (Figure 1.3). This band is also seen in the Raman spectra at all excitation wavelengths investigated [34].

Bohle *et al.* [35] performed density functional calculations for the gas phase formic acid dimer and suggested that for β-haematin, if the hydrogen bonded propionic acid group is deformed and non-planar then a Raman band at 1712 $cm^{-1}$ and an IR band at 1625 $cm^{-1}$ would be observed. These bands are either absent or very weak due to the propionic acid groups being flat or centrosymmetric and therefore there are no significant deviations from planarity [35].

Raman spectroscopy has been applied to the qualitative and quantitative analysis of organic, inorganic and biological systems and is a potentially useful source of information concerning the composition, structure and stability of coordination compounds [36]. Raman lines are more characteristic than infrared absorption bands of the skeletal vibrations of finite chains and rings of saturated and unsaturated hydrocarbons. Aromatic compounds have particularly strong spectra. Laser Raman spectroscopy is a powerful technique and has been used for making clear both structural and functional information on haem and other metalloporphyrins [37].

Micro-Raman spectroscopy of haemozoin was performed within the food vacuole of *Plasmodium falciparum* trophozoite-infected functional erythrocytes using 488, 514, 568, 633 and 780 nm excitation wavelengths (Figure 1.4). The enhancement of $\nu_4$ (1374 $cm^{-1}$) at 780 nm excitation enabled Raman imaging of haemozoin within a functional erythrocyte.

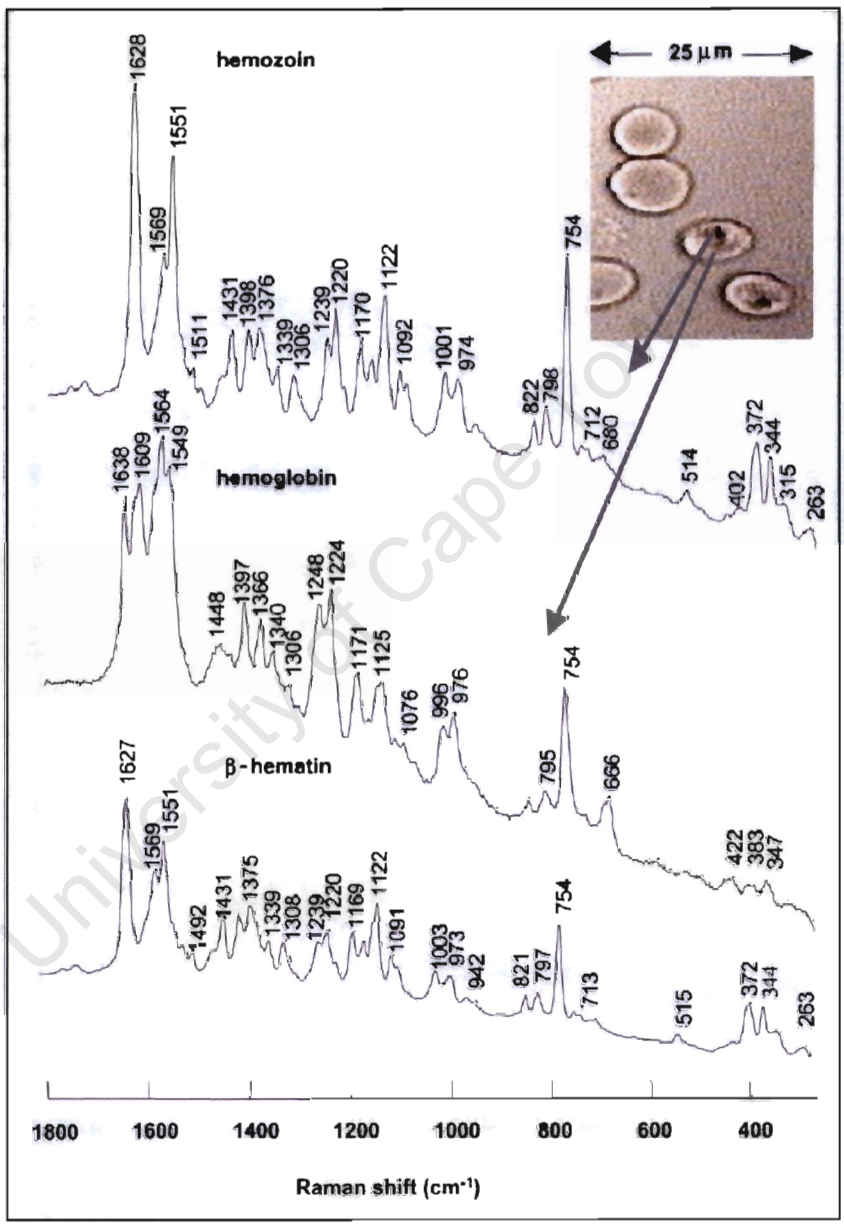


**Figure 1.4** Photomirograph of *P. falciparum* - infected erythrocytes (late trophozoite stage) showing the food vacuoles containing haemozoin. The arrows indicate the laser targets: the food vacuole and the surrounding haemoglobin. The corresponding spectra are compared with synthesized β-haematin [31].

The spectrum of β-haematin at this wavelength is identical to the spectrum of haemozoin within the cell (Figure 1.4), confirming that β-haematin and haemozoin are identical [31]. The spectrum of haematin differs from haemozoin and β-haematin mainly in terms of band enhancement (Figure 1.4 and1.5). In particular, bands at 1571, 1376, 1241-1240, 974, 944, 821, 796, 710, 678 $cm^{-1}$ are dramatically enhanced in haemozoin and β-haematin compared to haematin.

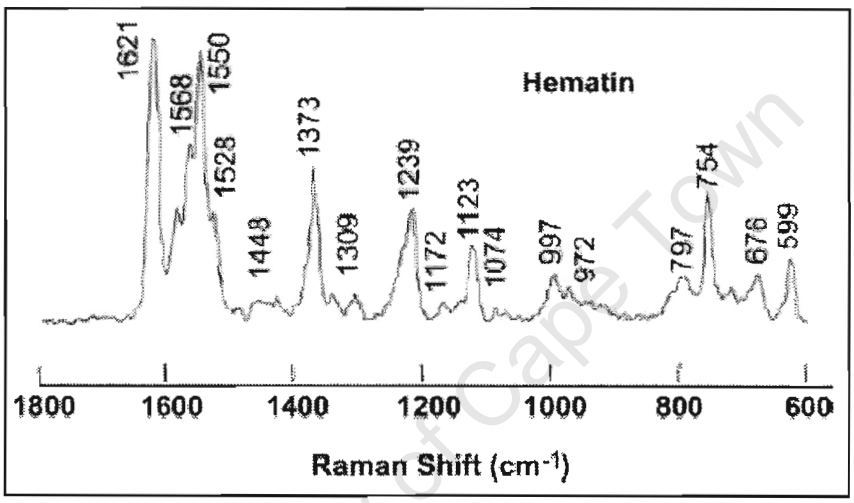


**Figure 1.5** Raman spectrum of haematin [31].

This may result from excitonic coupling between porphyrin moieties in the extended array because the haemozoin and β-haematin porphyrin array enables delocalised electrons to migrate between porphyrins *via* the coordinated propionate linkage [31].

### *1.3.2 Extended X-ray absorption fine structure*

Further evidence for carboxylate coordination to haematin was obtained from EXAFS analysis. EXAFS analysis, through mathematical simulation can provide information on the type, number and distance of the atoms in the first coordination sphere of a

metal ion [38]. The EXAFS spectra obtained from haemin and haemozoin are different (Figure 1.6a), indicating that a difference in the atoms surrounding iron exists between the two compounds.

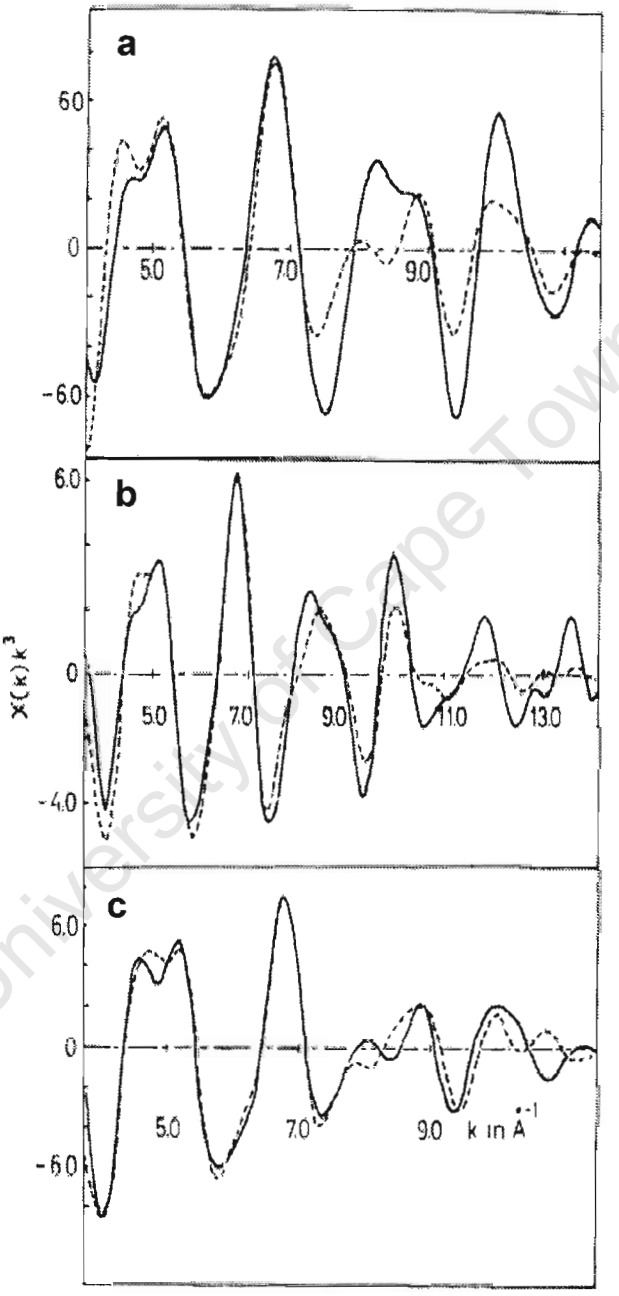


**Figure 1.6** EXAFS comparisons. (**a**) Haemin (—) and haemozoin (----), (**b**) haemin (—) and the best-fit haemin model (----), (**c**) haemozoin (—) and the best-fit haemozin model (----) [15].

The haemin model gave a poor fit to the experimental EXAFS of haemozoin (Figure 1.6a), but fitted well to the haemin experimental spectrum (Figure 1.6b). However when the chlorine atom was replaced with a single oxygen atom, there was a large improvement. The model became less accurate when two oxygen atoms were present but it improved when a single carbon atom was placed at 2.17 Å. A further improvement occurred when a second oxygen shell, containing one atom, was introduced at 3.7 Å (Figure 1.6c). This is very close to the calculated Fe-second oxygen shell bond length of 3.4 Å and consistent with the structure proposed. These oxygen and carbon atoms probably belong to a single carboxylate functional group in which only the first-shell oxygen is directly coordinated to the iron [15].

### *1.3.3 Electron paramagnetic resonance*

The oxidation and spin states of iron in haemozoin were determined using electron paramagnetic resonance spectroscopy (EPR). Electron paramagnetic resonance is an important spectroscopic method in bioinorganic chemistry [39]. It is used to map unpaired electron distributions in molecules and molecular fragments. Its effect depends on the presence of unpaired electrons [40] and detects changes in electron configuration [41].

Slater *et al.* claimed that at 10 K haemozoin gives an EPR spectrum indicative of low-spin ferric iron [15] while the iron in both haematin and haemin is in the high-spin ferric state as previously reported [42]. The g factor, the gyromagnetic ratio, has a value of 2.0023 for a free electron but varies significantly for paramagnetic ions in the

solid state. It depends on the particular paramagnetic ion, its oxidation state and coordination number and therefore the position of an EPR absorption peak [41]. Dominant signals for haemozoin were reportedly observed at g = 3.80 and 1.95 [15], but when Bohle *et al.* [26] performed EPR spectroscopy of β-haematin at different temperatures they found that for temperatures greater than 21 K, rapid relaxation leads to the loss of absorption intensity while at temperatures of 21 K and below, malaria pigment and synthetic β-haematin have a rhombic pattern with g = 5.79, 3.80 and 2.04 (Figure 1.7). Further cooling below 9 K resulted in the detection of a broad low-field feature at g = 12.03, characteristic of high spin Fe(III)PPIX. They suggested that the high field peak, that was found by Slater *et al.* [15] corresponding to a low-spin haem, may have been due to a contaminant.



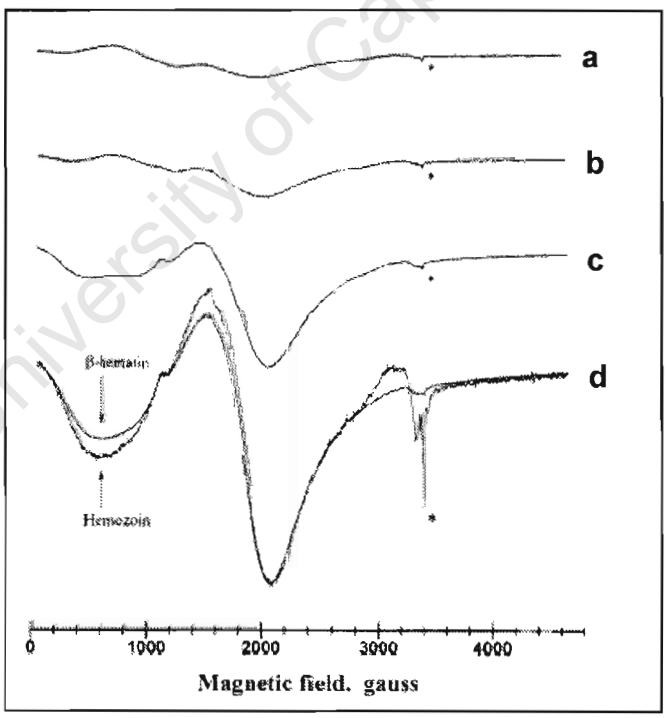


**Figure 1.7** EPR spectra for β-haematin at (**a**) 21 K, (**b**) 15.5 K, (**c**) 9.0 K, and (**d**) 5.6 K and also of haemozoin overlaid in **d** [26]. Microwave frequency = 9.464 GHz.

### 1.3.4 Mössbauer spectroscopy

Mössbauer spectroscopy has been widely used in studies of iron compounds such as haemoproteins and iron-sulfur proteins. Transitions between two nuclear energy levels of the $^{57}Fe$ nucleus (a less abundant isotope of iron) are observed. These levels are I = 1/2 and I = 3/2 levels, referring to the magnetic moment of the nuclear spin. Transitions can be observed between these nuclear energy levels corresponding to absorption of $\gamma$-radiation from an appropriate source. The energy separation, $\Delta E$, depends on both the electronic charge density and the asymmetry of charge at the nucleus. These parameters in turn depend on the electronic state of iron, i.e. the occupancy of the d orbitals. Characteristic spectra are obtained for different electronic and spin states of iron [43].

The Mössbauer spectrum of $\beta$-haematin in a weak applied field (Figure 1.8) [26], supports the conclusion about the iron environment drawn from the EPR spectra. The isomer shift and quadrupolar splitting values are indicative of a single high-spin ferric site in this lattice [26].

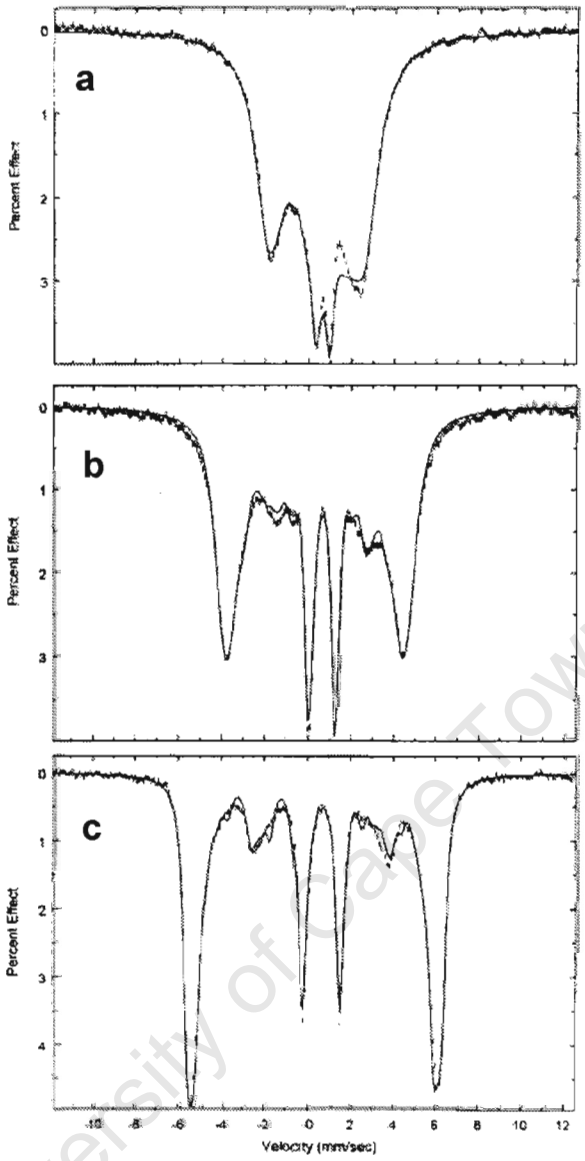


**Figure 1.8** Magnetic Mössbauer spectra of β-haematin at (**a**) 23.3 K, (**b**) 11.1 K and (**c**) 4.2 K. Dashed and solid lines represent experimental and calculated spectra respectively [26].

Prior to the study above Adams *et al.* reported a single asymmetric broad peak for β-haematin and haemozoin at 78K [44]. A recent study by Egan *et al.* also clearly demonstrated that haemozoin of freeze dried *P. falciparum* trophozoites and β-haematin at different temperatures are virtually identical (Figure 1.9) [13].

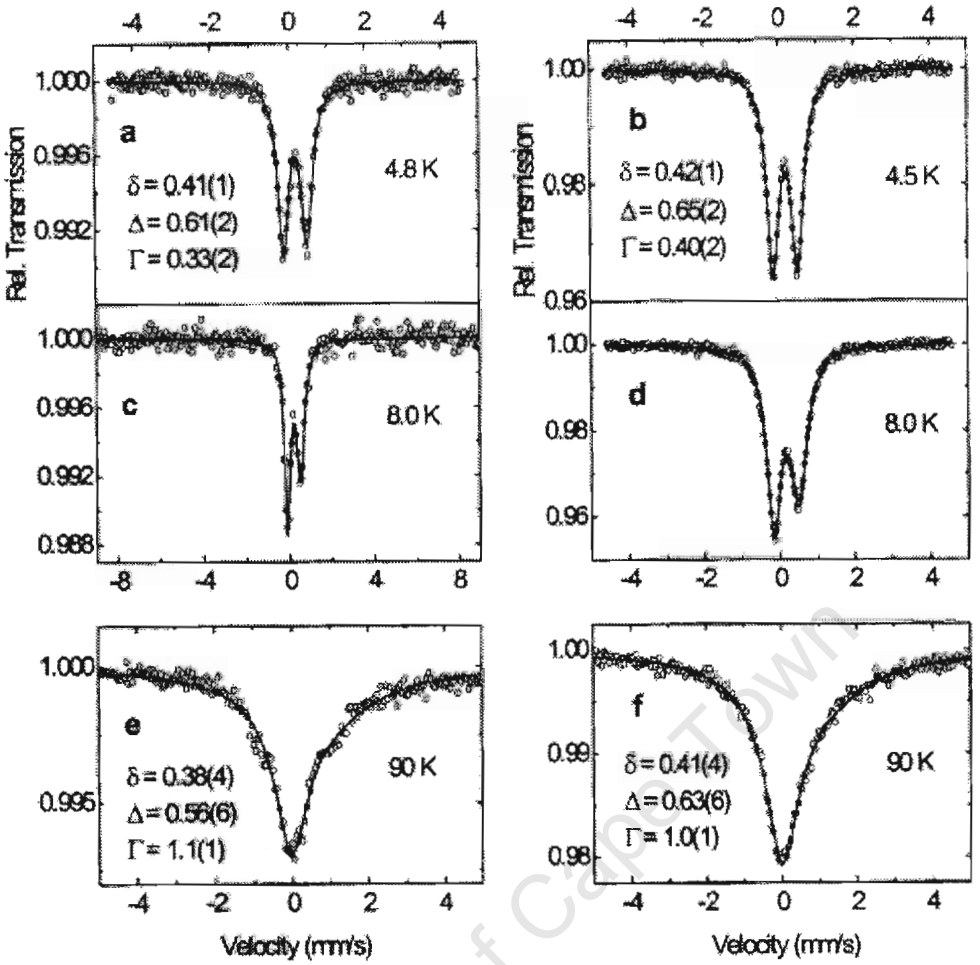


**Figure 1.9** Mössbauer spectra of (**a**, **c** and **e**) freeze-dried trophozoites and (**b**, **d** and **f**) β-haematin [13].

The correlations of ESR and Mössbauer spectroscopy with each other led to the conclusion that naturally occurring and synthetic β-haematin have a single high-spin S = 5/2 Fe(III) ion type [26].

### *1.3.5 X-ray diffraction*

Since the iron-carboxylate linkage between adjacent haems [15, 45] potentially allows two or more monomers to polymerise, haemozoin was believed to be a

coordination polymer of ferriprotoporphyrin IX with the direction of the chain propagation indicated by the arrows and hydrogen-bonded propionic dimerization between the chains (Figure 1.10).

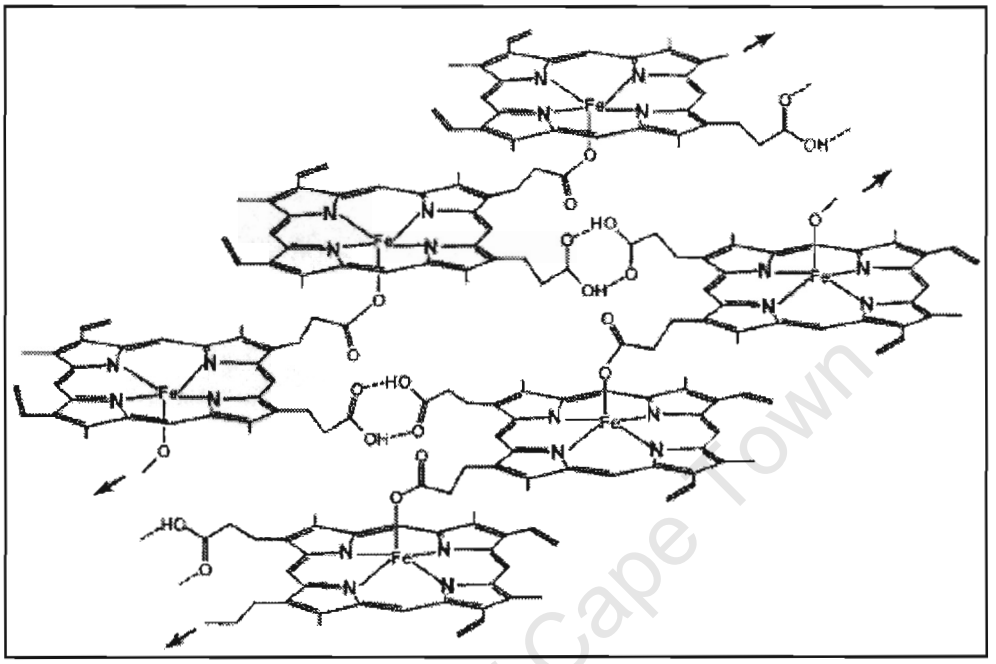

**Figure 1.10** Structure of β-haematin initially proposed by Bohle *et al.* [32].

When the structure was solved by Rietvield refinement from the high resolution X-ray powder diffraction pattern [33] however, it was found to be a porphyrin dimer in which the metal atoms are reciprocally coordinated by the propionate side chain with H-bond links between the dimers (Figure 1.11).

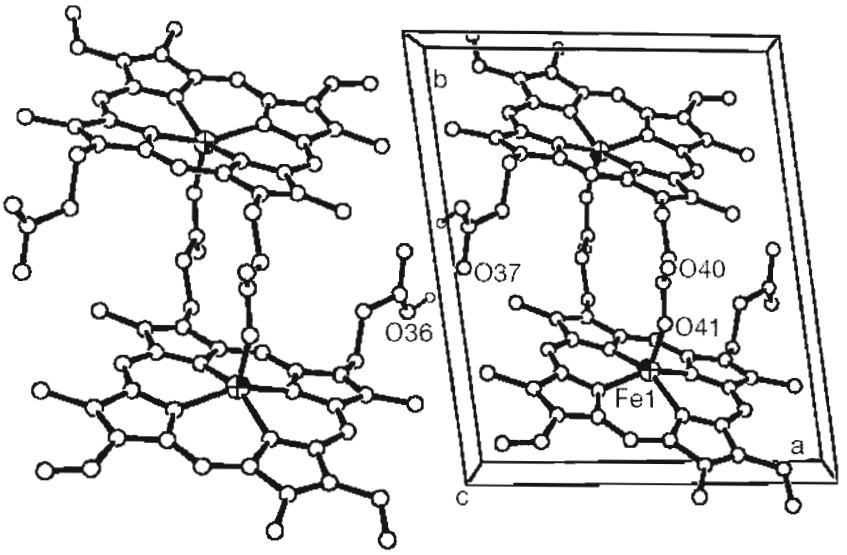


**Figure 1.11** Two unit cells of the crystal structure β-haematin [33].

The structure in Figure 1.11 is consistent with all of the known spectroscopic and magnetic properties of β-haematin. β-Haematin and malaria pigment are crystallographycally identical and they have the same unit cell and same atomic structure [33].

### *1.3.6 X-ray diffraction for characterisation purpose*

The diffraction patterns for trophozoites and uninfected erythrocytes have been measured by Bohle *et al.* (Figure 1.12a-d) [32]. The phenomenon of X-ray diffraction by crystals results from a scattering process in which X-rays are scattered by the electrons of the atoms without change in wavelength. Analysis of the positions of the diffraction effect leads immediately to a knowledge of the size, shape, and orientation of the unit cell [46]. An X-ray powder diffraction pattern is a set of lines or peaks, each of different intensity and position expressed as a d-spacing or Bragg angle θ.

For a given crystalline structure of a substance, the line positions are fixed and are characteristic of that substance. The intensities may vary somewhat from sample to sample, depending on the method of sample preparation and the instrumental conditions.

For identification purposes, principal note is taken of line positions together with a semi-quantitative consideration of intensities. Crystalline solids give diffraction patterns that have a number of sharp lines whereas non-crystalline solids give diffraction patterns that have a small number of very broad humps. Each crystalline substance has its own characteristic diffraction pattern which may be used for phase identification [41]. Both desiccated erythrocytes and parasitized erythrocytes scatter X-rays in two broad bands between 6 - 10 Å and 3 - 5 Å d values.



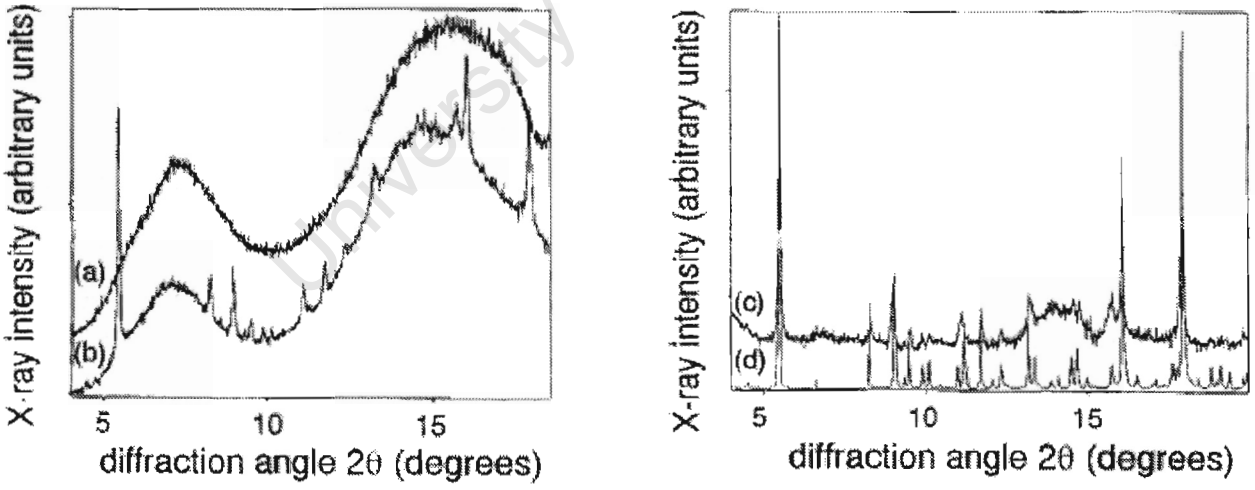


**Figure 1.12** Powder diffraction patterns of (**a**) lyophilised uninfected erythrocytes, (**b**) lyophilised erythrocytes infected with late trophozoites of *P. falciparum*, (**c**) difference of **a** and **b**, (**d**) synthetic β-haematin [32], ($\lambda$ = 1.1495).

Trophozoite-infected erythrocytes have clear Bragg diffraction peaks arising from a crystalline species not found in the uninfected erythrocytes, and these peaks are identical to the sharp diffraction pattern obtained from synthetic samples of β-haematin (Figure 1.12c and d). Haemozoin formed within trophozoites therefore crystallises in the same unit cell as β-haematin with identical spacings between layers of atoms in the crystal. The similar intensities of the two patterns further show that the materials are also crystallographically identical on the atomic level [32]. These findings unequivocally show that β-haematin is present in infected erythrocytes.

The synthetic method and subsequent sample treatment critically determines the phase homogeneity in aggregated haem samples. This is demonstrated by comparing diffractograms of β-haematin prepared by thermal methods in acetic acid [15, 16] and propionic acid, equation 1 and the dehydrohalogenation method, equation 2 [28]. Although haemozoin and β-haematin prepared by these methods have the same infrared spectrum, there is a marked difference in their crystallinity (Figure 1.13-1.14).



$$n[Fe(PP\text{-}IX)H_2Cl] \xrightarrow[18\ hr,\ 70^{\circ}C]{1.\ NaOH \quad 2.\ EtCO_2H} [Fe(PP\text{-}IX)H]_n \quad \beta\text{–haematin} \qquad 1.1$$

$$n[Fe(PP\text{-}IX)H_2Cl] \xrightarrow[-\ n\ HCl]{lutidine,\ MeOH,\ DMSO} [Fe(PP\text{-}IX)H]_n \quad \beta\text{–haematin} \qquad 1.2$$

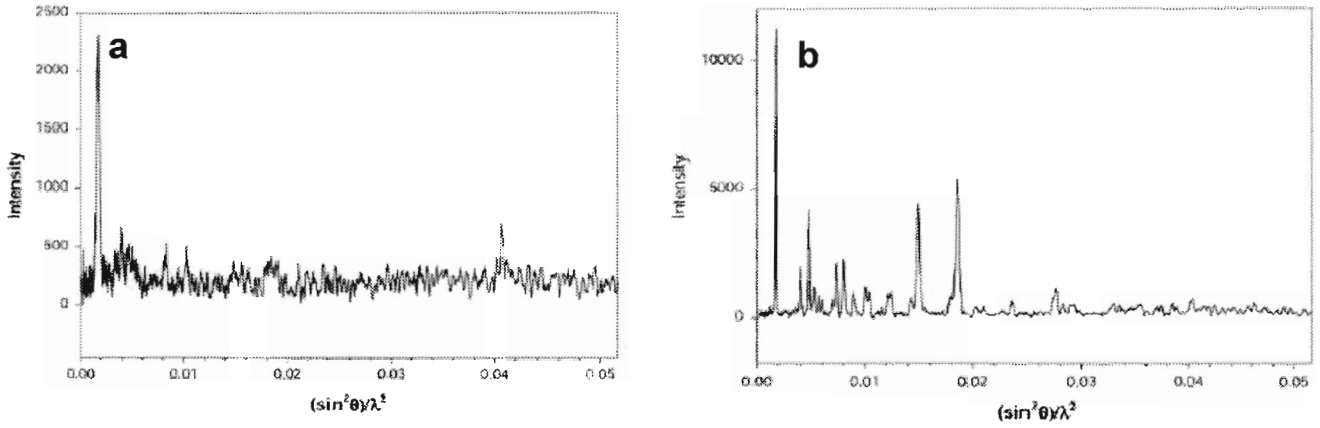


**Figure 1.13** Powder diffraction patterns for β-haematin prepared (**a**) in propionic acid and (**b**) by the dehydrohalogenation method [29].

The diffractogram in Figure 1.13a is of a product obtained from the reaction carried out in propionic acid and washed with water, methanol and sodium carbonate. The product formed from the reaction performed in acetic acid pH 2, 70°C for 12 hours and washed with water and sodium bicarbonate (Figure 1.14a) is more crystalline than the one prepared in propionic acid and has the same crystallinity as that prepared by the method of Egan *et al.* (Figure 1.14a) at pH 4.5, 60°C, 1 hour incubation.

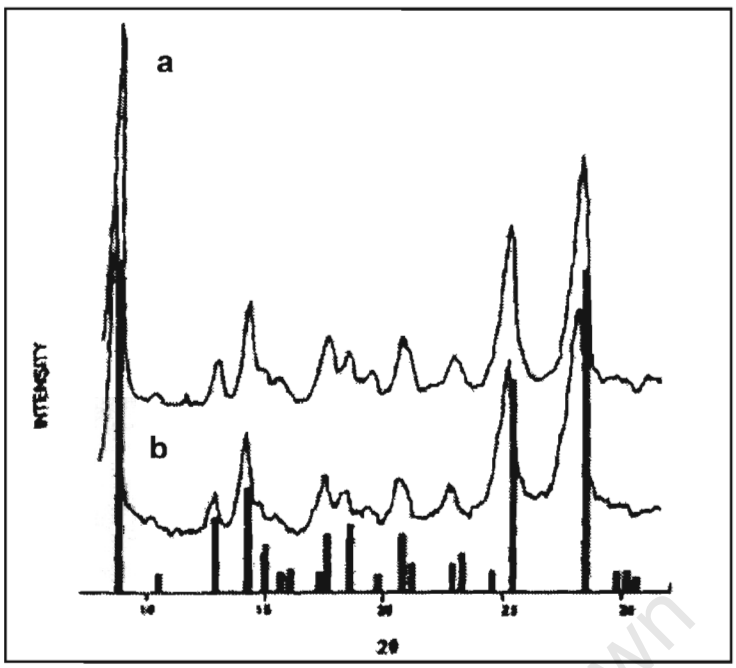


**Figure 1.14** X-ray powder diffraction patterns β-haematin prepared by the method of (**a**) Slater *et al.* [15] and by (**b**) Egan *et al.* [27] in acetic acid. The expected lines for Co Kα radiation calculated from the reported diffraction patterns of Bohle *et al.* [32] are shown as vertical lines and they were calculated peak from peak from the published pattern.



The crystallinity of the product of the dehydrohalogenation method is much higher. This implies that more crystalline samples of β-haematin result when the crystallization is slowed down and when completely soluble precursors and complexes are employed.

### *1.3.7 Scanning electron microscopy*

Scanning electron microscopy (SEM) has also been used both to characterize the external morphology of haemozoin (Figure 1.15a) [47] and β-haematin (Figure 1.15b-d) synthesized according to the methods mentioned in 1.3.6 above. SEM qualitatively

evaluates the external morphology of the products in great detail. It is an extremely versatile technique, capable of providing structural information over a wide range of magnification and features up to tens of micrometers in size can be seen. The resulting pictures have a definitive three dimensional quality because of the depth of focus of SEM [41].

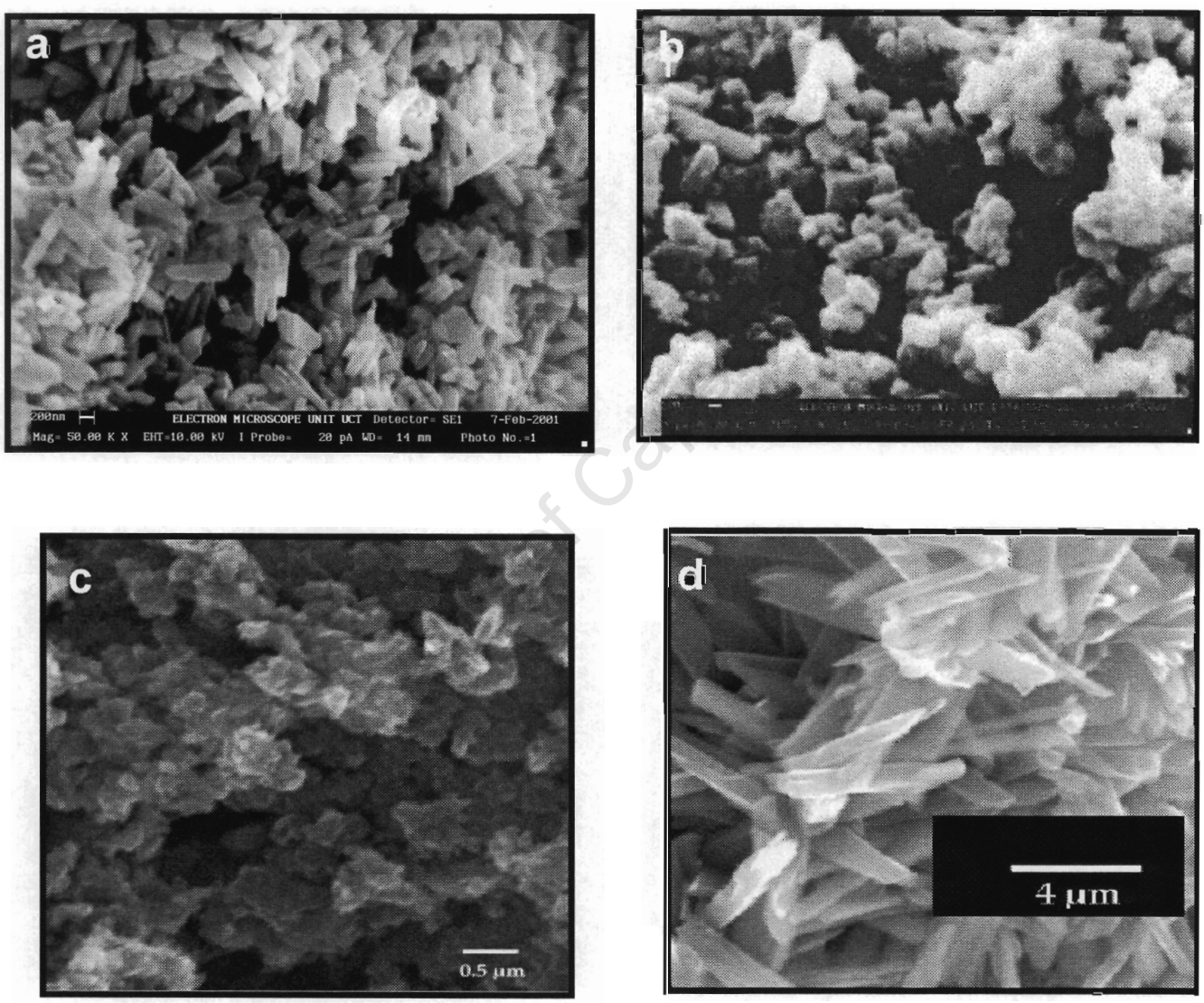


**Figure 1.15** Scanning electron micrograph of (**a**) haemozoin isolated from the D10 strain of *Plasmodium falciparum* [47] (Scale: 10 000:1 as shown) and (**b**) synthetic β-haematin formed in acetic acid [30] (Scale: 20 000:1 as shown) and by the reaction in equation 1.1 (c) and 1.2 (d) [29].

Crystals of haemozoin closely resemble those of β-haematin formed in acetic acid using the method by Egan *et al.*, although the latter are smaller and less regular in shape (Figure 1.15a and b). The crystallites formed in propionic acid have few distinguishable facets and have an upper estimate of 0.2 μm for the largest visible crystal dimension (Figure 1.15c) whereas the crystallites resulting from the method of Bohle *et al.* have maximum lengths 20 fold larger, with very regular morphologies and sizes throughout the sample. They are also similar to those formed by the parasite, in width and thickness but not in length (Figure 1.15d) [29].

### *1.3.8 Elemental analysis*

There have been literature discrepancies concerning the elemental composition of β-haematin and haemozoin (Table 1.1). The elemental compositions of the products produced by the methods above are slightly different from each other and from that of haemozoin.



**Table 1.1** Elemental analysis of haemozoin and β-haematin prepared using different methods

| | C | H | N |
|---|---|---|---|
| Haemozoin | 63.7 | 5.6 | 7.5 |
| β-Haematin$^{calc.}$ | 66.4 | 5.1 | 9.1 |
| β-Haematin [15] | 64.7 | 5.0 | 8.8 |
| β-Haematin [48] | 65.1 | 5.0 | 9.0 |
| β-Haematin [27] | 66.0 | 5.1 | 9.1 |

Bohle *et al.* [48] hypothesised that this may be due to the hygroscopic nature of β-haematin. They demonstrated that the amount of water absorbed by products of the dehydrohalogenation method is twice that of the product of the acid catalysed reaction, meaning that the amount of water absorbed is source dependent. To determine the degree of sample hydration, several different TGA experiments were conducted with various β-haematin samples, as well as by XRD, IR spectroscopy and by rehydration TGA. Rehydration led to subtle changes in the positions and relative intensities of the Bragg reflections in the powder diffraction pattern. There is also a sharp improvement in the signal to noise ratio of the diffraction profile upon hydration, suggesting that the sample becomes more ordered as it is allowed to rehydrate [48].

## 1.4 HAEMOZOIN FORMATION IN ORGANISMS OTHER THAN PLASMODIA



Haemozoin formation is not exclusive to *Plasmodium* parasites only. It is also found in the midgut of the blood-sucking insect *Rhodnius prolixus* [49]. It appears that this species of blood-sucking insect also makes haemozoin in order to escape the toxicity of free haem. This insect is an important vector of *Trypanosoma cruzi*, the causative agent of Chagas' disease [50]. The morbidity and mortality associated with South American trypanosomiasis in Latin America are more than one order of magnitude higher than those caused by malaria, schistosomiasis or leishmaniasis on that continent. It must be borne in mind that these places are nonendemic to malaria. Chagas disease is endemic from northern Mexico to Argentina and there are 18-20 million people infected with *T. cruzi* and another 40 million people are at risk of

acquiring the disease. Recent surveys indicate that there are approximately 200 000 new cases and 21 000 deaths associated with this condition every year. In addition, it has been recently estimated that this disease leads to 676 000 disability adjusted life years (DALYs) per annum [51].

Haemoglobin breakdown in *Schistosoma mansoni* also results in the formation of haemozoin [52, 53]. *Schistosoma mansoni* is one of the parasitic helminths [54] and is the main aetiological agent of human schistosomiasis. It belongs to the phylum Trematoda. Schistosomiasis is one of the most important parasitic diseases in humans. The human *Schistosomes* and most of the other species in mammals belong to the genus *Schistosoma* in the family Schistosomatidae. There are three species of *Schistosoma* which are habitual human parasites of wide distribution: *S. haemotobium, S. mansoni*, and *S. japonicum*. The first affects the urinary system, and the other two the intestine in which case the disease is referred to as intestinal *Schistosomiasis*. The diseases produced by various *Schistosomes* are similar in many respects but differ in details [2].



The map in Figure 1.16 below shows that malaria and schistosomiasis endemicity do not coincide everywhere, but they overlap almost completely in central Africa and Madacascar [55].

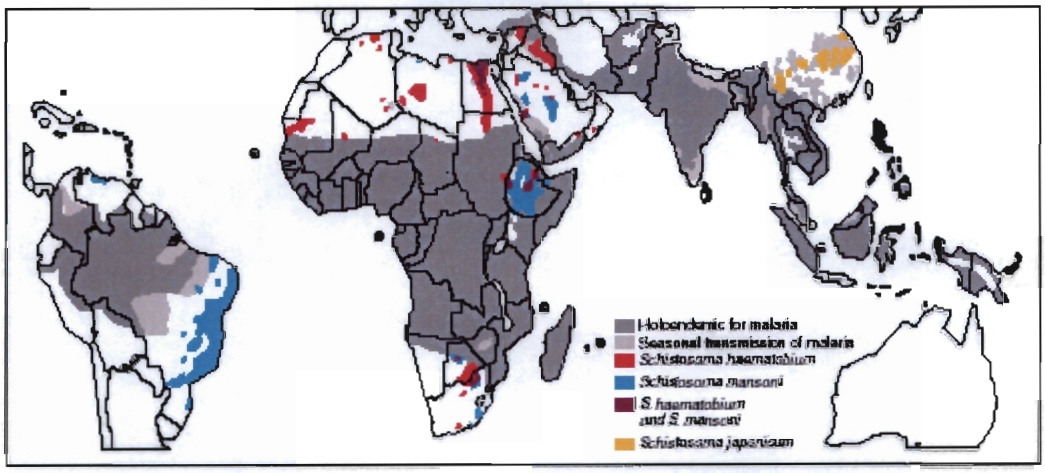


**Figure 1.16** Superimposing maps of endemicity for malaria and schistosomiasis [55].

Schistosomiasis remains one of the most prevalent parasitic infections in the world. It is estimated to afflict more than 300 million people worldwide. It is endemic in 76 countries and territories and continues to be a global public health concern in the developing world [56]. A recent study shows that 600 million people are at risk and more than 200 million cases are reported and there are 15 thousand deaths caused by this disease annually [1]. Schistosomiasis ranks second only to malaria in terms of parasite-induced human morbidity and mortality [57].

*Haemoproteus* species, close relatives of *Plasmodium* are apicomplexan protozoan parasites common in birds and they are relatively non-pathogenic. *Haemoproteus columbae* is transmitted by flies and it also synthesises a pigment chemically identical to the pigments of *P. falciparum* and *S. mansoni* but different in external morphology [58].

Haemozoin from *P. falciparum*, *Haemoproteus*, *Schistosoma*, and β-haematin were found to share the unit cell crystal structure of β-haematin but have different external morphologies (Figure 1.17) and differ in their susceptibility to $H_2O_2$ degradation that roughly correlates with a surface area to volume ratio in the observed three-dimensional shape [58].

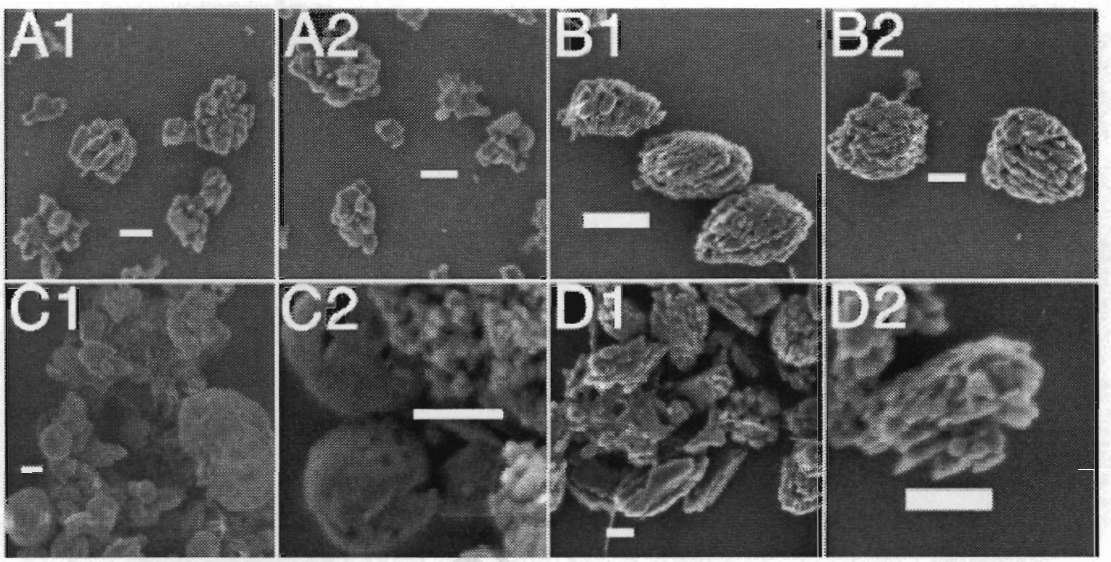


**Figure 1.17** Haemozoin from **A** *P. gallinaceum* (from erythrocytes), **B** *P. gallinaceum* (from ookinetes), **C** *Schistosoma*, **D** *Haemoproteus* [59].

The *Schistosoma* pigment is heterogeneous in size with a smoother round shape. Much of the *Schistosoma* pigment is spherical, unlike *Plasmodium* pigment, with a large range in size from 50 nm to a few microns in diameter. The haemozoins of the other human *Plasmodium species*, *P. vivax, P. ovale and P. malariae* were found to be very similar to *P. falciparum*. *P. falciparum* haemozoin is closer in appearance to other mammalian *Plasmodium* species than to the *avian* species (Figure 1.18). Different morphological shapes are thus observed as end products of haemozoin formation [59].

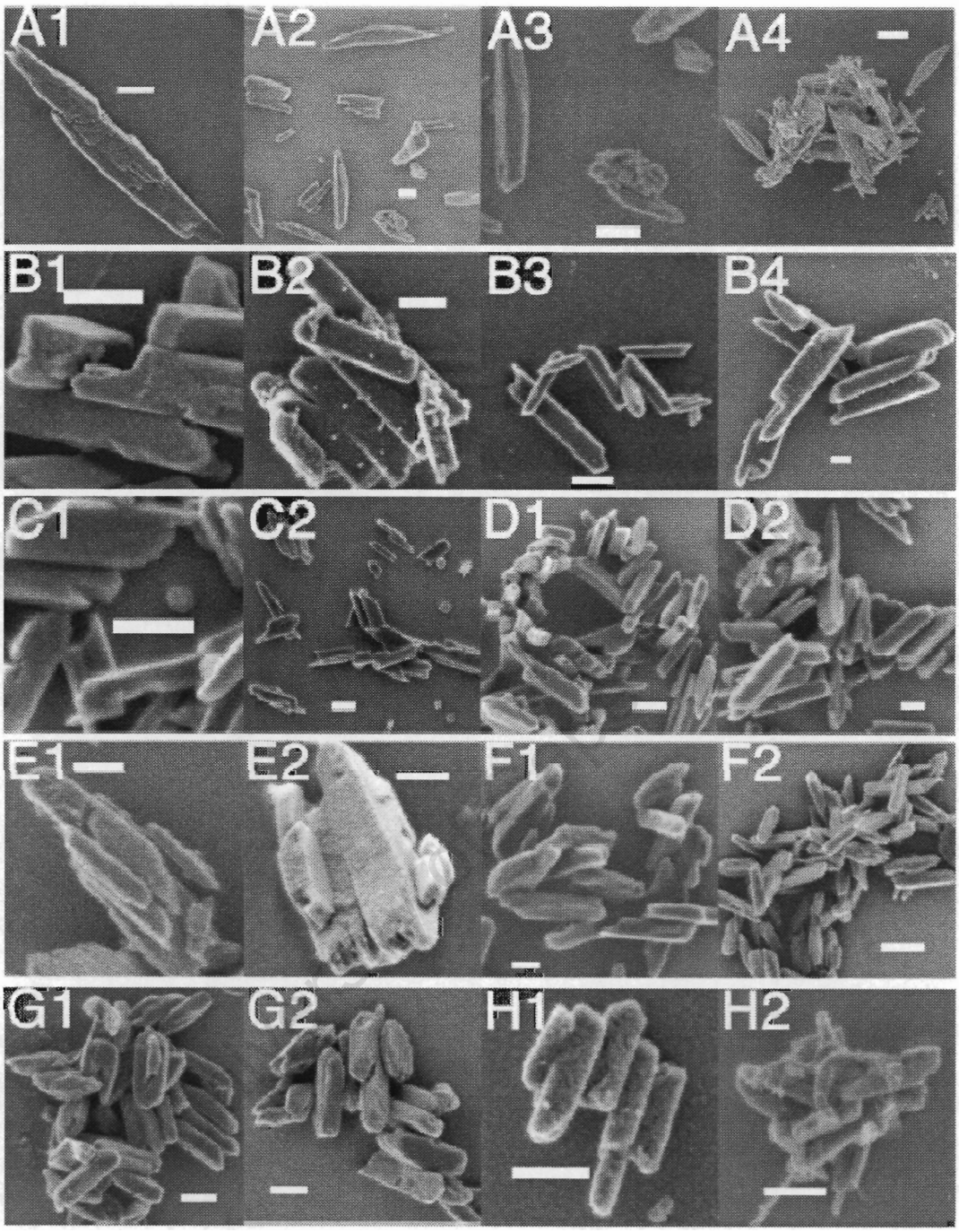


**Figure 1.18** Electron micrographs of β-haematin and *Plasmodium* haemozoin. **A** β-haematin, haemozoin from **B** *P. falciparum* clones, **C** *P. vivax*, **D** *P. ovale*, **E** *P. brasilianum*, **F** *P. knowlesi*, **G** *P. yoelli*, **H** *P. falciparum* [59].

## 1.5 METHODS FOR β-HAEMATIN SYNTHESIS

Various methods have been proposed to prepare β-haematin *in vitro*, the haem dimerization and crystallisation process leading to the formation of synthetic malaria pigment. Bohle *et al.* have synthesised β-haematin using a non-aqueous method where it was prepared by abstraction of HCl from haemin with the non-coordinating base 2, 6-lutidine in dry methanol [28].

The synthesis of β-haematin can also be brought about in acidic aqueous solution in the presence of organic acids such as acetic, benzoic, propionic or succinic acid [15] at 70°C. A number of studies have described β-haematin formation in acidic acetate solution in the presence of different materials to promote the reaction: parasite membrane [60], preformed β-haematin [61, 62], lipids [63], and histidine–rich proteins (HRP's) [64].



Most of the methods for β-haematin synthesis involve multiple laborious steps which involve washing, extractions, centrifugation and incubating for a considerable time. A more simplified method obtains β-haematin by dissolving haemin in NaOH and neutralising it with HCl followed by incubation in 4.5 M acetate at 60°C for 30-60 minutes [16]. It is a modified version of the method first reported by Slater *et al.* [15].

Blauer and Akkawi [65] recently reported the formation of β-haematin in ethanol, methanol or propanol-water mixtures containing dilute acid.

The identity of the products from the different methods has been confirmed using infrared spectroscopy in all the cases and also by means of differential solubility, XRD and elemental analysis and SEM in some cases.

## 1.6 THEORIES OF HAEMOZOIN FORMATION IN P. FALCIPARUM

The mechanism of haemozoin biosynthesis under physiological conditions within the malaria parasite digestive vacuoles, the physiological site for haemoglobin degradation, is still under debate.



An initial report suggested that haemozoin does not form spontaneously from either free haem or haemoglobin under physiological conditions [15, 20, 24]. It was assumed that haemozoin is polymeric and this led to the suggestion that an enzyme is required for haemozoin formation. Slater and Cerami [66] reported that a haem polymerase activity is present in parasite extracts of *Plasmodium falciparum* and they hypothesised that it catalyses haemozoin formation.

This was questioned by Dorn *et al.* [61] who proposed that the activity of β-haematin formation is protein-independent and is due to preformed haemozoin which could seed and support its own formation. They investigated the lability of the haem polymerase activity and found that parasite lysates retained their activity at 4°C for several weeks even after boiling. They also found that the activity is associated with the water insoluble fraction of the parasite lysate, which contains the digestive vacuoles. They then subfractionated crude digestive vacuoles into membrane,

digestive-vacuole and haemozoin fractions, and tested them for their ability to support β-haematin formation. From this they found that there was an enrichment of 'haem polymerase' activity in the haemozoin fraction and concluded that the activity in the membrane and vacuole fractions could be accounted for by the presence haemozoin in these fractions.

Addition of synthetic β-haematin was also found to promote its own formation at 37°C, confirming that it is a physicochemical process in which haemozoin supports its own formation and therefore the formation of haemozoin can be described as autocatalytic [61]. It should be noted that some mechanism would still be required to begin nucleation of the crystals in the parasite.

When Egan *et al.* performed the reaction *in vitro*, in 4.5 M acetate, with 10% preformed β-haematin, using two different assays *i.e.* Mössbauer [44] and infrared spectroscopy [30] , they did not observe that β-haematin formation was promoted by preformed β-haematin under these conditions and therefore proposed that β-haematin formation *in vitro* is spontaneous, as its formation does not require a catalyst. However, this is unlikely to be the case *in vivo*.

Bendrat *et al.*, through an analysis of trophozoites, proposed that lipids catalyse the formation of β-haematin in the absence of protein [67] and this was supported by Dorn *et al.* [62] and Fitch *et al.* [63]. Tripathi [68] demonstrated that plasma from mice infected with *P. yoelii* also catalyses *in vitro* β-haematin and haemozoin formation and that the plasma β-haematin synthesis activity was recovered in the lipid extract.

Formation of haemozoin in the midgut of the blood-sucking insect *Rhodnius prolixus* was found to be promoted by a particulate fraction from intenstine lumen and this fraction is composed of perimicrovilla membranes and a flocculent material. This particulate fraction was found to be heat-labile and this suggests a mechanism different from that described for *Plasmodium falciparum* where boiling trophozoites extracts did not change the ability to induce haemozoin formation [50].

Sullivan *et al.* [64] hypothesized that HRPII, a 30 kDa protein with histidine and alanine residues constituting 76% of the entire protein, could bind haem in the digestive vacuole and might play a role in haemozoin formation. Both catalytic as well as scaffolding roles have been proposed for HRPs. Papalexis *et al.* suggested that HRPII may perform different roles in different compartments to promote haemozoin formation and confirmed that HRPII is an efficient catalyst of β-haematin. They found that HRPII (and possibly HRPIII and IV) exist in the digestive vacuole and that HRPII and III are capable of mediating haemozoin formation [69].



However, the existence of a parasite clone, 3B-D5, that is deficient in both *Pf*HRPII and *Pf*HRPIII but still generates haemozoin, argues against an essential role for these proteins in haemozoin formation, but there may be multiple HRPs that are involved in protection against the toxic effects of haematin in *P. falciparum*. For example, *Pf*HRPIV has been suggested as a possible candidate for an additional protective HRP [64].

On the basis that haemozoin and β-haematin can seed the pigment formation reaction [61], Ziegler *et al.* suggested that HRPs are more likely to play a role in the nucleation of haemozoin and that the protein yields a functionalized surface that serves as a template for nucleation and that this may be a biomineralization process [70]. Biomineralization is known to act as a detoxification mechanism in other microorganisms, eg. mineralization of copper sulphide confers copper tolerance in *S. cerevisiae* [71]. This was supported by Egan *et al.*, who from their detailed study of kinetics of formation of β-haematin in acetate solution suggested that the formation of β-haematin proceeds *via* rapid precipitation of amorphous β-haematin, they proposed that the conversion proceeds by dissolution and re-precipitation, the latter process occurring *via* crystal nucleation and growth. It therefore resembles a mineral formation process and can be interpreted as a type of biomineralization [30]. They suggested that in common with other biomineralisation processes, haemozoin is likely to be formed directly from solution in the organism.

A study by Pandey *et al.* [72] suggests that haemozoin formation in the malaria parasite may be a coordinated two-step process involving both HRPs and lipids. Since too little HRPII is present in the parasite food vacuole to bring about haem detoxification on its own, it is suggested that HRPs may be mainly involved in haem binding and dimer formation by linking haem molecules together while lipids facilitate hydrogen bonding of the propionate side chains of two haem molecules and stabilise the structure by shielding these hydrogen bonds from competitive hydrogen binding with water. Lipids alone cannot mediate haem interactions of complexes that are insoluble. Similarly, the hydrogen bonding in the absence of lipids is poor, thus negatively affecting the rate of haemozoin formation by *Pf*HRPII alone [72].

It has recently been suggested that the rate of reaction could also be affected by the presence of the noncentrosymmetric β-haematin-like cyclic dimer, which may dock onto the growing crystal surface, leading to crystal growth inhibition [73]. It has been well established that minor amounts of a tailor-made additive, which structurally mimics the host molecule present in solution, may induce dramatic changes in the nucleation properties, growth rate and morphology of a crystal [74, 75].

Since the inhibition of crystal precipitation is best achieved by making use of additives designed to retard crystal growth, Buller *et al.* proposed the possibility that the growing haemozoin crystal surfaces act as template for formation of β-haematin centrosymmetric dimers. The noncentrosymmetric dimer is formed as a result of one of the two porphyrin rings of haematin reacting from its opposite face, leading to an interchange of the porphyrin ring's methyl and vinyl groups (Figure 1.19.).

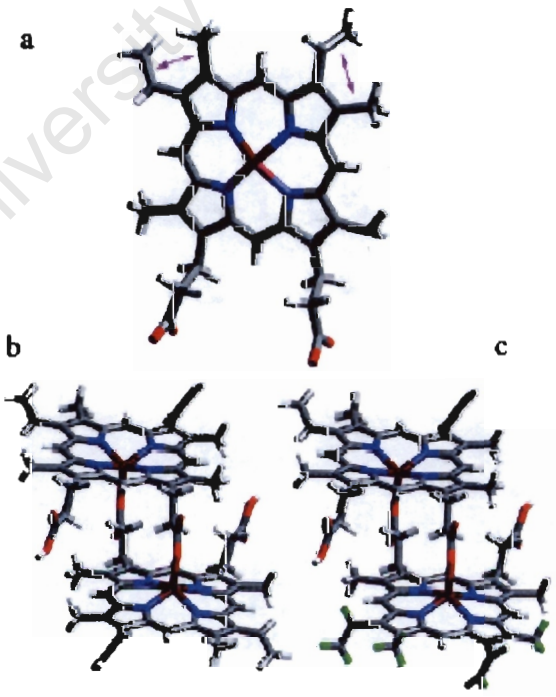


**Figure 1.19** (**a**) Molecular structure of haematin, (**b**) centrosymmetric cyclic dimer present in β-haematin, (**c**) noncentrocymmetric dimer proposed to retard crystal growth [73].

It is possible that the noncentrosymmetric isomer retards further crystal growth during β-haematin formation confining crystals to micron-sized crystals [73]. This may play a role in limiting crystal growth *in vivo*, or the parasite may have mechanisms for avoiding formation of this unwanted dimer.

To date, most authors have assumed that haemozoin formation occurs in the food vacuole, the site where it is found. However, recently Hempelmann *et al.* hypothesised a different site for the formation of haemozoin. They proposed that in addition to parasite nutrient acquisition and a role in the trafficking of parasite proteins to the host cell membrane, the parasitophorous vacuolar membrane, PVM, which topologically forms the inner membrane of the transport vesicles that traffic haemoglobin to the food vacuole, also functions in the biogenesis of haemozoin crystals by acting as a sacrificial membrane for decomposing hydrogen peroxide produced by the autoxidation of haem [76]. However, in their most recent paper Williams *et al.* [77] found that parasites grown outside the cell still produce haemozoin, although they do not have the parasitophorous vacuolar membrane. The other problem associated with Hempelmann's hypothesis is that haemoglobin monomers may produce large concentrations of proteolytic products which can increase the osmotic pressure inside the transport vesicle, finally destroying it [78].

Thus, at present there are many hypotheses for the mechanism and site of haemozoin formation *in vivo*, but little consensus.

## 1.7 KINETIC STUDIES OF β-HAEMATIN FORMATION

Understanding the chemical mechanism of β-haematin formation is important in that it sheds light on how the haemozoin formation process might occur *in vivo*. Several assays have been developed to study the mechanisms of β-haematin formation. These assays differ mostly in the conditions of reaction such as pH, temperature and duration. They also differ in the methods used to identify and quantify the reaction products. Most of the studies of β-haematin formation have been done in acetate solution. In a number of reports, the amount of β-haematin formed at fixed intervals was measured under different reaction conditions [60, 62, 79-82].

A few studies have been done where the extent of β-haematin formation was investigated, but the rate constant for product formation was not determined. Dorn *et al.* reported a spontaneous time-course for formation of β-haematin from haematin in aqueous sodium acetate in the absence of additional reagents, at 37°C. The incorporation of haematin into β-haematin was quantified by scintillation counting using the Topcount™ Microplate Scintillation system [62]. Slater and Cerami investigated the time dependence of haemozoin formation by measuring the amount formed at different intervals [66]. In their assay Basilico *et al.* determined the time course of β-haematin formation by stopping the reaction at different time intervals and measuring the amount of porphyrin present in each fraction, in microtitre wells [83]. Berger *et al.* measured the disappearance of free haematin detected in 20 µl injections of haematin sampled at sequential time points during incubation in acetic

acid at 70°C, by spectrophotometric absorbance at 400 nm [84]. None of these studies proposed a kinetic model for the process.

Two studies have been reported which give detailed kinetic analyses of β-haematin formation, Mössbauer spectroscopy and IR pectroscopy were used to monitor the reaction. Mössbauer spectroscopy was used to measure the relative amounts of haematin and β-haematin present during the course of the reaction [44]. Any given sample obtained between t = 0 and t = 60 minutes consists of a mixture of haematin and β-haematin and therefore the observed spectrum is a composite of two asymmetric quadrupole doublets. The curve-fitting procedure was greatly simplified by using the isomer shifts for haematin and β-haematin as fixed parameters in the optimisation process, and their percentage contribution to the observed spectrum was determined. This allowed construction of kinetic curves for either β-haematin formation or for haematin decay, with time. The reaction was performed in 4.5 M acetate, pH 4.3 at 60°C and it required 15 mg of sample for each time point. Samples were quenched by cooling and dried for measurement. This stops all further reaction in the sample.



For each sample the spectrum was accumulated over approximately 12 hours. These kinetic experiments suggested that the reaction is a zero-order process and that it is not autocatalytic since there was no evidence of an induction phase and that seeding with β-haematin did not increase the rate of the reaction [44]. In a subsequent study where infrared spectroscopy was used to monitor the reaction kinetics, it was demonstrated that the proposal of zero-order kinetics was erroneous, probably due to

the relative insensitivity of the Mössbauer method. Instead, the kinetics were found to be sigmoidal, in accordance with what was reported by Dorn *et al.* (Figure 1.19) [62], indicative of a process of nucleation and growth.

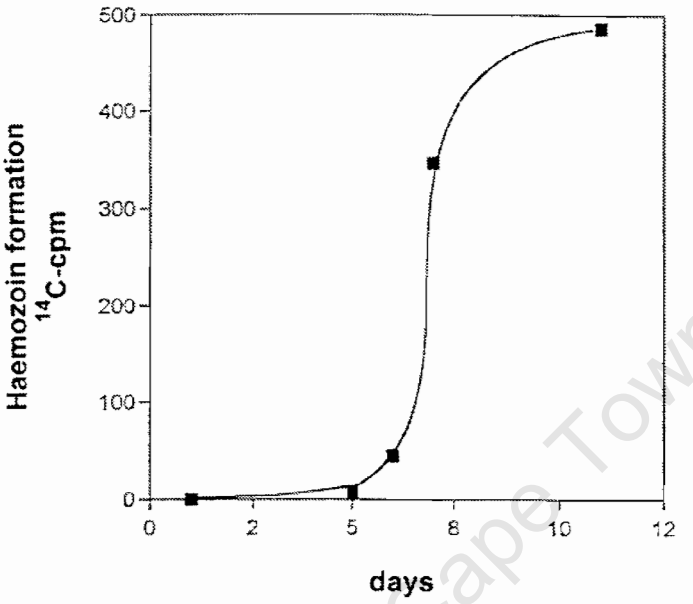


**Figure 1.20** Sigmoidal curve for the formation of β-haematin in 0.5 M sodium acetate, pH 4.8 at 37°C [62].

The kinetics using IR were studied by monitoring the growth of the β-haematin peak at 1210 $cm^{-1}$ from the shoulder of the peak at 1229 $cm^{-1}$ (Figure 1.21a) [30]. For each time point, approximately 1.5 mg sample was removed from the reaction mixture, quenched on ice, filtered and washed with deionised water. Although a kinetic run required only an hour of incubation, the product had to be dried at room temperature for at least 48 hours over silica gel and $P_4O_{10}$. A calibration plot (Figure 1.21b) was prepared by mixing well-characterized samples of haematin and β-haematin in known mass proportions and the mass fraction of haematin was approximated by using Equation 1.3 below.

$$\frac{m}{m_0} = 1 - \frac{\Delta A}{\Delta A_\infty} \qquad 1.3$$

where $m$ is the mass of haematin remaining in the sample, $m_0$ is the initial mass of haematin in the sample. $\Delta A$ is the difference absorbance at 1210 $cm^{-1}$ due to β-haematin as shown in Figure 1.21a. $\Delta A_\infty$ is the final difference absorbance at the end of the reaction.

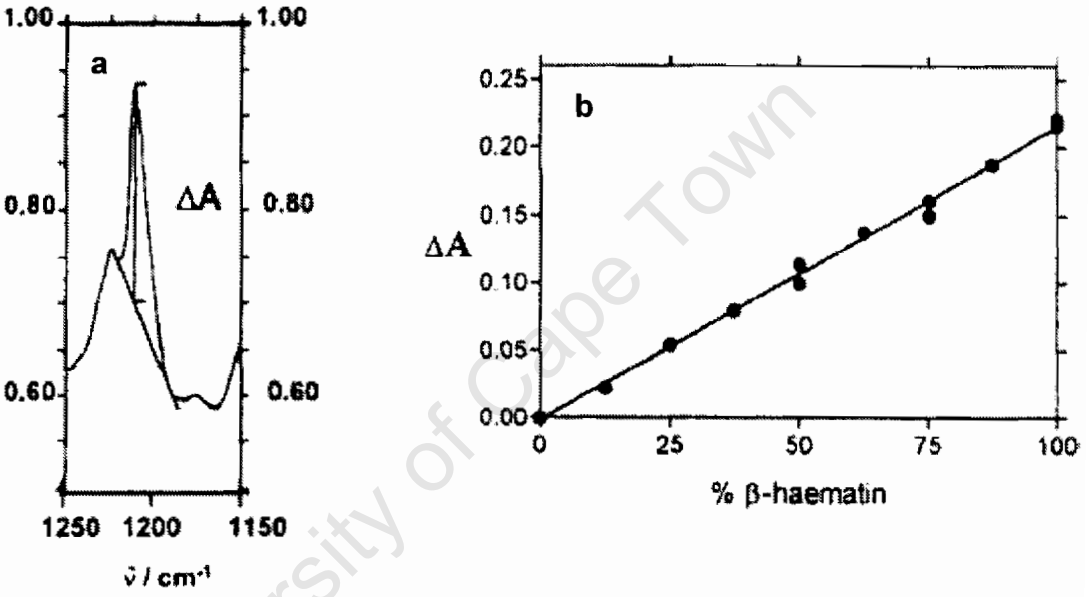


**Figure 1.21** (**a**) Typical infrared absorbance spectrum of a sample obtained during β-haematin formation showing how the difference absorbance readings were obtained from the spectrum, (**b**) calibration plot showing $\Delta A_{1210}$ as a function of β-haematin percentage in samples made up by mixing known masses of haematin and β-haematin [30].

Rate constants were obtained by fitting the data to the Avrami equation, a semi-theoretical model that relates the rate of a process to the rates of nucleation and growth (Equation 1.4). Phase transition kinetics in many systems are described on the grounds of this model [85].

$$\Delta A = \Delta A_{\infty}\left\{1 - \exp\left(-zt^{n}\right)\right\} \qquad 1.4$$

where $z$ is the empirical rate constant and $n$ is a constant known as the Avrami constant, an integer ranging between 1 and 4, The combinations of the type of nucleation and growth giving rise to different values of $n$ are shown in Table 1.2 below.

**Table 1.2** Values for the Avrami exponent, $n$, for different types of nucleation and growth [86].

| $n$ | type of nucleation and growth |
|---|---|
| 4 (3 + 1) | sporadic nucleation and spherical (3D) growth |
| 3 (3 + 0) | instantaneous nucleation and spherical (3D) growth |
| 3 (2 + 1) | sporadic nucleation and disk-like (2D) growth |
| 2 (2 + 0) | instantaneous nucleation and disk-like (2D) growth |
| 2 (1 + 1) | sporadic nucleation and rod-like (1D) growth |
| 1 (1 + 0) | instantaneous nucleation and rod-like (1D) growth |



Sporadic or time-dependent nucleation is a first order process with nucleation sites appearing continuously throughout the reaction whereas instantaneous or random nucleation is a zero order process with nucleation sites being formed immediately at the beginning of the process and no new sites appear during the process.

When the data for β-haematin formation at 60°C in 4.5 M acetate, pH 4.5, were fitted to the Avrami equation, the value of $n$ was found to be closer to 4 than to any values less than 4 (Figure 1.22) and was therefore fixed to 4 to reduce the standard

deviation in the fitted value of *z*. The kinetics show a sigmoidal shape indicative of a process of nucleation and growth, a process that resembles many mineral formation processes.

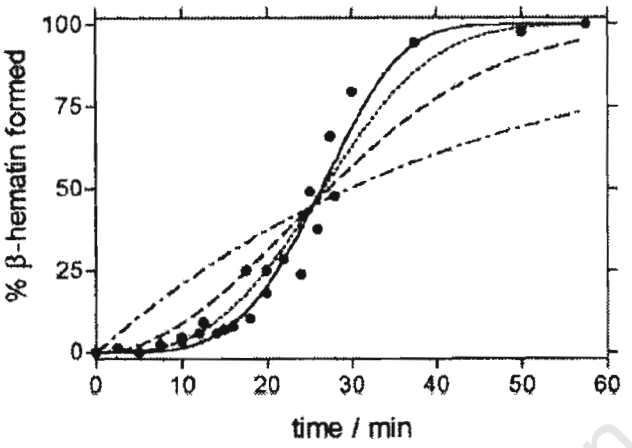


**Figure 1.22** Time course of β-haematin formation measured by infrared spectroscopy (•) in 4.5 M acetate, pH 4.5, 60°C. Lines are best fits of the data to the Avrami equation with (–) $n = 4$, (· · ·) $n = 3$, (– –) $n = 2$, (– · –) and $n = 1$ [30].

The time course for this process observed by IR spectroscopy was in excellent agreement with the changes in the diffraction pattern (Figure 1.23) and in external morphology (Figure 1.24). The diffraction pattern shows the change from amorphous haematin to crystalline β-haematin.

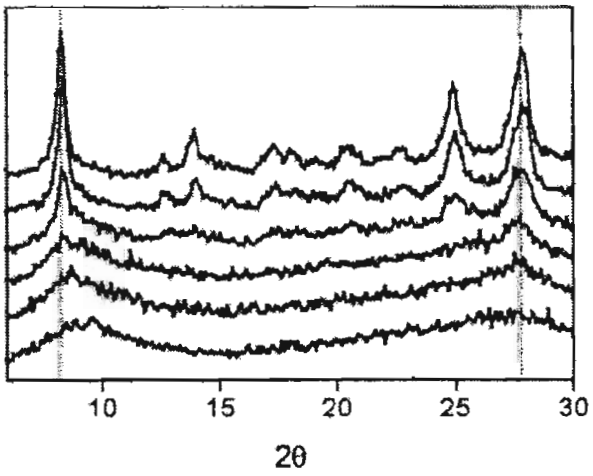


**Figure 1.23** XRD patterns of dried samples of β-haematin obtained from the reaction under the same conditions as in figure 1.22 at 0, 5, 15, 20, 30, and 60 minutes (from bottom to top) [30].

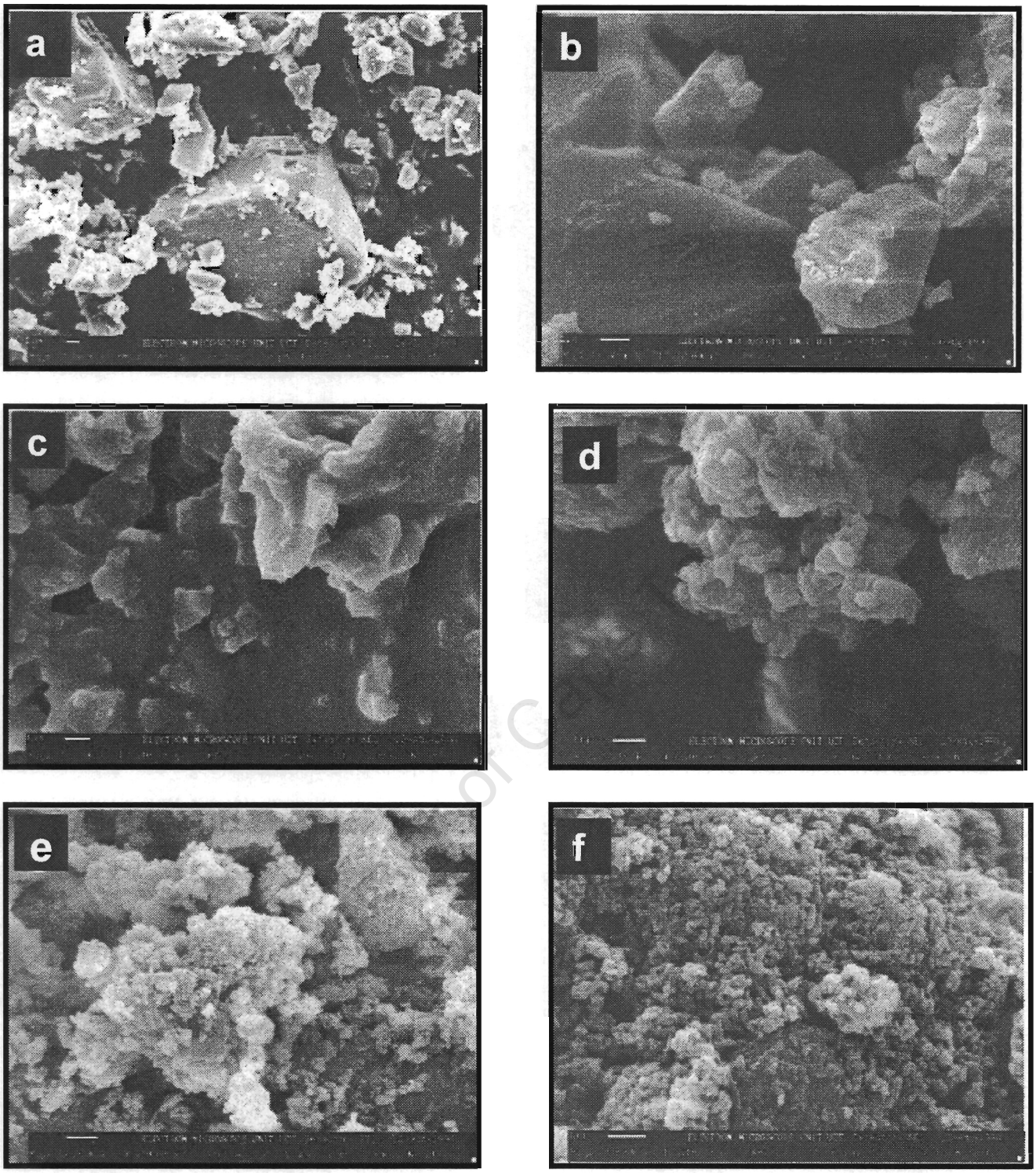


**Figure 1.24** Scanning electron micrographs of dried samples of β-haematin at (**a**) 0, (**b**) 5, (**c**) 15, (**d**) 20, (**e**) 30, (**f**) 60 minutes, reactions were carried out under the same conditions as in Figure 1.22 [30]. (Scales: (a) 667:1, (b-e) 5000:1, (f) 6000:1 as shown).

The effect of stirring, temperature, pH, acetate concentration and seeding with β-haematin were investigated and it was found that the rate of formation of β-haematin is strongly dependent on stirring rate, temperature and concentration of acetate. Changes in the stirring rate and concentration also bring about a change in the value of *n*. Seeding with β-haematin did not have an effect on the rate of formation of β-haematin. The pH dependence showed a bell-shaped plot with maximal rate at pH 3.5, consistent with an equation that assumes two protonation sites on the Fe(III)PPIX, with only the monoprotonated species reacting at an appreciable rate. According to these results, β-haematin formation occurs by rapid precipitation of amorphous haematin, followed by slow conversion to the less soluble, thermodynamically more stable β-haematin, very typical of a biomineralization process [30].



## 1.8 BIOMINERALIZATION PROCESSES

The most important biominerals are calcium carbonate, calcium phosphate, calcium oxalate, metal sulfates, amorphous silica and iron oxides. Their different functions are mechanical support, storage, deposition and detoxification [87].

The ability of organisms to exert a suprising level of control over mineral deposition has been illustrated by the biological formation and stabilisation of amorphous calcium carbonate, a phase which is intrinsically unstable thermodynamically and kinetically at physiological pH, temperature, and pressure [88].

Silification of microorganisms occurs in abundance in many hot spring environments where they are exposed to geothermal waters supersaturated with respect to amorphous silica. Recent studies have demonstrated that repeatedly exposing cyanobacteria to freshly prepared supersaturated polymerizing silica solution by regularly replacing the experimental fluid can induce extensive biomineralization similar to that observed in hot springs. Furthermore it has been shown that cyanobacteria continue to metabolise and function during extensive silification [89]. It is well established that the growth and aggregation of polymers, particularly silica, in solution is affected by pH, ionic strength, temperature and surfactant concentration and type.

Copper is an essential element for normal cell physiology. Although it is an essential nutrient, excess copper in the environment can lead to toxicosis. Cells have evolved mechanisms to balance intracellular copper levels between nutritious and toxic, by converting it to CuS [71] by means of biomineralisation.

Magnetotactic bacteria synthesise intracellularly enveloped, single magnetic domain crystals of magnetite ($Fe_3O_4$, $Fe^{2+}Fe^{3+}O_4$) and/or greigite ($Fe_3S_4$) in compartments called magnetosomes. The magnetosomes contain well-ordered crystals that have narrow size distributions and consistent species and/or strain–specific morphologies. These characteristics are features of biologically–controlled mineralization in which an organism exerts a great degree of crystallochemical control over the nucleation and growth of the mineral particle [90].

Haemozoin formation appears to have many features in common with these processes and may be a unique biologically-controlled biomineralisation-like process in which the crystal is formed, not from a mineral salt but from an iron porphyrin.

## 1.9 β-HAEMATIN FORMATION IN THE PRESENCE OF BENZOIC ACID SOLUTION

Slater *et al.* reported the formation of β-haematin in the presence of organic acids such as acetic, benzoic, propionic or succinic acid [15]. In a preliminary study done in our laboratory in benzoic acid, at a concentration which is about one-fiftieth of the concentration of acetate, and at the same pH and temperature as that used for β-haematin formation in acetic acid, it was revealed that benzoic acid is more active in promoting the formation of β-haematin.



The use of benzoic acid as opposed to acetic acid is better in that much lower concentrations of benzoic acid are required for the formation of β-haematin, and the electronic properties of the acid can be varied by simply changing the substituents at the para, meta or ortho positions on the benzene ring.

There are a number of empirical methods for describing the electronic properties of substituents. The most successful and intensively investigated are the linear free energy relationships, with the Hammet equation as the most prominent example [91]. The Hammet equation states that the electronic effect of substituents on the

ionization of benzoic acids can be used as a model for the electronic effect of substituents on other reaction centers attached to aromatic systems and can be expressed by Equation 1.5 below,

$$\sigma(X) = \frac{\log K_X - \log K_H}{\rho} \qquad 1.5$$

where $K_H$ is the ionization constant for benzoic acid in water at 25°, $K_X$ is the ionization constant for a para or meta derivative under the same experimental conditions and $\rho$ is a measure of the sensitivity of such a reaction to the electronic effect of X as compared to the effect of substituents on the ionization of benzoic acids where, by definition, $\rho$ = 1.0 when the measurements are made in water at 25°C [92].

The primary values of $\sigma$ are obtained simply from $pK_a$ values of the substituted and unsubstituted benzoic acids according to Equation 1.5. Positive values of $\sigma$ represent electron withdrawal by the substituent from the aromatic ring and negative $\sigma$ values indicate electron release to the ring.

Hammett constants are position-dependent; that is $\sigma$ for a given substituent in the meta position is different from that in the para position [93]. A collection of $\sigma$ values for ortho substituents and the development of a general approach for dealing with the electronic effects of ortho substituents has been carried out by Charton [94] and Fujita [95] respectively.

## 1.10 AIMS AND OBJECTIVES

The aim of this project is to study the kinetics of β-haematin formation in benzoic acid, using a newly developed pyridine assay [96]. The assay makes use of the observation that haematin and not β-haematin forms a soluble, intensely coloured complex with pyridine, and therefore the disappearance of haematin as the reaction proceeds is easily measured by removal of samples, followed by reaction with pyridine.

In this study the rate of formation will be studied by varying pH, seeding, concentration, temperature, stirring rate and substituents at the para positions (Figure 1.25) since conjugation is generally more effective at the para positions.

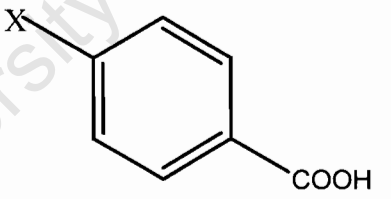


**Figure 1.25** Benzoic acid derivatives used for studying the effect of electronic properties and $pK_a$ on the formation of β-haematin, X = H, $NO_2$, $OCH_3$, CN, $NH_2$, $SO_2CH_3$, $SO_2NH_2$, CHO.

Specific objectives of the study are:

- To confirm that the product formed in 0.05 M benzoic acid is β-haematin, using infrared spectroscopy, X-ray diffraction (XRD) and scanning electron microscopy (SEM) and to compare it with that formed in 4.5 M acetic acid.

- To determine if data obtained from the kinetic study of β-haematin formation in benzoic acid gives sigmoidal behaviour and whether it fits the Avrami equation.
- To validate the pyridine assay for studying the kinetics of formation of β-haematin by performing the reaction in acetic acid and comparing with the results found when infrared spectroscopy was used.
- To compare the activity of benzoic acid with that of acetic acid in promoting formation of β-haematin.
- To confirm that β-haematin forms during incubation and not during drying by following the kinetics on wet β-haematin using XRD.
- To investigate the effect of temperature, stirring, seeding with preformed β-haematin, and pH and concentration of benzoic acid on the kinetics.
- To determine the relationship between the rate of formation of β-haematin and different substituents in the para position of benzoic acid.
- To study the effect of $pK_a$ of 4-cyanobenzoic acid and 4-aminobenzoic acid on the pH maxima of haematin during formation of β-haematin.

# 2. MATERIALS AND METHODS

The following materials were purchased and used as received. Haemin chloride, 4-chlorobenzoic acid, 4-cyanobenzoic acid, 4-aminobenzoic acid, 4-carboxybenzenesulfonamide, 4-methylsulfonylbenzoic acid, 4-nitrobenzoic acid, 4-carboxyaldehydebenzene, 4-methoxybenzoic acid, 4-toluic acid and N-[2-hydroxyethyl]piperizine-N'-[2-ethanesulfonic acid] (HEPES) were obtained from Sigma. Sodium hydroxide was purchased from Orion chemicals. Phosphate buffer solutions of pH 4 and 7, pyridine, dimethyl sulfoxide (DMSO) and hydrochloric acid were obtained from BDH Laboratory Supplies. Benzoic acid was obtained from Associated Chemical Enterprise. Phosphorous Pentoxide ($P_2O_5$) was obtained from Riedel-déHaën.

All reactions were performed in a 50 ml titration cell covered with a watch-glass, on a Snijders magnetic stirrer, and connected to a GRANT Y6 thermostated water bath set at 60°C unless stated otherwise. The contents of the vessel were stirred with a stirrer bar of length 15 mm and diameter 4.5 mm. Absorbance and spectral measurements were collected on a Varian Cary 100 UV-Vis spectrophotometer. pH measurements were done on a Crison MicropH 2000 pH meter that was calibrated using standard solutions of pH 4 and 7. All solid chemicals were weighed on a Sartorius electronic balance and all volumes were delivered using Eppendorf micropipettes. Distilled water was used throughout in the preparations of solutions.

## 2.1. PREPARATION OF SODIUM BENZOATE/BENZOIC ACID SOLUTION

A stock solution of 0.07 M sodium benzoate acid was prepared by dissolving 4.274 g (35 mmol) benzoic acid in 25 ml of 1 M NaOH (prepared by dissolving 4.0 g (100 mmol) NaOH pellets in 100 ml distilled $H_2O$ in a volumetric flask). The solution was made up to 450 ml with distilled $H_2O$. The pH was then adjusted to 4.5 by adding the 1 M NaOH solution in a dropwise manner. When the pH was at 4.5 the solution was made up to 500 ml with water. Although this solution is a mixture of benzoic acid and sodium benzoate salt, it will be referred to as benzoic acid throughout.

## 2.2 FORMATION OF β-HAEMATIN IN BENZOIC ACID

In a reaction vessel connected to a thermostated water bath, 30 mg haemin chloride was dissolved in 2.6 ml of 0.1 M NaOH and stirred until all the haemin was dissolved. To this was added 0.26 ml 1.00 M HCl, to neutralise the NaOH. After about 2 minutes, formation of β-haematin was initiated by adding 7.14 ml of 0.07 M benzoic acid solution to the reaction mixture to give a final concentration of 0.05 M benzoic acid. The reaction was stirred continuously. After 2.5 hours distilled water was added to the reaction mixture to stop any further reaction. The product was filtered, using a 0.22 μm cellulose nitrate filtration disk, washed with water and dried at room temperature over silica gel and $P_2O_5$ for 48 hours.

## 2.3 FORMATION OF β-HAEMATIN IN ACETIC ACID

At 60°C, 30 mg haemin chloride was dissolved in 2.6 ml of 0.1 M NaOH and stirred until all the haemin was dissolved. To this was added 0.26 ml 1.00 M HCl, to neutralise the NaOH. After about 2 minutes, formation of β-haematin was initiated by adding 3.49 ml of 12.9 M acetic acid stock solution, pH 5. The mixture was then diluted to 7.14 ml with distilled water to give a final acetic concentration of 4.5 M and a pH of 4.5.

## 2.4 CHARACTERISATION OF THE PRODUCT

### *2.4.1 Infrared spectroscopy*

To obtain IR spectra, KBr pellets were prepared by grinding a 2 mg sample of β-haematin with 200 mg KBr using a mortar and pestle. The resulting powder was compressed under 10 ton/psi pressure to produce a disk of 16 mm diameter. The spectrum was collected from 2000 to 1000 $cm^{-1}$ on a Perkin-Elmer FT-IR Spectrum 100 spectrometer.

### *2.4.2 X-ray diffraction*

For X-ray diffraction, the β-haematin formation reaction was carried out on a larger scale to obtain enough product (about 200 mg). A piece of Mylar was fitted into the specimen holder. Using a template, a rectangular film of Paratone N was spread so

as to cover the marker of the template and to enable the product to stick to the Mylar. About 200 mg of the product, finely ground, was spread onto the Paratone N. The specimen holder was fitted on a flat sample holder. In cases where XRD was performed on wet product, it was not necessary to use Paratone N. The sample holder was mounted on a flat oscillation device 670.1. Diffractogram data was collected on a HUBER Imaging Plate Guinier Camera 670 with a Cu Kα radiation source of λ = 1.5418 Å operating at 20 mA and 40 kV over the 2θ range of 4° - 30° at a step resolution of 0.005°.

### *2.4.3 Scanning electron microscopy*

Scanning electron microscopy was carried out by the University of Cape Town electron microscopy unit on a LEO S440 scanning electron microscope. The samples were sprinkled on aluminium stubs coated with a mixture of graphite and glue. The samples were then coated with gold-palladium.



## 2.5 PYRIDINE ASSAY FOR β-HAEMATIN FORMATION

### *2.5.1 Preparation of 0.2 M HEPES buffer*

In 95 ml distilled water, 4.766 g of HEPES was dissolved and the pH was adjusted to 7.5 using a saturated solution of NaOH. The solution was then made up to 100 ml with distilled water.

### 2.5.2 Preparation of pyridine solution

Pyridine solution for monitoring the formation of β-haematin was prepared by mixing 10 ml of 0.2 M HEPES buffer, pH 7.5, with 5 ml pyridine in a 100 ml volumetric flask. The mixture was then made up to 100 ml with distilled water.

## 2.6 MONITORING THE FORMATION OF β-HAEMATIN

From the reaction mixture, 5 μl aliquots were removed at predetermined time intervals. This was continued for varying times depending on how long the reaction took to reach completion. The aliquot was suspended in 2 ml pyridine solution and the absorbance of the supernatant was measured on a spectrophotometer at 405 nm after the undissolved β-haematin had settled. In all the reactions, the absorbance measured is proportional to the amount of haematin remaining in the reaction mixture.



## 2.7 DATA ANALYSIS

Kinetic data was analysed by fitting to the well known and widely used [30, 85, 86] Avrami equation (Equation 2.1) using a non-linear least squares fitting program.

$$A_t = \{(A_i - A_f)\exp(-zt^n)\} + A_f \qquad 2.1$$

Where $A_t$ is the absorbance at time t, $z$ is an empirical rate constant, $n$ is a constant known as the Avrami constant, which is usually an integer which ranges between 1

and 4, $A_i$ is the initial absorbance, i.e. absorbance at the beginning of the reaction and $A_f$ is the final absorbance, i.e. absorbance at the end of the reaction.

## 2.8 KINETICS OF β-HAEMATIN FORMATION IN BENZOIC ACID

### *2.8.1 Effect of stirring*

The reactions were performed under the conditions described above for β-haematin formation (2.2) but at different stirring rates. Where the reaction was carried out unstirred, stirring was stopped immediately after adding the benzoic acid solution. To obtain homogeneity the solution was agitated briefly before taking each aliquot.

### *2.8.2 Effect of temperature*

The formation of β-haematin was studied at 37, 55, 60, 65, and 70°C. The amount of haemin chloride, concentration of benzoic acid, pH and stirring rate were all kept constant and reactions were carried out as described in 2.2 above.

### *2.8.3 Effect of concentration*

The volume of benzoic acid was varied so as to have final concentrations of 0.05, 0.04, 0.03, 0.02, and 0.01 M in the reaction vessel. Temperature, total reaction volume (10 ml), amount of haemin chloride and pH were all kept constant. The volumes of HCl and NaOH were also kept constant.

### *2.8.4 Effect of pH*

Solutions of the benzoic acid stock solutions with pH 2.5, 3.0, 3.5, 4.0, 4.5 and 5.0 were prepared using the same procedure described in 2.1 except for adjustment of the final pH value. The effect of pH was studied at a constant concentration of 0.05 M benzoic acid and a temperature of 60°C. The volumes of HCl and NaOH were kept constant.

### *2.8.5 Effect of seeding*

The procedure used is the same as above (2.2) except that 3 mg of β-haematin was added to the reaction vessel just before adding benzoic acid.

## 2.9 KINETICS OF β-HAEMATIN FORMATION IN SUBSTITUTED BENZOIC ACIDS

The reactions were carried out as in benzoic acid (2.2) and the amounts of haemin chloride, NaOH, HCl, temperature and pH were kept constant. The kinetics were studied at the same concentration of 0.02 M except for 4-methoxybenzoic acid which was not soluble at this concentration. As a result a concentration study was consequently performed in order to extrapolate the rate constant to 0.02 M.

## 2.9.1 4-Nitrobenzoic acid

### 2.9.1.1 Preparation of 4-nitrobenzoic acid solution

A stock solution of 0.03 M was prepared by dissolving 2.5073 g of 4-nitrobenzoic acid in 20 ml of 0.1 M NaOH. Approximately 450 ml of distilled water was added. The pH was adjusted to 4.5 using 0.1 M NaOH solution. The solution was made up to 500 ml with distilled water.

### 2.9.1.2 Effect of concentration

The reactions were performed under the same conditions as in 2.2 using the 0.03 M stock solution of 4-nitrobenzoic acid. Appropriate dilutions were performed to give different concentrations at a pH of 4.5. The concentrations studied were 0.005, 0.01, 0.015, 0.018 and 0.02 M.



### 2.9.1.3 Effect of temperature

The effect of temperature was studied in 0.02 M 4-nitrobenzoic acid, pH 4.5 at 37, 50, 55, 60 and 65°C using the method described above in 2.2.

## 2.9.2 4-Amino benzoic acid

### 2.9.2.1 Preparation of 4-aminobenzoic acid solution

A stock solution of 0.06 M 4-aminobenzoic acid was prepared by dissolving 0.4114 g of 4-aminobenzoic acid in 2 ml of 1 M NaOH. Approximately 45 ml distilled water was added and the pH was adjusted to 4.5 using 0.1 M NaOH. The solution was made up to 50 ml with distilled water.

### 2.9.2.2 Effect of pH

Solutions of 0.06 M 4-aminobenzoic acid with pH values 3.5, 3.8, 4.0, 4.5, 5.0 and 5.5 were prepared using the same procedure as above (2.9.2.1). The effect of pH was studied at a constant concentration of 4-aminobenzoic acid of 0.04 M and a temperature of 60°C. The volumes of HCl and NaOH were also kept constant.



## 2.9.3 4-Methoxybenzoic acid

### 2.9.3.1 Preparation of 4-Methoxybenzoic acid solution

A stock solution of 0.01 M was prepared by dissolving 0.1522 g in 2 ml of 0.1 M NaOH. Approximately 95 ml distilled water was added and the pH was adjusted to 4.5 using 0.1 M NaOH. The solution was made up to 100 ml with distilled water.

#### 2.9.3.2 Effect of concentration

The reactions were carried out under the same conditions as in 2.2 using the 0.01 M stock solution of 4-methoxybenzoic acid. Appropriate dilutions were performed to give different concentrations at a pH of 4.5. The concentrations studied were 0.005, 0.0055, 0.0058, 0.006, 0.0065, and 0.007 M.

### 2.9.4 4-Cyanobenzoic acid

#### 2.9.4.1 Preparation of 4-cyanobenzoic acid solution

A stock solution of 0.03 M was prepared by dissolving 0.2207 g in 5 ml of 0.1 M NaOH. Approximately 45 ml distilled water was added and the pH was adjusted to 4.5 using 0.1 M NaOH. The solution was made up to 50 ml with distilled water.



#### 2.9.4.2 Effect of pH

Solutions of 0.01 M 4-cyanobenzoic acid with pH values 2.5, 3.0, 3.5, 4.0, 4.3, and 4.5 were prepared using the same procedure as above (2.9.4.1). The effect of pH was studied at a constant concentration of 4-cyanobenzoic acid of 0.007 M and a temperature of 60°C. The volumes of HCl and NaOH were also kept constant.

## 2.9.5 4-Carboxybenzenesulfonamide

### 2.9.5.1 Preparation of 4-Carboxybenzenesulfonamide solution

A stock solution of 0.03 M was prepared by dissolving 0.3018 g in 5 ml of 0.1 M NaOH. Approximately 45 ml distilled water was added and the pH was adjusted to 4.5 using 1 M NaOH. The solution was made up to 50 ml with distilled water.

## 2.9.6 4-Methylsulfonylbenzoic acid

### 2.9.6.1 Preparation 4-Methylsulfonylbenzoic acid solution

A stock solution of 0.03 M was prepared by dissolving 0.3003 g in 0.5 ml of 1 M NaOH. Approximately 45 ml distilled water was added and the pH was adjusted to 4.5 using 0.1 M NaOH. The solution was made up to 50 ml with distilled water.



## 2.9.7 4-Carboxybenzaldehyde

### 2.9.7.1 Preparation of 4-Carboxybenzaldehyde solution

A stock solution of 0.03 M was prepared by dissolving 0.2252 g in 1 ml of 0.1 M NaOH. Approximately 45 ml distilled water was added and the pH was adjusted to 4.5 using 0.1 M NaOH. The solution was made up to 50 ml with distilled water.

# 3. CHARACTERISATION OF β-HAEMATIN AND EVALUATION OF THE PYRIDINE ASSAY FOR STUDYING β-HAEMATIN FORMATION KINETICS

## 3.1 CHARACTERISATION OF β-HAEMATIN

β-haematin formed in 0.05 M benzoic acid, pH 4.5 at 60°C, was characterised by infrared spectroscopy, scanning electron microscopy and x-ray diffraction. β-haematin formed in acetic acid under conditions described by Egan *et al.* [16, 30] was also characterised by these methods for comparison.

### *3.1.1 Infrared spectroscopy*

The infrared spectrum of haematin formed in 0.05 M benzoic acid is shown in Figure 1a together with that of β-haematin formed under the same conditions (Figure 1b). The infrared spectrum of β-haematin formed in 4.5 M acetic acid is also shown (Figure 1c). Both spectra of β-haematin are significantly different from that of haematin and they are identical to each other.

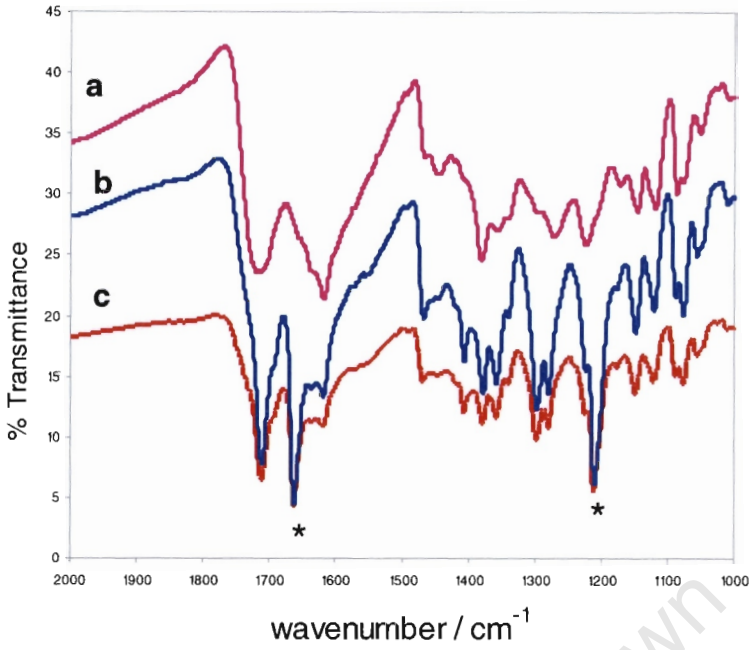


**Figure 3.1** Infrared spectra of (**a**) haematin, (**b**) β-haematin formed in 0.05 M benzoic acid and (**c**) β-haematin formed in 4.5 M acetic acid, pH 4.5, 60°C. The asterisks indicate characteristic peaks of the iron-caboxylate bond.



When the carboxylate coordinates to the metal centre of a porphyrin, peaks are observed at 1660 and 1210 $cm^{-1}$ [15]. The presence of peaks in the β-haematin samples, which are absent in haematin, confirms coordination between $COO^-$ and the Fe(III) centre.

Besides the major features at 1662 and 1210 $cm^{-1}$, all the peaks in the spectrum of haematin are broader, while the spectrum of β-haematin is more sharply resolved. This difference has previously been ascribed to a reduction in intermolecular hydrogen bonding in β-haematin [15].

### 3.1.2 X-ray diffraction

X-ray diffraction was performed in order to confirm the identity and structural composition of β-haematin formed in benzoic acid. The diffraction patterns of β-haematin formed in 0.05 M benzoic acid (Figure 3.2a) and in 4.5 M acetic acid (Figure 3.2b), measured from 4 to 30° were found to be identical.

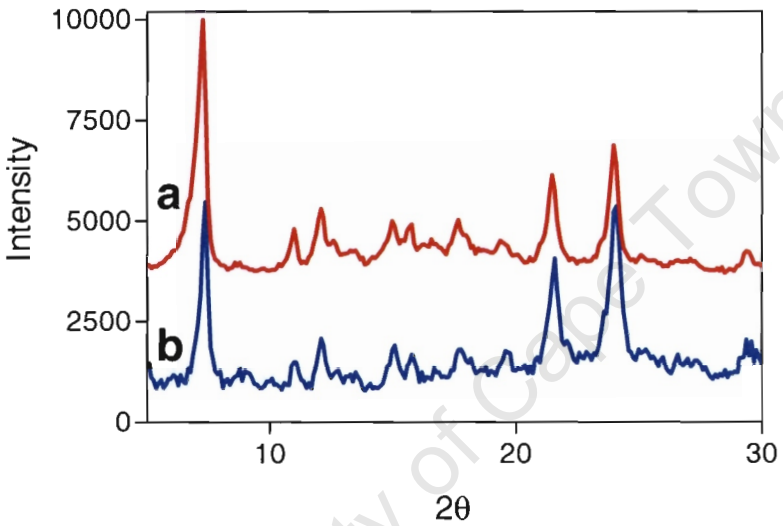


**Figure 3.2** X-ray diffraction pattern of dried β-haematin formed in (**a**) acetic acid and (**b**) benzoic acid. Data collected with a Cu Kα radiation source of λ = 1.5418 Å.



These peaks also correspond to d-spacings reported for lyophilised late trophozoites of *P.falciparum* [45]. The identical peak positions and similar relative intensities of these patterns confirm that the materials are crystallographically identical at the atomic level.

The d-spacings of β-haematin formed in benzoic acid were compared with those of β-haematin prepared by other methods [28, 45]. As can be seen in Table 3.1 below, the d-spacings from the different methods are in good agreement with each other.

The 2θ values for β-haematin were extracted from a diffractogram in Figure 2 of Bohle *et al.* [32].

**Table 3.1** Comparison of d spacings of β-haematin prepared from different methods [28, 45]

| **Bohle *et al.*** [a] | | **This work** [b] | |
|---|---|---|---|
| 2θ values | d (Å) | 2θ values | d (Å) |
| 5.5 | 0.12 | 7.3 | 0.12 |
| 8.22 | 8.02 | 11.0 | 8.03 |
| 9.01 | 7.32 | 12.1 | 7.30 |
| 11.71 | 5.63 | 15.8 | 5.60 |
| 13.22 | 4.99 | 17.7 | 5.00 |
| 14.5 | 4.55 | 19.4 | 4.59 |
| 16.18 | 4.08 | 21.5 | 4.13 |
| 18.09 | 3.65 | 24.0 | 3.60 |

[a] Bohle *et al.* [32], λ = 1.1495 Å; [b] β-haematin prepared in benzoic acid in this study, λ = 1.5418 Å

### *3.1.3 Scanning electron microscopy*

Scanning electron microscopy was used to observe the external appearance of both the initial and the final product. The scanning electron micrographs of haematin and β-haematin are shown in Figure 3.3 below.

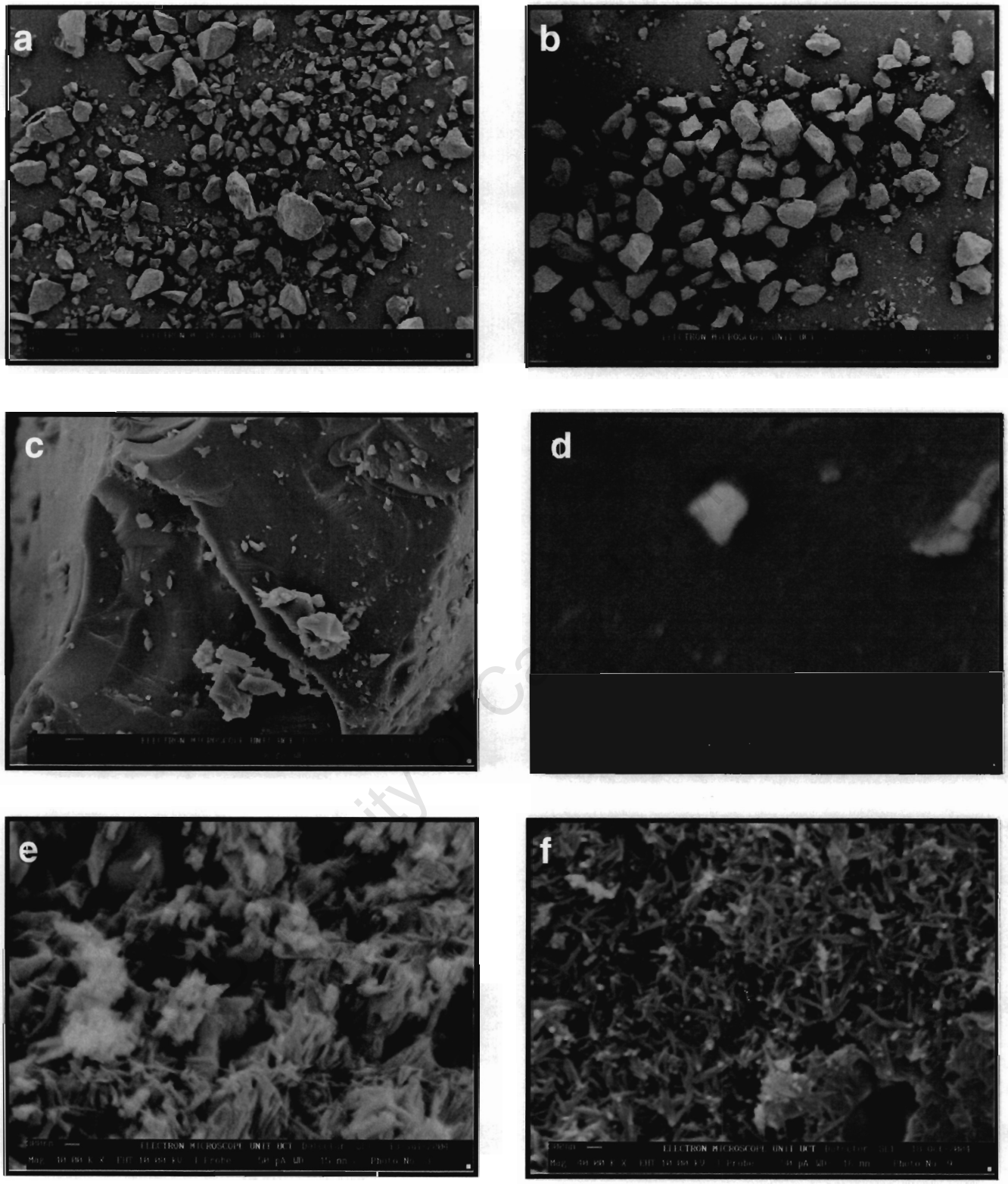


**Figure 3.3** Scanning electron micrographs of (**a**, **c**, and **d**) haematin, (**b** and **e**) β-haematin formed in 0.05 M benzoic acid and (**f**) β-haematin formed in 4.5 M acetic acid acid. (Scales: (a and b) 20:1, (c) 1 000:1, (d) 20 000:1, (e and f) 10 000:1 as shown).

At low magnification these materials appear to be similar (Figure 3.3a and b) but look quite different at higher magnification (Figure 3.3c and e) where there is a distinct difference in the morphology and the shape. At a magnification of 5 000 X (1 000 times as diplayed) (Figure 3.3c) haematin displays a smooth surface.

No crystals were visible even at a magnification of 100 000 X (20 000 times as shown) (Figure 3.3d) and this confirms that it is amorphous or consists of nanocrystals. The smallest resolvable feature in Figure 3.3d is 10 nm. Thus if any crystallites are present, they are considerably smaller than this and this is in agreement with a maximum possible size of 2 to 4.4 nm which was previously determined from XRD [30]. β-haematin crystals (Figure 3.3e) formed in benzoic acid resemble those of β-haematin formed in acetic acetic acid (Figure 3.3f). As noted before [30] the results above suggest that formation of β-haematin involves a change in phase from a non-crystalline or nanocrystalline haematin solid to a crystalline β-haematin solid.



## 3.2 COMPARISON OF KINETIC RESULTS OBTAINED USING A PYRIDINE ASSAY WITH THOSE USING AN IR ASSAY

The kinetics of β-haematin formation have previously been studied using infrared spectroscopy where the growth of the band at 1210 $cm^{-1}$ peak was monitored [30]. A different assay has been used to study the mechanism of formation of β-haematin in this work. The reaction was performed in 4.5 M acetic acid; pH 4.5 at 60°C. Under the same conditions, the rate of the reaction was monitored using the pyridine assay described in the introduction. This assay measures the amount of haematin

remaining in the reaction as the reaction progresses. Data from the earlier infrared study are also presented for comparison as percentage of β-haematin formed. For the purpose of comparison of the two assays, normalisation was carried out as follows: For data collected using the pyridine assay, the fraction of haematin remaining was calculated according to Equation 3.1 below.

$$A_{ft} = \frac{A_t - A_\infty}{A_0 - A_\infty} \qquad 3.1$$

Where $A_{ft}$ is the fraction of haematin remaining at time t,

$A_t$ is the absorbance of the pyridine complex formed with unreacted haematin,

$A_\infty$ is the absorbance at the end of the reaction,

$A_0$ is the absorbance at the beginning of the reaction.

For IR, data were extracted from Figure 6.4 of the PhD thesis of Mavuso [97] (a plot of % β-haematin formed as a function of time), and normalised using equation 3.2 below.

$$A_{ft} = 1 - \frac{\%\beta - haematin}{100} \qquad 3.2$$

The normalised data of the two assays were each fitted to the Avrami equation to obtain the rate constant *z* with the Avrami constant *n* fixed at 4 (Table 3.2).

**Table 3.2** Comparison of rate constants for formation of β-haematin using the pyridine and infrared assays. Rate constants (*z*) were obtained by non-linear least squares fitting of the data to the Avrami equation

| Assay method | *n* (fixed) | *z* ($min^{-4}$) |
|---|---|---|
| Pyridine | 4 | $2.3 \pm 0.1 \times 10^{-6}$ |
| Infrared | 4 | $1.8 \pm 0.2 \times 10^{-6}$ |

The two assays gave rate constants that are the same within experimental error. This result confirms the reliability of the new pyridine assay, demonstrating that results obtained are essentially the same as those using infrared monitoring. It is also clear in Figure 3.4 below that the data from the two assays are virtually identical, but with less data scatter from the pyridine assay.



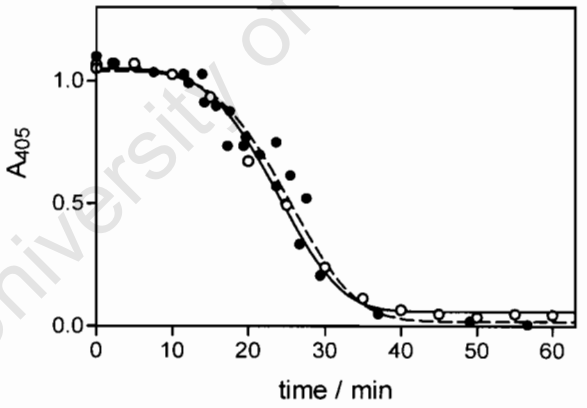


**Figure 3.4** Comparison of kinetic results for β-haematin formation in 4.5 M acetic acid, pH 4.5, 60°C, obtained using the pyridine and IR assays. Data collected using the pyridine assay are shown by open circles (○); data extracted from a plot of % β-haematin formed as a function of time using the IR assay are displayed as solid circles (●) [97]. Solid and dashed lines represent best fits to the Avrami equation with *n* = 4 for the pyridine and IR assays respectively.

## 3.3 FORMATION OF β-HAEMATIN IN BENZOIC ACID MEDIUM MONITERED BY X-RAY DIFFRACTION

The diffraction patterns of the wet product extracted from the reaction mixture at different time intervals are shown in Figure 3.5 below. The reaction was performed in 0.05 M benzoic acid, pH 4.5. Non-crystalline solids give diffraction patterns that consist of broad featureless humps [41]. Two broad humps were observed in the diffractogram of the sample collected at time 0 minutes where only amorphous haematin is present (Figure 3.5).

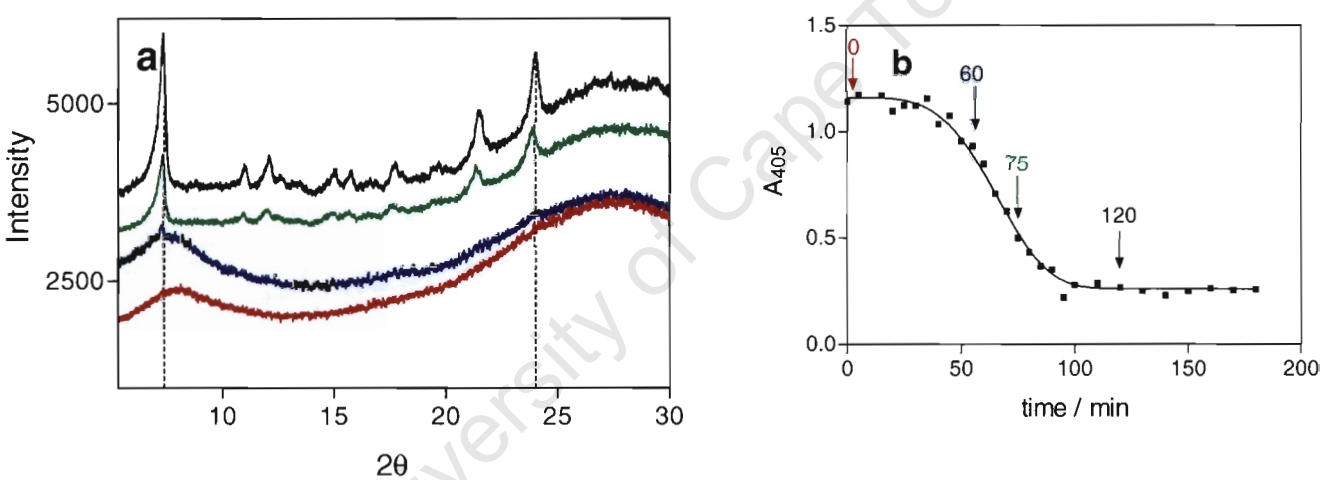


**Figure 3.5** (**a**) X-ray diffraction patterns of wet products at different time intervals, 0, 60, 75, and 120 minutes, from bottom to top. (**b**) Kinetics of β-haematin formation monitored using the pyridine assay. Time points indicated correspond to the time points at which the diffraction data in (a) were collected.

Only after an hour does the surface begin to change and the characteristic peaks of β-haematin start to appear. A major change occurs after 75 minutes where the entire characteristic pattern of the product can be seen. The positions of the strongest characteristic peaks (dotted lines on Figure 3.5a) do not occur at the same 2θ values as the two broad peaks of haematin. Therefore the total disappearance of the broad

peaks suggests that all the haematin is converted to β-haematin. (The broad peak at at $2\theta \sim 28°$ is due to water).

The observed diffraction pattern of the final product is identical to that obtained on the dry product of the reaction in 4.5 M acetic acid [30] and 0.05 M benzoic acid solutions, pH 4.5, except for the broad peaks at a $2\theta$ of approximately 28° which is due to the presence of water.

It has previously been noted [30] that the observation of the characteristic diffraction pattern for the wet product is definitive evidence that β-haematin forms during incubation and not during drying over $P_2O_5$ as suggested by other authors [65]. This study further shows that β-haematin forms during incubation since diffraction patterns were measured in wet β-haematin prior to drying.

It is possible to follow the kinetics of formation of β-haematin using X-ray diffraction, but this method is not practical for obtaining rate constants because it is too time consuming and makes use of too much material to obtain sufficient number of data points. For this reason the kinetics were followed using the pyridine assay. The observed time dependence observed with this method, as shown in Figure 3.5b above is in excellence qualitative agreement with the diffraction data.

## 3.4 FORMATION OF β-HAEMATIN IN BENZOIC ACID MEDIUM MONITERED BY THE PYRIDINE ASSAY

A sigmoidal curve similar to that reported by Dorn *et al.* [62] and Egan *et al.* [30] was observed when the data for formation of β-haematin formation at 60°C in 0.05 M benzoic acid, pH 4.5, with stirring collected. These data were fitted into the Avrami equation and the value of *n*, the Avrami constant, was found to be closest to 4. There is a very strong cross-correlation between *n* and *z* when performing non-linear least squares fitting, so when they are both allowed to refine freely the standard deviations of the rate constant is unacceptably large (Table 3.3). Fixing *n* however, results in values of *z* with acceptable standard deviations as shown in Table 3.3 below. The curves for five repeat reactions are shown below (Figure 3.6).



**Table 3.3** Rate constants (*z*) and Avrami constants (*n*) obtained by nonlinear least squares fitting of the data to the Avrami equation

| Data | *n* (fitted) | *z* ($min^{-n}$) (fitted) | *n* (fixed) | *z* ($min^{-n}$) (fixed) |
|---|---|---|---|---|
| a | $4.6 \pm 0.3$ | $(3.0 \pm 4.0) \times 10^{-9}$ | 4 | $(3.7 \pm 0.2) \times 10^{-8}$ |
| b | $5.6 \pm 0.7$ | $(5 \pm 10) \times 10^{-11}$ | 4 | $(4.5 \pm 0.4) \times 10^{-8}$ |
| c | $4.3 \pm 0.4$ | $(1 \pm 2) \times 10^{-8}$ | 4 | $(3.7 \pm 0.2 \times 10^{-8}$ |
| d | $3.6 \pm 0.2$ | $(18 \pm 20) \times 10^{-8}$ | 4 | $(3.0 \pm 0.2 \times 10^{-8}$ |
| e | $4.3 \pm 0.2$ | $(1.0 \pm 1.0) \times 10^{-8}$ | 4 | $(3.8 \pm 0.1) \times 10^{-8}$ |
| f | $4.2 \pm 0.2$ | $(2 \pm 2) \times 10^{-8}$ | 4 | $(3.9 \pm 0.1) \times 10^{-8}$ |

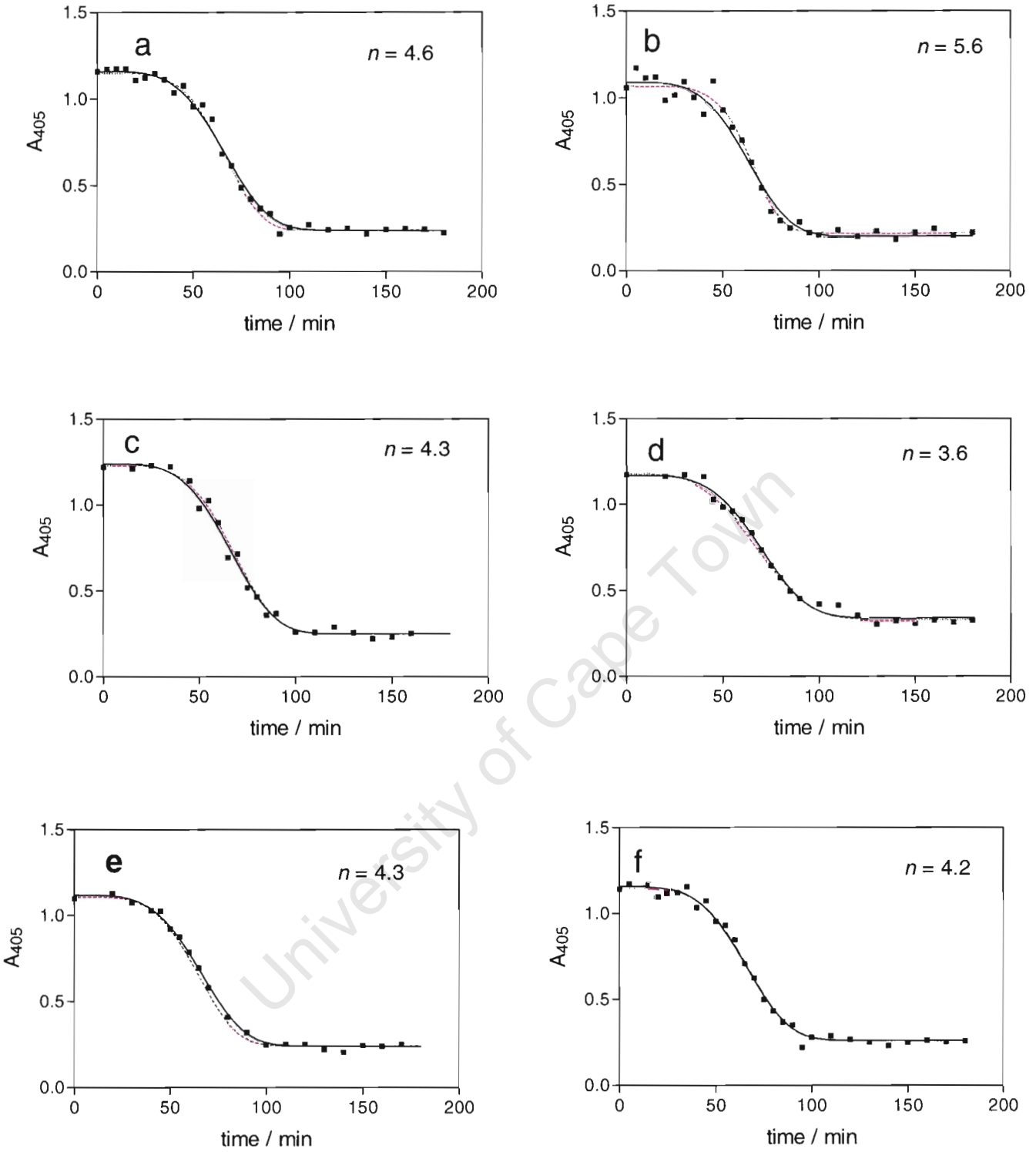




**Figure 3.6** Plots comparing fits with different values of *n*. Black solid lines represent a fit where n is fixed at 4 and dashed pink lines represent best fit values of *n* as specified on the graphs and shown in Table 3.3, **a-e** correspond to individual reactions and **f** is the average of the five reactions.

In cases where the value of *n* was greater than 4, it was fixed to 4 since theoretically the value of *n* cannot be greater than 4 (see introductory chapter). These were assumed to be due to errors in the experimental data (Figure 3.4a). The value of *n* obtained from the average data for reactions a-e is 4.2 and closest to 4. It is clear from Figure 3.4 that when the data are fitted to the Avrami equation with $n = 4$, there are only very subtle differences from those where *n* is allowed to refine freely. The plots a-f in Figure 3.4 illustrate that the integer value of *n* that best fits the data is 4. Therefore for all subsequent cases where *n* was close to or greater than 4 it was fixed at 4.

## 3.5 COMPARISON OF BENZOIC ACID WITH ACETIC ACID

To compare the rate of formation of β-haematin in benzoic acid with that in acetic acid, reactions were carried out in 4.5 M acetic acid and 0.05 M benzoic acid at the same temperature, pH and stirring rate. Although the concentration of acetic acid is ninety times larger than that of benzoic acid, the rate of formation of β-haematin in benzoic acid is a factor of sixty faster (Table 3.2, Figure 3.7).



**Table 3.2** Comparison of rate constants for formation of β-haematin in acetic acid and benzoic acid

| | Concentration (M) | n (fixed) | z ($min^{-4}$) |
|---|---|---|---|
| benzoic acid | 0.05 | 4 | $3.9 \pm 0.1 \times 10^{-8}$ |
| acetic acid | 4.5 | 4 | $2.3 \pm 0.1 \times 10^{-6}$ |

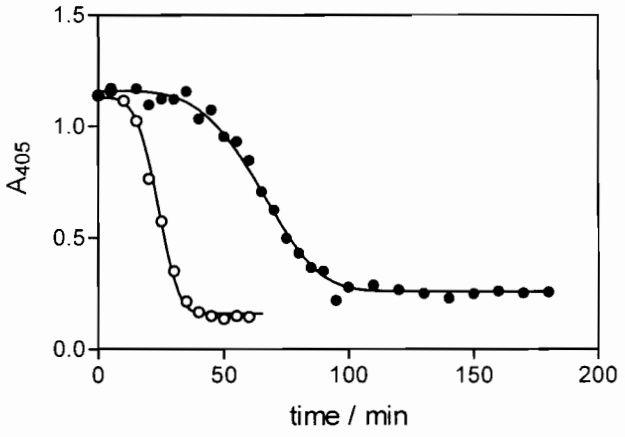


**Figure 3.7** Comparison of benzoic acid and acetic acid. The symbols (○) and (●) represent the data collected from the reaction in acetic acid (4.5 M) and benzoic acid (0.05 M) respectively, pH 4.5, 60°C. Solid lines are best fit of the data to the Avrami equation, with $n$ = 4.



## 3.6 CONCLUSIONS

Infrared spectra, scanning electron microscopy and X-ray diffraction unequivocally demonstrate that the product formed in benzoic acid is β-haematin. The reaction is easy to follow using the pyridine assay and it gives results essentially identical to those found using infrared spectroscopy to monitor the reaction. As in acetic acid the process of β-haematin formation appears to occur by rapid precipitation of non-crystalline haematin and slow conversion to the crystalline product. It is not clear what the role of the acid is during the conversion of haematin to β-haematin. Data collected gave excellent fits to the Avrami equation with $n$ = 4. In terms of the Avrami model, this means that nucleation sites appear continuously throughout the reaction, and crystal growth from these sites is spherical (three-dimensional). The time dependence of the changes in the diffraction pattern is in excellent agreement with

the pyridine assay observations. β-haematin forms in only a fourfold longer time in benzoic acid compared to acetic acid despite the concentration being ninety times lower than the acetic acid concentration.

# 4. KINETICS OF β-HAEMATIN FORMATION IN BENZOIC ACID

Having confirmed that the material formed in benzoic acid is indeed β-haematin, and that the pyridine assay gives essentially identical results to those obtained by infrared spectroscopy, detailed kinetic studies were carried out. These are concerned with the rates of formation of β-haematin, the factors that influence these rates and their interpretation in terms of chemical changes taking place in known intervals of time i.e., the detailed way in which haematin and β-haematin behave during a reaction. The factors that might be important for the formation of β-haematin are temperature, stirring rate, pH, concentration of benzoic acid and seeding of the reaction with preformed β-haematin. The results are presented and discussed below. All data represent an average of two or more reactions, solid lines represent a fit to the Avrami equation with $n = 4$.



## 4.1 EFFECT OF STIRRING

As shown in Table 4.1 and Figure 4.1, whether the reaction is carried out stirred or unstirred has no significant effect on the rate of formation of β-haematin. This makes it relatively easy to obtain reproducible results, as stirring rate is difficult to control.

**Table 4.1** Effect of stirring on the rate constants for the formation of β-haematin in 0.05 M benzoic acid, pH 4.5 and 60°C

| | *n* (fixed) | *z* ($min^{-4}$) |
|---|---|---|
| Stirring | 4 | $3.9 \pm 0.1 \times 10^{-8}$ |
| No stirring | 4 | $3.6 \pm 0.1 \times 10^{-8}$ |

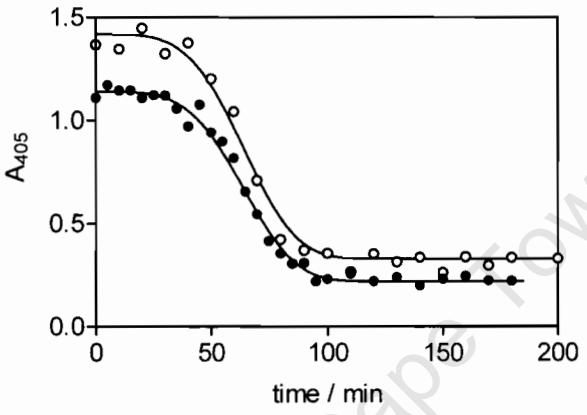


**Figure 4.1** Effect of stirring. The filled circles (●) represent a reaction carried out with stirring, and open circles (○) represent a reaction carried out without stirring. The solid lines represent best fits to the Avrami equation with $n = 4$.



This result is surprising as it was not the case when the reaction was performed in acetic acid. Here both the reaction rate constant and the value of *n* were affected when the reaction was carried out unstirred [30]. The lack of sensitivity to stirring is not an artefact of the pyridine assay, because when the kinetics were followed using the pyridine assay, in 4.5 M acetic acid, pH 4.5 at 60°C, sensitivity to stirring was confirmed (Table 4.2, Figure 4.2).

It is very clear in the case of acetic acid that that the data collected using the pyridine assay does not fit to $n = 4$ but fits well to $n = 2$ (Figure 4.2), and the rate constant obtained is similar to that reported using the IR assay (Table 4.2) in an unstirred reaction. This result also further confirms the validity of this new pyridine assay in monitoring these reactions.

**Table 4.2** Effect of no stirring on the rate constants and Avrami constants for the formation of β-haematin in 4.5 M acetic acid, pH 4.5 and 60°C

| | *n* (fixed) | *z* ($min^{-4}$) | *z* ($min^{-4}$) (infrared data)[a] |
|---|---|---|---|
| Normal stirring | 4 | $2.3 \pm 0.1 \times 10^{-6}$ | $1.2 \pm 0.1 \times 10^{-6}$ |
| No stirring | 2 | $7.3 \pm 0.7 \times 10^{-4}$ | $1.7 \pm 0.2 \times 10^{-4}$ |

[a] data reported in Table 1 by Egan *et. al.* [30]

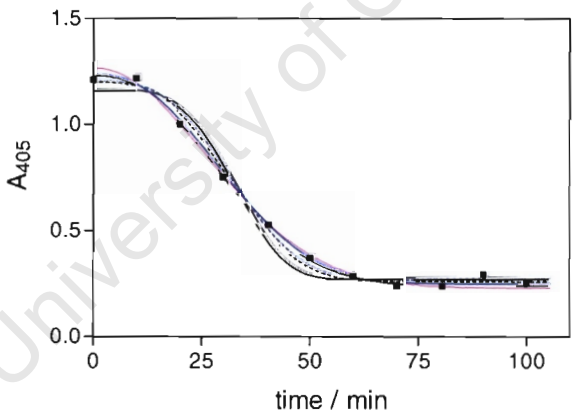


**Figure 4.2.** Effect of not stirring on β-haematin formation in acetic acid, monitored using the pyridine assay. The pink and blue solid lines are for $n = 2$ and $n = 2.3$ respectively, black solid line is for $n = 4$ and the black dotted line is for $n = 3$.

Surprisingly, when the reaction was carried out at a faster than usual stirring rate in benzoic acid solution, there was a deviation from the Avrami equation (Figure 4.3a and b). This was interpreted as evidence that vigorous stirring disrupts the initial

nucleation of β-haematin prolonging the induction time. This causes the formation of β-haematin to follow the Gompertz equation [1] (Equation 4.1) instead of the Avrami equation.

$$A_t = A_i - (A_i - A_f)\exp\left[-\exp\left\{\left(\frac{\mu e}{A_i - A_f}\right)(\lambda - t) + 1\right\}\right] \qquad 4.1$$

The Gompertz equation, a purely empirical, with no theoretical content was first proposed in 1825 [98]. The growth of most human populations [99], some human tumours [100], visceral organs [101] etc. are well described by this equation.

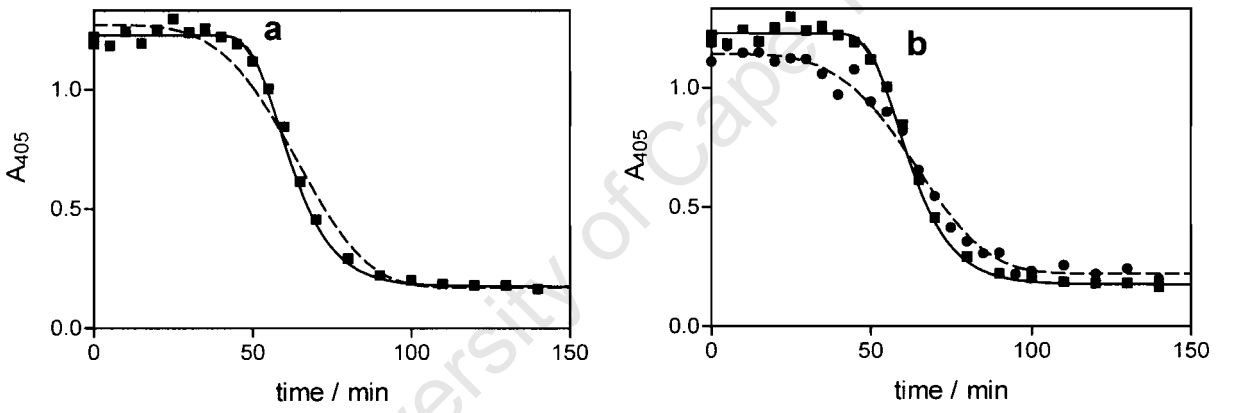


**Figure 4.3** Plots showing the effect of stirring at a faster than usual stirring rate on formation of β-haematin in 0.05 M benzoic acid, pH 4.5. (**a**) (■) Data collected at a vigorous stirring rate, (**b**) (●) data collected at normal stirring rate fitted to the Avrami equation $n$ = 4. Solid lines and dashed lines represent fits to the Gompertz and Avrami equation respectively.

As shown in Figure 4.3, at the early stage of the reaction where $t << \lambda$, we have

$$\left\{\left(\frac{\mu e}{A_i - A_f}\right)(\lambda - t) + 1\right\} \approx \left\{\left(\frac{\mu e}{A_i - A_f}\right)\lambda + 1\right\} = const$$

$$\therefore A_t \approx A_i - (A_i - A_f)\exp\left[-\exp\{const\}\right] = A_i - (A_i - A_f)\cdot c$$

So $A_t \approx (1-c)A_i + cA_f$

Here $c$ is a constant and must necessarily be << 1, since $A_t = A_i$ when t = 0. This means that $A_t$ remains essentially equal to $A_i$ as long as $t << \lambda$, and this corresponds to the induction phase. Once $t >> \lambda$, then $\lambda - t \approx -t$ and

$$\exp\left\{\left(\frac{\mu e}{A_0 - A_f}\right)(\lambda - t) + 1\right\} \approx \exp\left\{-\left(\frac{\mu e}{A_0 - A_f}\right) \times t\right\}$$

corresponding to an exponentially decreasing function. Thus, the term in square brackets will become more negative, initially very quickly and then more slowly (i.e. exponentially). Consequently, the outer exponential will decrease exponentially, but very rapidly at first and then much more slowly later on. When $t \rightarrow \infty$, the overall exponential term $\rightarrow$ 0 and as exp(-0) = exp(0) = 1, we have

$$A_t \rightarrow A_i - (A_i - A_f) = A_f$$

This describes a function which begins at $A_i$, shows no significant change for a period of time and then decreases very rapidly at first, but then more gradually (the curvature being much greater than an exponential function) and finally levelling off towards $A_f$.

If the data is forced to fit the Avrami equation, the fit is obviously unsatisfactory (Figure 4.3a), but gives the same rate constant as that for normal stirring (Table 4.3).

**Table 4.3** Effect of vigorous stirring on the rate of formation of β-haematin in 0.05 M benzoic acid, pH 4.5 and 60°C

| | *n* (fixed) | *z* ($min^{-4}$) |
|---|---|---|
| Normal stirring | 4 | $3.9 \pm 0.1 \times 10^{-8}$ |
| Vigorous stirring | 4 | $4.3 \pm 0.4 \times 10^{-8}$ |

Information obtained from the Gompertz equation is the rate constant μ and the induction time I. The rate constant was found to be 0.04 ± 0.002 and induction time was 49.3 ± 0.6. Unfortunately, as the Gompertz equation is purely empirical it provides little information about the mechanism of formation of β-haematin.

The destruction of crystal nuclei by collision has been reported in other studies to produce fragments that are too small to permit crystal nucleation and therefore slows down crystal formation [102]. This suggests that fewer but bigger crystals may be formed under these conditions. This was confirmed by comparing crystals obtained from normal stirring and vigorous stirring rate using SEM (Figure 4.4). The crystals from vigorous stirring (Figure 4.4b-d) appear to be slightly bigger than those obtained with normal stirring (Figure 4.4a).

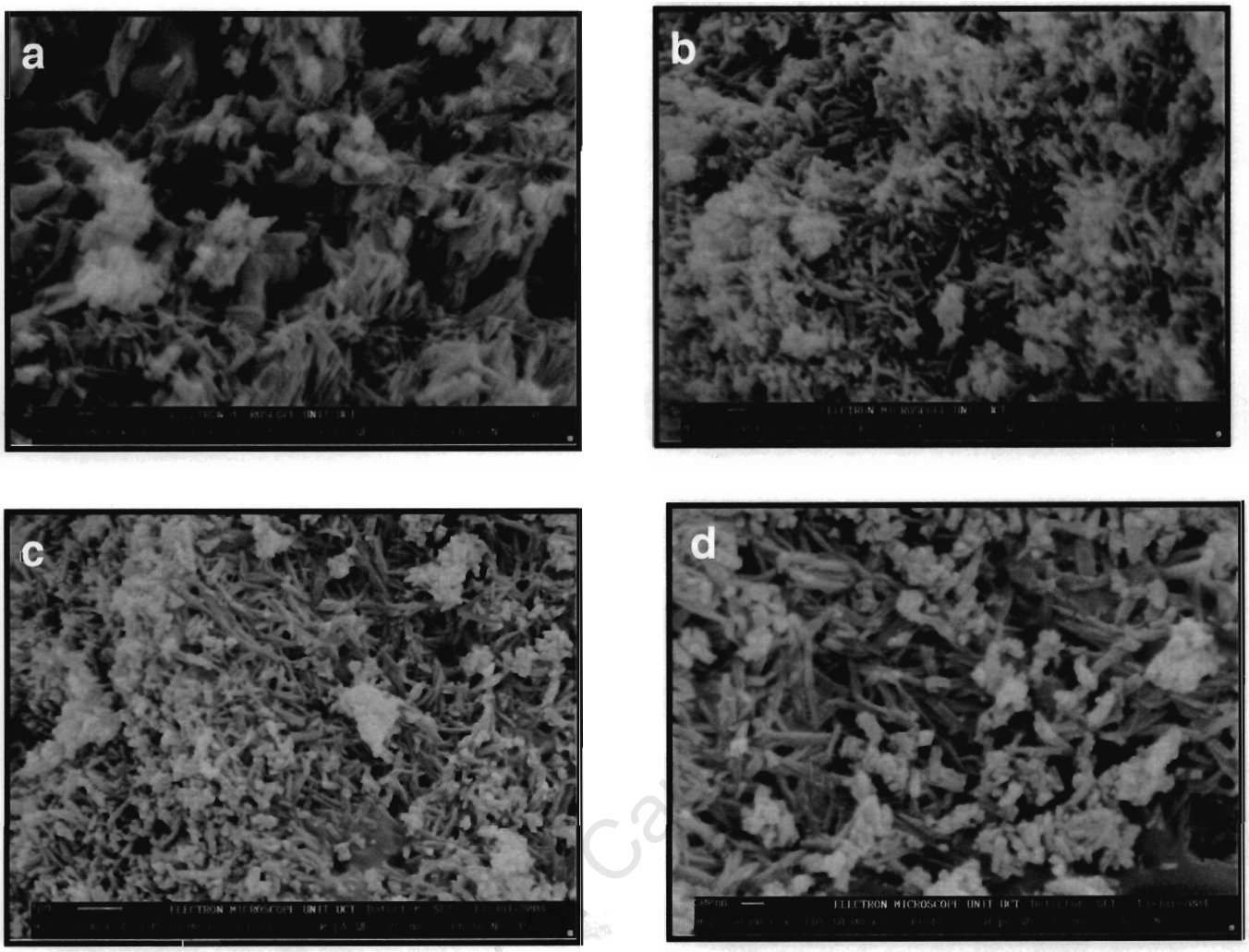


**Figure 4.4** Scanning electron micrograph of β-haematin obtained from a reaction in 0.05 M benzoic acid, pH 4.5 and 60°C (**a**) with stirring and (**b**, **c**, **d**) vigorous stirring rate. (Scale: (a, b and d) 10 000:1, (c) 6 000:1 as shown).

## 4.2 EFFECT OF TEMPERATURE

As expected, the reaction takes a longer time to reach completion at lower temperatures and is faster at higher temperatures. At temperatures ranging from 37 - 70°C the Avrami constant is 4 (Figure 4.5 and Table 4.4).

**Table 4.4** Effect of temperature on the rate of formation of β-haematin in 0.05 M benzoic acid, pH 4.5.

| Temperature (°C) | *n* (fixed) | *z* ($min^{-4}$) |
|---|---|---|
| 37 | 4 | $(5.1. \pm 0.3) \times 10^{-12}$ |
| 55 | 4 | $(1.2 \pm 0.1) \times 10^{-8}$ |
| 60 | 4 | $(3.9 \pm 0.1) \times 10^{-8}$ |
| 65 | 4 | $(1.5 \pm 0.1) \times 10^{-7}$ |
| 70 | 4 | $(2.0 \pm 0.1) \times 10^{-6}$ |



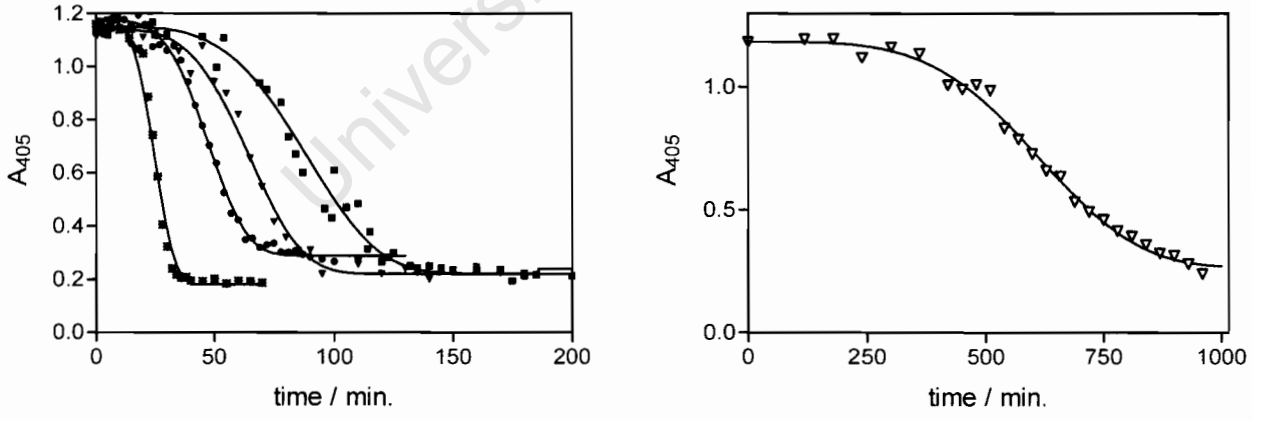


**Figure 4.5** Effect of temperature on the formation of β-haematin in 0.05 M benzoic acid, pH 4.5 at (▽) 37, (■) 55, (▼) 60, (●), 65, and (⋆) 70 °C. Solid lines represent best fits of the data to the Avrami equation with *n* = 4.

Rate constants obtained from the temperature study conform to the Arrhenius equation (Figure 4.6). An activation energy of 334 ± 17 kJ/mol was obtained from the Arrhenius plot in Figure 4.6, very close to the 331 ± 13 kJ/mol obtained when the temperature study was carried out in acetic acid [30].

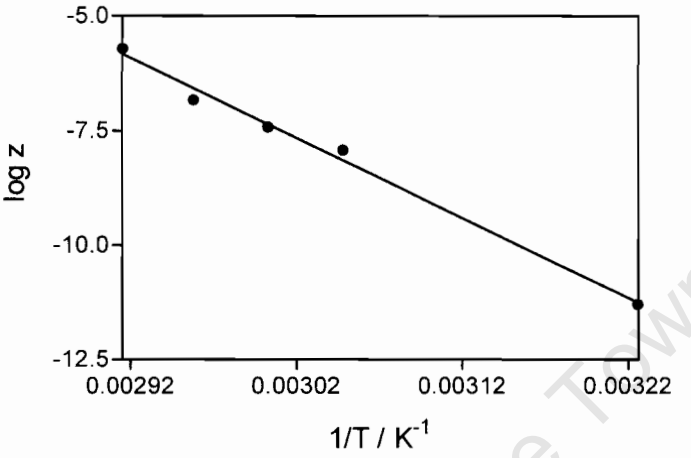


**Figure 4.6** Arrhenius plot for β-haematin formation in 0.05 M benzoic acid, pH 4.5.



These values seem rather too high. Activation energies of this magnitude have been reported for the diffusion of cobalt ions in the silicates as follows: basalt (220 kJ/mol) and andesite (280 kJ/mol) [103]. The viscosity of silicate melts is also strongly dependent on temperature and reflects an increase in activation energy which increases with silica content in the order: basalt (230 kJ/mol), rhyolite (350 kJ/mol), silica (500 kJ/mol) [104]. The crystallization of Corning 9608, a glass ceramic generally used as a cookware also has a high activation energy of 369.13 kJ/mol [105]. It seems unrealistic that formation of β-haematin can require the same activation energy as these processes. It has been reported that the activation energy calculated from the rate constants obtained from the Avrami equation are only physically meaningful if the rate constant is expressed as a $4^{th}$ root for $n = 4$, in order

to have a unit of time$^{-1}$ [106]. The activation energy obtained this way is 84 ± 4 kJ/mol, a far more reasonable value.

## 4.3 EFFECT OF BENZOIC ACID CONCENTRATION

On increasing the concentration of benzoic acid from 0.01 M to 0.05 M, there is an increase on the rate of formation of β-haematin and a decrease in the induction time. Data collected conform to $n$ = 4 when fitted to the Avrami equation. The rate constants (Table 4.5) obtained by fitting the data in Figure 4.7 to the Avrami equation with $n$ = 4 show that there is a linear dependence of rate constant on concentration (Figure 4.8).

**Table 4.5** Effect of concentration of benzoic acid pH 4.5 on the rate constant for formation of β-haematin at 60°C

| Concentration (M) | $n$ (fixed) | $z$ (min$^{-4}$) |
|---|---|---|
| 0.01 | 4 | $(1.1 \pm 0.1) \times 10^{-9}$ |
| 0.02 | 4 | $(8.0 \pm 1) \times 10^{-9}$ |
| 0.03 | 4 | $(1.6 \pm 0.1) \times 10^{-8}$ |
| 0.04 | 4 | $(2.8 \pm 0.1) \times 10^{-8}$ |
| 0.05 | 4 | $(3.9 \pm 0.1) \times 10^{-8}$ |

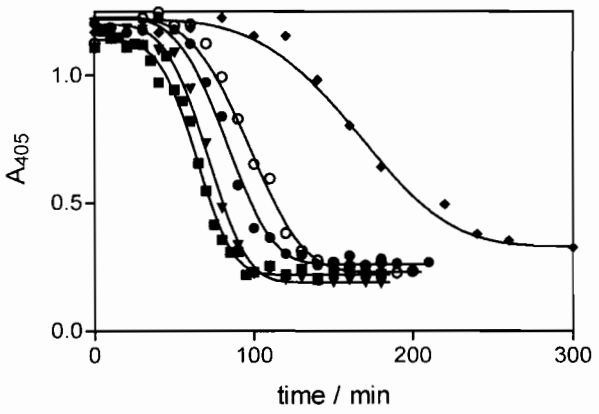


**Figure 4.7.** Effect of benzoic acid concentration on the formation of β-haematin at 60°C and pH 4.5 in (◆) 0.01, (○) 0.02, (●) 0.03, (▼) 0.04, (■) 0.05 M benzoic acid. Solid lines represent best fits of the data to the Avrami equation with $n = 4$.

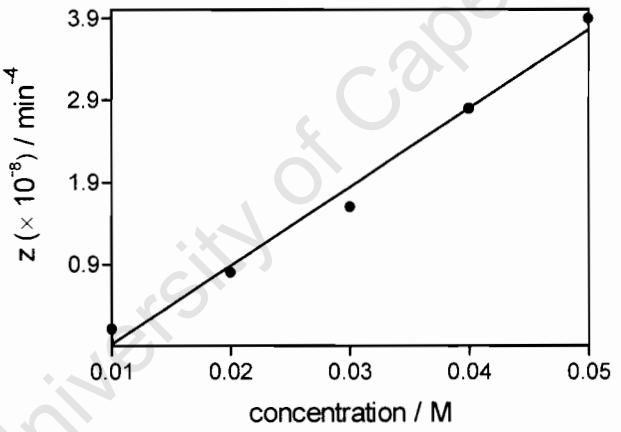




**Figure 4.8** Linear dependence of rate constant $z$ for formation of β-haematin on benzoic acid concentration.

A possible explanation is that at higher concentrations of benzoic acid, more haematin is solubilised and therefore there is a higher steady-state concentration available to precipitate as β-haematin. In acetic acid, an increase in concentration also brought an increase on the rate of formation of β-haematin but with a change in

the value of *n* [30], which made it difficult to determine the dependence of *z* on acetic acid concentration.

## 4.4 EFFECT OF SEEDING

Under the conditions used in this study, seeding with 10% preformed β-haematin does not have an effect on the rate of formation of β-haematin (Table 4.6, Figure 4.9).



**Table 4.6** Effect of seeding the reaction with 10% preformed β-haematin on the rate of formation of β-haematin in 0.05 M acetic acid, pH 4.5 and 60°C

| | *n* (fixed) | z ($min^{-4}$) |
|---|---|---|
| Unseeded | 4 | $3.9 \pm 0.1 \times 10^{-8}$ |
| 10% seeding | 4 | $4.2 \pm 0.4 \times 10^{-8}$ |

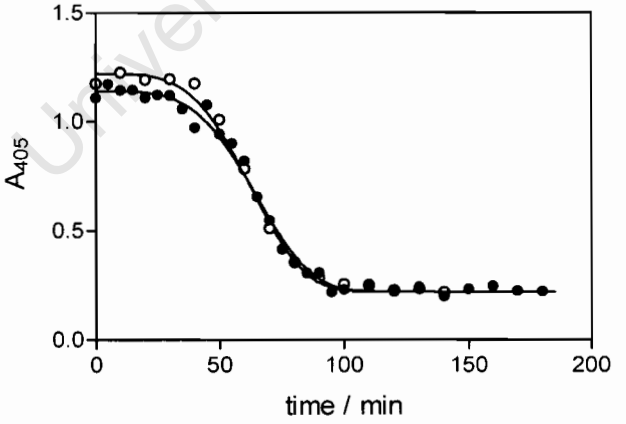


**Figure 4.9** Lack of effect of seeding on the rate of formation of β-haematin in 0.05 M benzoic acid at 60°C and pH 4.5. The filled circles (●) represent a reaction carried out unseeded, and open circles (○) represent a reaction carried out seeded with 10% preformed β-haematin. The solid lines represent a fit to the Avrami equation with *n* = 4.

This agrees with the reported observation in acetic acid, where the kinetics were studied using IR [30] and Mössbauer [44] spectroscopy and in turn contrasts with the suggestion that β-haematin autocatalyzes its own formation and acts as a nucleation site for rapid growth of β-haematin [58, 61].

## 4.5 EFFECT OF pH

The rate constants from the pH study (Table 4.7) for formation of β-haematin in benzoic acid display a pH optimum (Figure 4.10).

**Table 4.7** Effect of pH of benzoic acid (0.05 M) on the rate constant for formation of β-haematin at 60°C

| pH | *n* (fixed) | *z* ($min^{-4}$) |
|---|---|---|
| 2.5 | 4 | $(5.9 \pm 1.3) \times 10^{-8}$ |
| 3.0 | 4 | $(7.1 \pm 1.1) \times 10^{-7}$ |
| 3.5 | 4 | $(1.1 \pm 0.5) \times 10^{-6}$ |
| 4.0 | 4 | $(3.5 \pm 1.0) \times 10^{-7}$ |
| 4.5 | 4 | $(3.9 \pm 0.1) \times 10^{-8}$ |
| 5.0 | 4 | $(1.0 \pm 0.5) \times 10^{-8}$ |

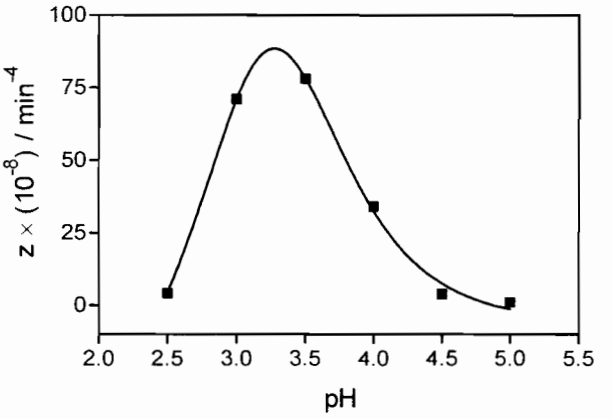


**Figure 4.10** Dependence of rate constant of formation of β-haematin at 60°C in 0.05 M benzoic acid on the pH in the range 2.5–5. The solid line is a fit obtained from an equation that describes two protonation equilibria and assumes that only the monoprotonated species reacts at an appreciable rate, where the fraction of mono-protonated species is given by: $1/\{(K_{a2}/[H^+]) + ([H^+]/K_{a1}) + 1)\}$. The $pK_{a1}$ and $pK_{a2}$ values obtained from the above fit are 3.4 ± 0.9 and 3.0 ± 0.8 respectively.

The pH optimum probably arises from the effect of differing states of protonation of the propionate side-chains Figure 4.11.

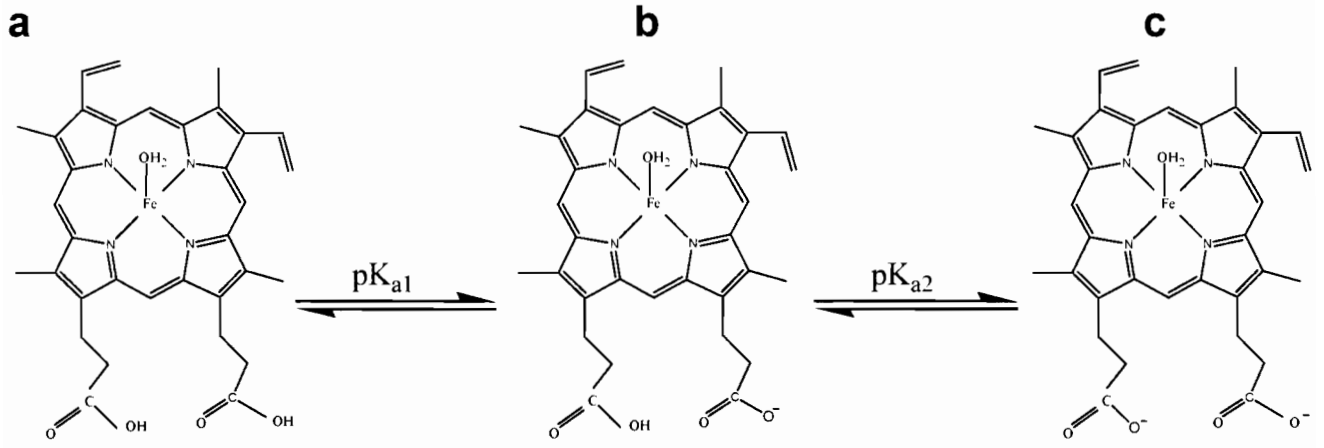


**Figure 4.11.** Different protonation states of haematin propionic acid groups, (**a**) diprotonated, (**b**) monoprotonated and (**c**) deprotonated.

In order for β-haematin to form one of the deprotonated carboxylate groups must be available for coordination to the Fe(III) center of the second haematin molecule and the protonated carboxylate group must be available for intermolecular H-bonding between the two dimers. This corresponds to species b in Figure 4.11.

At pH values below the optimum pH of 3.3, where the diprotonated species of haematin (Figure 4.11a) is likely to predominate, the reaction becomes slower with decreasing pH. The reaction also becomes slower with increasing pH values higher than 3.3 where the unprotonated species of haematin (Figure 4.11b) probably starts to dominate.

The pH profile shown in Figure 4.10 is similar to one that was obtained when the reaction was carried out in 4.5 M acetic acid at 60°C [30]. A study of the dependence of yield of β-haematin in acetic acid medium as a function of pH also illustrated that

there is maximal yield at a pH of around 3.5 [82]. The pH profile of haematin dimerization induced by haemozoin and an acetonitrile extract of trophozoite lysate have a pH optimum of 4-5 [62], slightly higher than what was found in acetic and benzoic acid. A higher pH optimum was also observed when the reaction was carried out in mono-oleoylglycerol in citrate/phosphate buffered medium [63]. This change in the value of the pH optimum suggests that the $pK_a$ values of the propionate groups of haematin are dependent on the medium in which the reaction is carried out.

It must also be recognised that the thermodynamic stability of the β-haematin product is also likely to influence these $pK_a$ values, so the $pK_a$s obtained from kinetic studies of β-haematin formation may not be the same as those of free haematin.



## 4.6 CONCLUSIONS

It is possible to study the kinetics of β-haematin formation in conditions milder than those of 4.5 M acetic acid using benzoic acid (0.05 M) and the data collected using the pyridine assay gave excellent fits to the Avrami equation. The observed Arrhenius behaviour and linear dependence on concentration makes it possible to predict the rate at any given temperature and concentration. Seeding has negligible effects, as was observed in acetic acid. There is also no change in the rate and induction time when the reaction is carried out unstirred. Vigorous stirring appears to disrupt nucleation and causes the formation of β-haematin to follow the Gompertz equation instead of the Avrami equation and gives rise to slightly bigger crystals. When the rates were fitted to an equilibrium equation that describes two protonation equilibria and assumes that only the monoprotonated species reacts at an

appreciable rate, a good fit was obtained to the observed pH dependence of the reaction with an optimum at around 3.3. In all these respects, the kinetics of β-haematin formation in benzoic acid closely resembles those in acetic acid. The only major difference is that far lower concentrations of benzoic acid are required and that stirring rate has no effect on the reaction rate, except at high stirring rates where nucleation appears to be disrupted.

# 5. KINETICS OF β-HAEMATIN FORMATION IN THE PRESENCE OF SUBSTITUTED BENZOIC ACIDS

## 5.1 EFFECT OF TEMPERATURE AND CONCENTRATION ON THE FORMATION OF β-HAEMATIN IN 4-NITROBENZOIC ACID

### *5.1.1 Effect of temperature*

The effect of temperature on the formation of β-haematin was also studied in 0.02 M 4-nitrobenzoic acid, pH 4.5. The rate constants are shown in Table 5.1 below.

**Table 5.1** Effect of temperature on the rate constant for formation of β-haematin in 0.02 M 4-nitrobenzoic acid, pH 4.5

| Temperature (°C) | *n* (fixed) | *z* ($min^{-4}$) |
|---|---|---|
| 37 | 4 | $(3.8 \pm 0.2) \times 10^{-12}$ |
| 50 | 4 | $(1.6 \pm 0.2) \times 10^{-9}$ |
| 55 | 4 | $(1.6 \pm 0.2) \times 10^{-8}$ |
| 60 | 4 | $(1.3 \pm 0.1) \times 10^{-7}$ |
| 65 | 4 | $(1.1 \pm 0.1) \times 10^{-6}$ |

There is an increase in the induction time and growth rate with a decrease in temperature from 65 to 37 °C (Figure 5.1), as observed in acetic acid and benzoic acid.

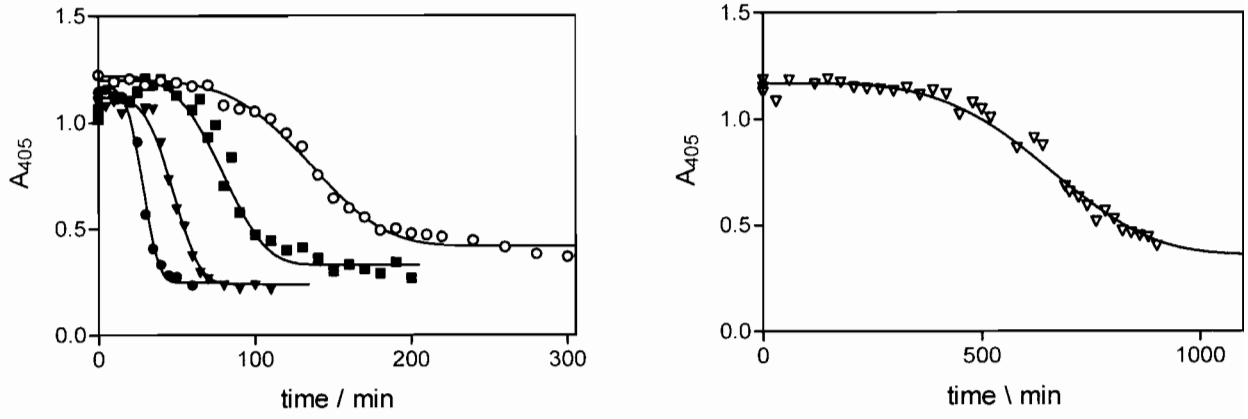


**Figure 5.1** Effect of temperature on the formation of β-haematin in 0.02 M 4-nitrobenzoic acid, pH 4.5 at (▽) 37, (○) 50, (■) 55, (▼) 60, and (●), 65 °C. Solid lines represent best fits of the data to the Avrami equation with $n = 4$.

The reaction exhibits Arrhenius behaviour (Figure 5.2) and this is further confirmation of the validity of the rate constants obtained from reactions performed in acetic [30] and benzoic acids. An activation energy of 98 ± 1 kJ/mol was obtained (value obtained as explained in 4.2 above) and it is similar to that obtained from studies in acetic [30] and benzoic acid.

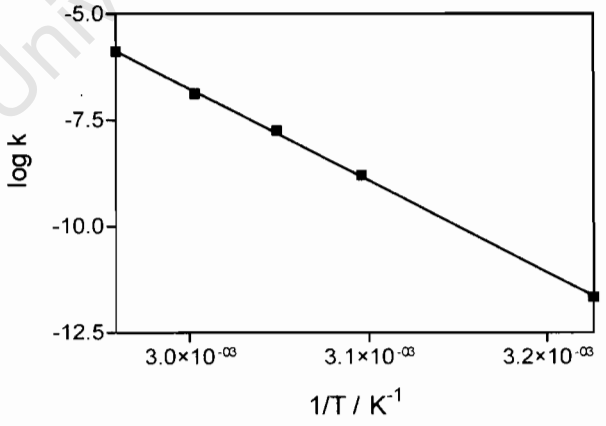


**Figure 5.2** Arrhenius plot for β-haematin formation in 4-nitrobenzoic acid.

## 5.1.2 Effect of 4-nitrobenzoic acid concentration

The effect of concentration of 4-nitrobenzoic acid on the rate of formation of β-haematin was studied at concentrations shown in Table 5.2.

**Table 5.2** Effect of concentration of 4-nitrobenzoic acid on the rate of formation of β-haematin at 60°C, pH 4.5

| Concentration (M) | *n* (fixed) | *z* ($min^{-4}$) |
|---|---|---|
| 0.005 | 4 | $(1.6 \pm 0.1) \times 10^{-9}$ |
| 0.010 | 4 | $(3.6 \pm 0.3) \times 10^{-8}$ |
| 0.015 | 4 | $(7.6 \pm 0.1) \times 10^{-8}$ |
| 0.018 | 4 | $(10.4 \pm 0.8) \times 10^{-8}$ |
| 0.020 | 4 | $(13.3 \pm 0.7) \times 10^{-8}$ |

Similar behaviour to that in benzoic acid, at these low concentrations of 4-nitrobenzoic acid was observed (Figure 5.3).

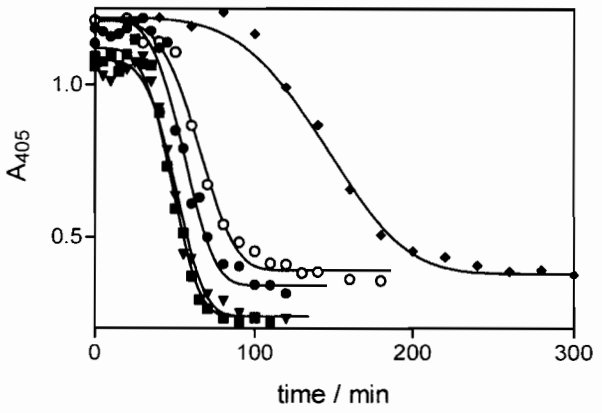


**Figure 5.3.** Effect of 4-nitrobenzoic acid concentration on the formation of β-haematin at 60°C and pH 4.5 in (◆) 0.005, (○) 0.010, (●) 0.015, (▼) 0.018, (■) 0.020 M 4-nitrobenzoic acid. Solid lines represent best fits of the data to the Avrami equation with $n$ = 4.

The value of $n$ is not affected by the change in concentration and there is a linear dependence of the rate constant on concentration (Figure 5.4). Higher concentrations were not accessible due to poor solubility of 4-nitrobenzoic acid.



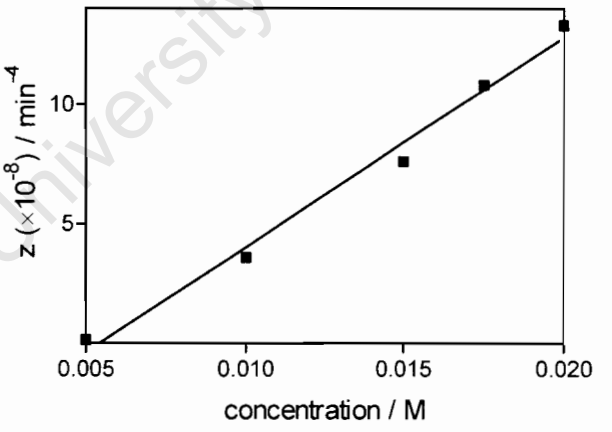


**Figure 5.4** Linear dependence of rate constant (z) for formation of β-haematin on 4-nitrobenzoic acid concentration.

## 5.2 EFFECT OF pH ON THE FORMATION OF β-HAEMATIN IN 4-AMINOBENZOIC ACID AND 4-CYANOBENZOIC ACID

The effect of pH on the rates of reaction in 4-aminobenzoic acid and 4-cyanobenzoic acid was determined. As in benzoic and acetic acid [30], optimum values are observed. There is no notable shift in the pH optimum (Table 5.3, Figure 5.5). It was not possible to compare the *z* values of the pH optima of these acids directly because of poor solubility of 4-cyanobenzoic acid and slow kinetics in 4-aminobenzoic acid. The pH study for 4-aminobenzoic acid was performed in 0.04 M, while for 4-cyanobenzoic acid 0.007 M acid was used.

**Table 5.3** Effect of pH on the rate constants for formation of β-haematin obtained by performing reactions in 4-aminobenzoic acid (0.04 M) and 4-cyanobenzoic acid (0.007 M)

| **4-Aminobenzoic acid** | | | **4-Cyanobenzoic acid** | | |
|---|---|---|---|---|---|
| pH | *n* (fixed) | *z* ($min^{-4}$) | pH | *n* (fixed) | *z* ($min^{-4}$) |
| 3.4 | 4 | $(1.7 \pm 0.3) \times 10^{-10}$ | 2.5 | 4 | $(3.0 \pm 0.4) \times 10^{-11}$ |
| 3.6 | 4 | $(1.3 \pm 0.1) \times 10^{-10}$ | 3.0 | 4 | $(8.0 \pm 0.5) \times 10^{-10}$ |
| 4.0 | 4 | $(2.4 \pm 0.1) \times 10^{-9}$ | 3.5 | 4 | $(2.0 \pm 0.3) \times 10^{-9}$ |
| 4.5 | 4 | $(3.5 \pm 0.8) \times 10^{-9}$ | 4.0 | 4 | $(3.9 \pm 0.2) \times 10^{-9}$ |
| 5.0 | 4 | $(7.9 \pm 0.3) \times 10^{-10}$ | 4.3 | 4 | $(1.2 \pm 0.09) \times 10^{-9}$ |
| 5.5 | 4 | $(5.1 \pm 1.0) \times 10^{-11}$ | 4.5 | 4 | $(7.0 \pm 0.4) \times 10^{-10}$ |

The plots of rate constants against pH clearly indicate a bell shaped curve (Figure 5.5) consistent with what was found when the study was done in benzoic acid and what has been previously reported for acetic acid [30].

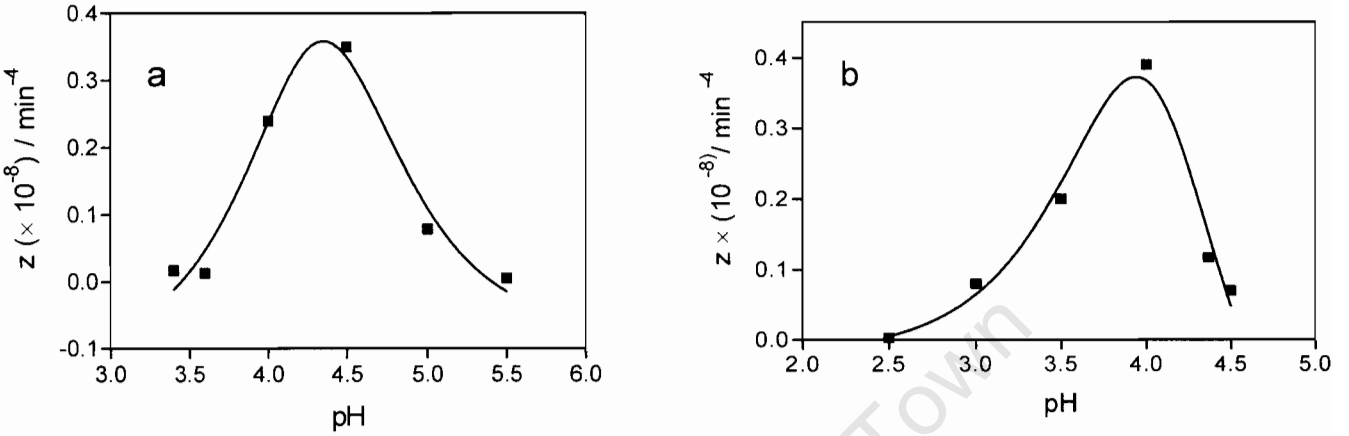


**Figure 5.5** Effect of pH of 4-aminobenzoic acid (**a**) and 4-cyanobenzoic acid (**b**) on the rate constants formation of β-haematin. Solid lines are a fit obtained from an equation that describes two protonation equilibria and assumes that only the monoprotonated species of haematin reacts at an appreciable rate, where the fraction of mono-protonated species is given by: $1/\{(K_{a2}/[H^+]) + ([H^+]/K_{a1}) + 1)\}$. The $pK_{a1}$ and $pK_{a2}$ values obtained from the above fits are 6.4 and 2.3 respectively in 4-aminobenzoic acid and 5.8 and 2.3 in 4-cyanobenzoic acid. The standard deviations of these $pK_a$ values are however too high to be considered reliable and the fits are essentially qualitative.

There does not seem to be a relationship between the pH at which the rate constant is a maximum and the $pK_a$ of the acid. When the optimum pH values are plotted against $pK_a$ of these acids (4-cyanobenzoic acid, 4-aminobenzoic acid, benzoic acid, and acetic acid) no relationship is evident (Figure 5.6). This suggests that the optimum is mainly a property of the haem propionates of haematin and not of the acid.

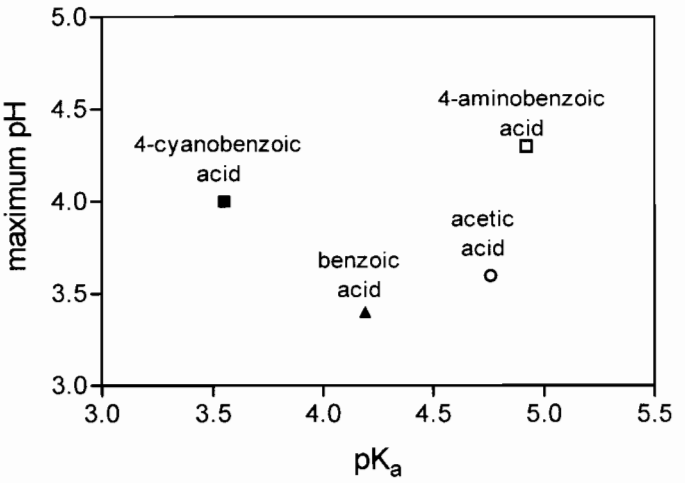


**Figure 5.6** Plot illustrating no correlation between pH optimum of formation of β-haematin in different acids (acetic acid (4.5 M), benzoic acid (0.05 M), 4-aminobenzoic acid (0.04 M) and 4-cyanobenzoic acid (0.007 M)) and their $pK_a$s.

## 5.3 EFFECT OF BENZOIC ACID SUBSTITUENTS ON THE RATE OF FORMATION OF β-HAEMATIN

The rate of formation of β-haematin was determined in the presence of different substituted benzoic acids, with substituents at the para position (Figure 5.7). Measurements were performed at 0.02 M acid concentration and a pH of 4.5, 60°C.

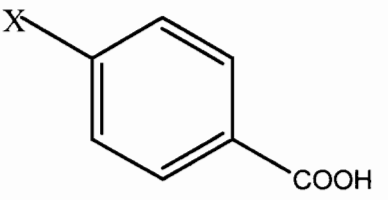


**Figure 5.7** Benzoic acid derivatives investigated, X = H, $NO_2$, $SO_2CH_3$, CN, $SO_2NH_2$, CHO, $OCH_3$, $NH_2$.

For 4-methoxybenzoic acid, a concentration of 0.02 M could not be achieved because of its low solubility. A concentration study was therefore carried out (Figure 5.8) and the rate constant at the required concentration for comparison with the other acids was estimated by extrapolation. Low solubility of other acids like 4-chlorobenzoic acid and 4-methylbenzoic acid prevented their use in this study.

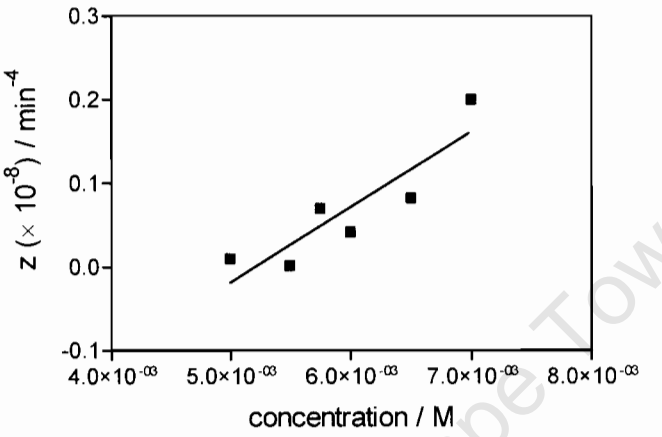


**Figure 5.8** Linear dependence of rate constant for β-haematin formation on concentration of 4-methoxybenzoic acid.

The rate constants obtained for β-haematin formation, Hammet constants and molar refractivity (a measure of substituent size) for the different substituents are listed in Table 5.4 below. The substituents are listed in the order of decreasing Hammett constant with the amino and nitro groups rated as strongly electron donating and withdrawing respectively.

**Table 5.4** Effect of substituent at the para position of benzoic acid on the rate constant (*z*) for formation of β-haematin in 0.02 M carboxylic acid at pH 4.5 and 60°C (in order of decreasing $\sigma_p$)

| X | *n* (fixed) | *z* ($min^{-4}$) | $\sigma_p$ | MR |
|---|---|---|---|---|
| $NO_2$ | 4 | $(1.3 \pm 0.7) \times 10^{-7}$ | 0.78 | 7.36 |
| $SO_2CH_3$ | 4 | $(2.5 \pm 0.2) \times 10^{-9}$ | 0.72 | 13.50 |
| CN | 4 | $(3.6 \pm 0.4) \times 10^{-8}$ | 0.66 | 6.3 |
| $SO_2NH_2$ | 4 | $(5.1 \pm 0.4) \times 10^{-10}$ | 0.57 | 12.28 |
| CHO | 4 | $(2.5 \pm 0.5) \times 10^{-8}$ | 0.42 | 6.9 |
| H | 4 | $(8.0 \pm 1.0) \times 10^{-9}$ | 0.00 | 1.03 |
| $OCH_3$ | 4 | $(1.3 \pm 0.1) \times 10^{-8}$ | -0.27 | 7.88 |
| $NH_2$ | 4 | $(1.2 \pm 0.2) \times 10^{-9}$ | -0.66 | 5.42 |

Electron withdrawing groups (all those listed above H in Table 5.4) decrease the electron density in the benzoic acid ring through a resonance withdrawing effect, making it less nucleophilic and more acidic than benzoic acid; whereas electron donating groups (all listed below H in Table 5.4) increase electron density through a resonance donating effect, making it more nucleophilic and a weaker acid than benzoic acid.

The effect of these electron donating and electron withdrawing groups on the rate of formation of β-haematin is shown in Figure 5.9 below.

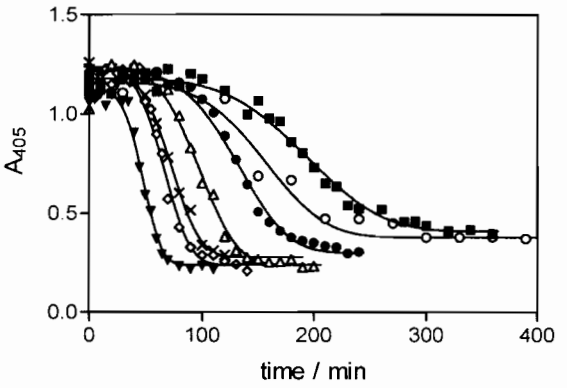


**Figure 5.9** Different reaction rates due to the presence of different substituents at the para position of the benzoic acid ring. (■) $SO_2CH_3$, (○) $NH_2$, (●) $SO_2NH_2$, (△) H, (×) CHO, (◇) CN and (▼) $NO_2$. Acid concentration is 0.02 M, pH 4.5, 60°C.

These findings show that electron donating groups on the benzoic acid ring slow down the reaction whereas when there is decreased electron density in the ring the reaction is faster, with the exception of methylsulfonyl and sulphonamide derivatives. There is a good correlation between the rate of formation of β-haematin and the Hammett constant of the remaining substituents (Figure 5.10).

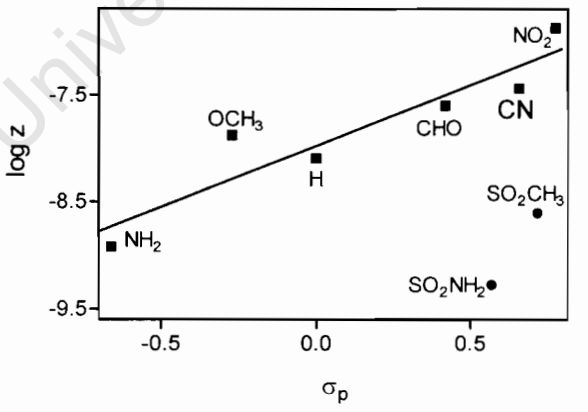


**Figure 5.10** Relationship between electron withdrawing and electron donating groups on the benzoic acid ring and the Hammet constant for the formation β-haematin.

The anomalous behavior of the methylsulfonyl and sulphonamido derivatives may arise from their very large sizes as reflected by their molar refractivity values (a measure of volume occupied by an atom or group) in Table 5.4 which are about double the size of the next largest substituent. Rate constants are thus strongly dependent on the nature of the group at the para position of the benzoic acid ring.

## 5.4 CONCLUSIONS

β-haematin forms in substituted benzoic acids and the kinetics can be studied using the same pyridine assay. There is a linear dependence of the rate constant for formation of β-haematin and concentration for 4-nitrobenzoic acid and a temperature study using this acid follows Arrhenius behaviour with an activation energy similar to that obtained in benzoic acid and acetic acid. The dependence of the rate constant for formation of β-haematin on the Hammett constant is an indication that electronic effects play a major role in the activity of the acid during this reaction. The pH optima of haematin formation in different acids are independent of their $pK_a$ values.

# 6. GENERAL CONCLUSIONS, IMPLICATIONS AND FUTURE RECOMMENDATIONS

## 6.1 GENERAL CONCLUSIONS

β-Haematin formed in 0.05 M benzoic acid, pH 4.5 and 60°C was characterised using infrared spectroscopy, scanning electron microscopy and x-ray diffraction. It is identical to that formed in 4.5 M acetic acid. The three methods confirm that there is a difference between haematin and β-haematin in structure, morphology and crystallinity. XRD and SEM suggest that the formation of β-haematin occurs by conversion of amorphous haematin to crystalline β-haematin.

The kinetics of formation of β-haematin were successfully studied using a pyridine-based assay and follow a sigmoidal reaction profile indicating a process of nucleation followed by growth. The data obtained fits the Avrami equation and the rate and Avrami constants were obtained under different conditions.

Almost identical rate constants were obtained for β-haematin formation in aqueous acetic acid from the pyridine-based assay to those reported for the infrared assay. The activity of benzoic acid was found to be 90 times greater

than that of acetic acid in terms of the time required for the reaction to reach completion.

XRD measurements performed on wet β-haematin at different time intervals during the reaction confirmed that β-haematin is formed during incubation and not during the drying stage. The kinetics followed this way were consistent with those from the pyridine assay.

The rate of formation of β-haematin depends on temperature, pH and concentration of benzoic acid but, does not depend on stirring rate and seeding except that excessive stirring rates lead to a change in the reaction profile. Temperature dependence follows Arrhenius behaviour and there is a linear dependence of the rate constant on the concentration of benzoic and 4-nitrobenzoic acid, without a change in the value of *n*.



Although carrying out the reaction without stirring did not have any effect on the rate of formation of β-haematin, stirring vigorously seems to disrupt nucleation and causes the reaction to follow the Gompertz equation instead of the Avrami equation. This is probably because crystal formation is slowed down since crystal nuclei are destroyed.

A bell-shaped curve with a pH optimum was obtained from a study performed on the effect of pH on the rate constant in benzoic acid, 4-aminobenzoic acid

and 4-cyanobenzoic acid. No correlation was found between the $pK_a$ of the acid and the pH optimum of the reaction.

When reactions for the formation of β-haematin were performed in benzoic acids with substituents at the para positions, a linear dependence between the Hammett constant and the rate of formation of β-haematin was obtained except for substituents which had much larger molar refractivities (and hence probably affected by steric hindrance). The more electron-deficient acids were found to be more effective in promoting formation of β-haematin.

## 6.2 DISCUSSION OF IMPLICATIONS

It was previously suggested [16, 44, 30] that the role of the acid during the formation of β-haematin is to solubilise haematin by coordination to the Fe(III) center, facilitating re-precipitation as β-haematin. Based on this, when the study of the relationship between the Hammett constant and rate of formation of β-haematin was carried out, it was expected that the most electron rich acid would promote formation of β-haematin better than the less electron rich acids because stronger electron donors would be expected to form stronger complexes with the metal [107]. However, the opposite was observed, suggesting that the acid may not act by binding to the Fe(III) centre of haematin.

Supporting this conclusion, an attempt to obtain the association constants of benzoic acid (0.2 M) with haematin in 40% DMSO did not show any evidence of interaction in the visible spectrum. In addition, no evidence of haematin solubilisation by benzoic acids was observed.

The dependence of the rate constants for β-haematin formation on pH in acetic acid and benzoic acid suggests that the haematin species at the pH where there is an optimum rate has one propionic group deprotonotated and the other one protonated. This is the required protonation state for coordination of the one propionate to the Fe(III) and the other for intermolecular hydrogen bonding in β-haematin. The diprotonated species ($MH_2$) is dominant at lower pH whereas the unprotonated species (M) is dominant at higher pH as shown in the speciation plot in Figure 6.1. (Both the $pK_a$ values of the haem propionates are likely to be influenced by coordination to Fe(III) and hydrogen bonding. The values at the $pK_a$ have not been established, so Figure 6.1 is semi-qualitative).

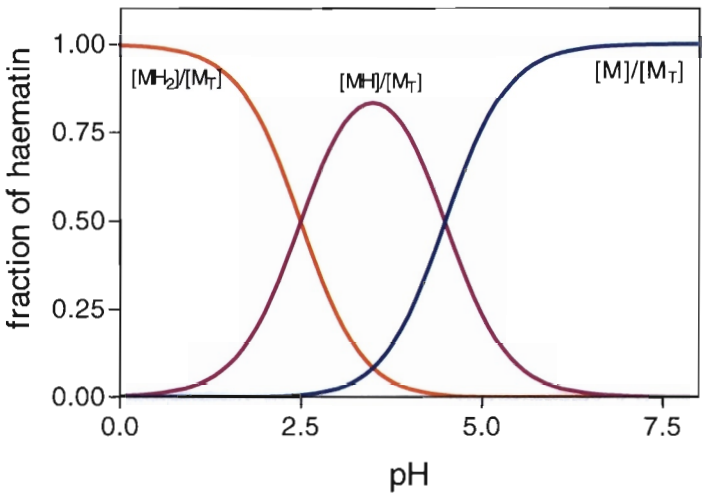


**Figure 6.1** Existence of different species of haematin at different pH where $MH_2$ is the diprotonated species in which both propionates are protonated, MH is the monoprotonated species and M is the unprotonated species.

Based on the proposal that the catalytic acid present in the reaction coordinates to the Fe(III) centre, another possibility is that the acid may need to also have the correct protonation state for optimum β-haematin formation. The unprotonated acid would associate with Fe(III) more strongly as competition with protons would be avoided. In that case, the maximum rate would be expected to also depend on the $pK_a$ of the acid. The fraction of unprotonated benzoic acid, 4-cyanobenzoic acid or 4-aminobenzoic acid at a given pH is dependent on the $pK_a$ of the acid. The fractions present as a function of pH are shown in Figure 6.2.

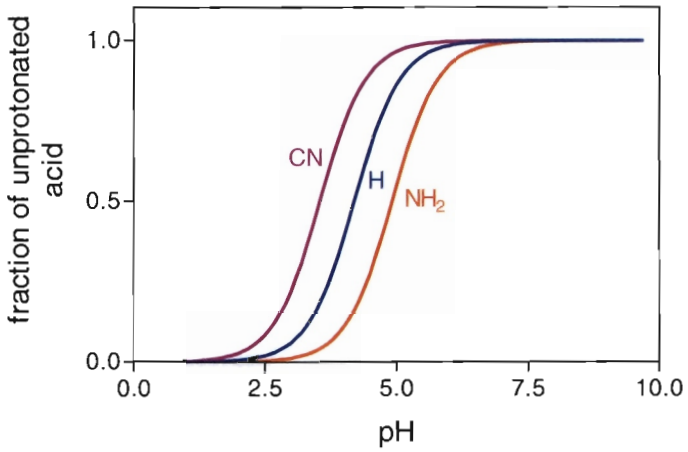


**Figure 6.2** The fraction of unprotonated benzoic acid derivatives as a function of pH in acids with different $pK_a$s, $pK_a$ values used are from literature [108]. Cyanobenzoic acid (3.55), benzoic acid (4.19), aminobenzoic acid (4.92).



If it is assumed that the overall (conditional) rate constant for β-haematin formation depends on the product of the concentration of unprotonated benzoic acid [B] and the monoprotonated haematin [MH] as shown in equation 6.1 below, the resulting rate constant will have the appearance shown in Figure 6.3.

$$z \propto [B][MH] \qquad 6.1$$

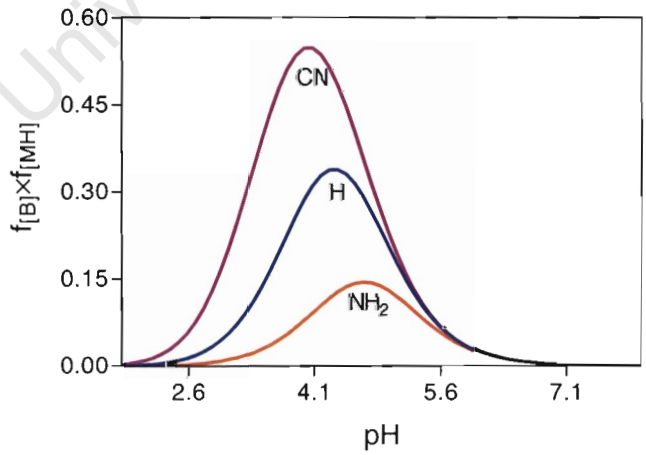


**Figure 6.3** Expected plots for formation of β-haematin in acids with different $pK_a$s assuming that *z* is proportional to the concentration of MH and unprotonated acid. $f_{[B]} = [B]/[B]_T$ and $f_{[MH]} = [MH]/[M]_T$.

In that case, the acid with the lowest $pK_a$ will produce the fastest reaction. In addition optimum rate constant for each acid would increase as the $pK_a$ increases. The maximum rate constant would be observed at the highest pH for 4-aminobenzoic acid.

Experiments carried out to investigate the above possibility showed no simple relationship between $pK_a$ and the pH optima (see Figure 5.6), suggesting that this is not the basis for the substituent effects observed with these acids. This leaves the electronic effects in the benzene ring as the most likely cause of the observed changes in the rate constant and not the strength of the acid as such. It may be that $\pi$-$\pi$ interactions between haematin and the benzoic acid derivatives are important in accelerating the reaction.

Indeed, the observed dependence of rate constants on the electronic properties of the substituents is in line with what is expected in the Hunter and Sanders' model [108] of $\pi$-$\pi$ interactions between a porphyrin and aromatic molecule. According to this model, electron-deficient molecules are able to form stronger $\pi$-$\pi$ interactions than electron-rich molecules. 4-Nitrobenzoic acid is the most electron-deficient acid and is therefore likely to be able to form good $\pi$-interactions with the porphyrin whereas there is repulsion between the 4-aminobenzoic acid $\pi$ cloud and the porphyrin $\pi$ cloud.

It is interesting to speculate how such interactions may assist β-haematin formation. Amorphous haematin consists of individual haematin molecules,

randomly arranged and probably linked together by hydrogen bonds involving the axial water molecule, the propionic acid groups and the propionates as shown schematically in Figure 6.4a. On the other hand, the only hydrogen bonding that occurs in β-haematin is between one β-haematin dimer and the next *via* the propionic acid groups. Thus it is likely that many H-bonds in haematin as well as π-π interactions between the haematin molecules need to be disrupted in the formation of β-haematin. Acetic acid may therefore promote β-haematin formation not by coordinating to Fe(III), but by disrupting some of these hydrogen bonds by itself forming hydrogen bonds with haematin and therefore weakening the existing hydrogen bonding networks. Benzoic acids are also expected to form hydrogen bonds with haematin as for acetic acid. However, in addition, they can probably disrupt π-π interactions between haematin molecules by themselves π-stacking with haematin. This disruption of hydrogen bonding and π-stacking may allow reorientation of the porphyrin rings to form β-haematin as indicated in Figure 6.4b and c.



This type of process may facilitate, not only nucleation (Figure 6.4c and d), but also subsequent growth of the β-haematin crystal. More electron deficient benzoic acids, such as 4-nitrobenzoic acid, which are able to form stronger π-π interactions, are then more efficient in promoting β-haematin formation.

It is not to be expected that carboxylic acids would promote formation of β-haematin, since their carboxylic acid groups have the potential to compete with the propionic groups of haematin in binding to the Fe(III) center and

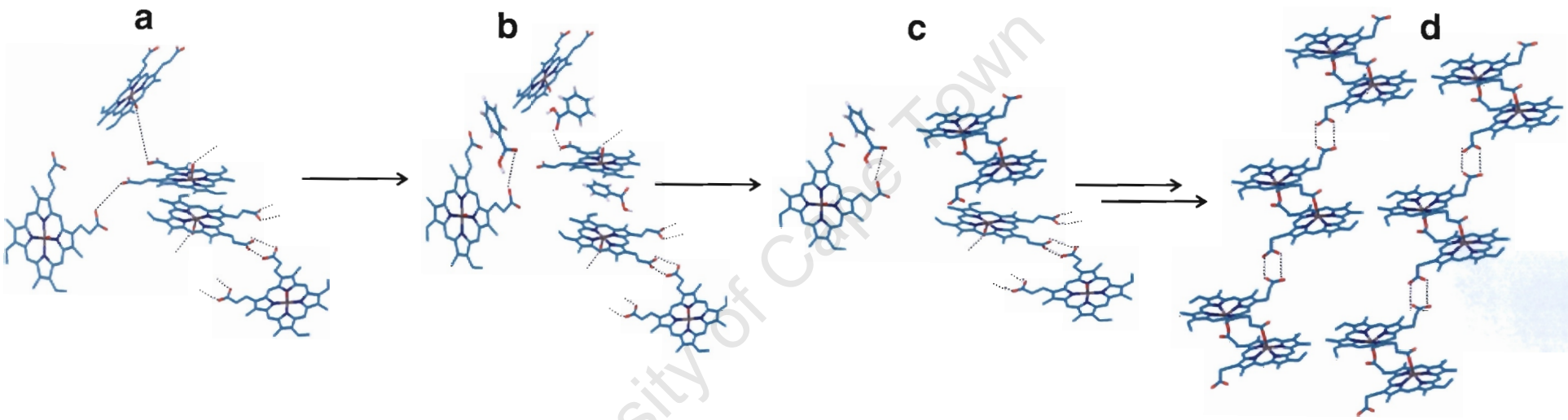




**Figure 6.4** Proposed mechanism for the formation of β-haematin in the presence of benzoic acid. (**a**) Amorphous haematin randomly orientated and linked together by hydrogen bonds, (**b**) benzoic acid competes with haematin for hydrogen bonding and π-stacking, (**c**) haematin orientate properly to form β-haematin in **d**.

hydrogen bonding, and therefore would be expected to inhibit formation of β-haematin. This suggests that their activity instead involves interaction with haematin, which then promotes conversion to β-haematin. There is no evidence of significant precipitation of haematin in the parasite. Rather, it seems likely that it is directly incorporated to haemozoin from solution, consistent with many biomineralization processes [87-90]. The need for acids and high temperatures to overcome the high activation energy of β-haematin formation *in vitro* probably reflects the difficulty of breaking up hydrogen bonding and π-stacking interactions in haematin. *In vivo*, haematin precipitation would probably represent a dead-end process; a lot to do with the haematin acting as a reservoir for dissolution of small amounts into the membranes, with deleterious consequences to the parasite. This is not observed in the parasite under normal conditions. Consequently the formation of β-haematin *in vitro* probably does not mimic the *in vivo* process very well, because too much haematin is introduced at the beginning. All of the methods reported to date for β-haematin formation in an aqueous environment involve introduction of a bolus of haematin into the reaction which rapidly precipitates and then very slowly converts to β-haematin. This emphasises the need to develop a method of introducing haematin at a steady state and to then nucleate β-haematin in a way that mimics the biological process.

## 6.3 FUTURE RECOMMENDATIONS

More work still needs to be done in order to understand how haematin is converted to β-haematin especially under physiological conditions. The following investigations are recommended to better understand this process:

- Study the nature of haematin in aqueous solution in order to better understand the properties that prevent its rapid conversion to β-haematin.
- Introduce haematin continuously into the reaction mixture using for example an automated burette in order to nucleate β-haematin directly from solution and to mimic the biological process.
- Attempt to study the nucleation process in more detail, possibly using atomic force microscopy (AFM) to look for evidence of nucleation process during formation of β-haematin. (β-haematin nuclei are too small to be visualised by electron microscopy).
- To test the hypothesis that the acids promote β-haematin formation by virtue of their ability to disrupt hydrogen bonding by studying the kinetics of β-haematin formation in the presence of substances that are stronger disruptors of hydrogen bonding.
- Investigate β-haematin formation in the presence of meta-substituted benzoic acids in order to further investigate the relationship between electronic properties of the benzene ring and the rate of formation of β-haematin.

- Determine the activity of different antimalarial drugs by performing the reactions in benzoic acid using the new pyridine hemichrome inhibition of β-haematin (PHIβ) assay.

# REFERENCES

[1] B. M. Watkins, Trends Parasitol. 19 (2003) 477-478.

[2] A. C. Chandler in: Introduction to Parasitology, Wiley, New York, 1955, p. 187.

[3] W. H. Wernsdorfer, I. McGregor, Malaria: Principles and practice of malariology, Churchill-Livingstone, Edingburgh, 1998.

[4] M. A. Rudzinska, W. Trager, R. S. Bray, J. Protozool. 12 (1965) 563-576.

[5] W. Trager, J. B. Jensen, Science 193 (1976) 673-675.

[6] H. Ladan, Y. Nitzan, Z. Malik, FEMS Microbiol. Lett. 112 (1993) 173-178.

[7] P. Manson in: Tropical Diseases, William Wood and Company, New York, 1899, p. 26.

[8] W. Metzger, B. Mordmuller, P. Kremsner, Trans R. Soc. Trop. Med. Hyg. 89 (1995) 637-638.

[9] G. M. Edington, Br. Med. J. 1 (1967) 715-718.

[10] C. L. A. Laveran, Excerpted in Reviews of infectious diseases 4 (1982) 908-911.

[11] R. Ross, Br. Med. J. 1 (1897) 1786-1788.

[12] T. Hanscheid, E. Valadas, M. P. Grobusch, Parasitol. Today 16 (2000) 549-551.

[13] T. J. Egan, J. M. Combrinck, J. Egan, G. R. Hearne, H. M. Marques, S. Ntenteni, B. T. Sewell, P. J. Smith, D. Taylor, D. A. van Schalkwyk, J. C. Walden, Biochem. J. 365 (2002) 343-347.

[14] A. C. Chou, R. Chevli, C. D. Fitch, Biochemistry 19 (1980) 1543-1549.

[15] A. F. G. Slater, W. J. Swiggard, B. R. Orton, W. D. Flitter, D. E. Goldberg, A. Cerami, G. B. Henderson, Proc. Natl. Acad. Sci. USA 88 (1991) 325-329.

[16] T. J. Egan, D. C. Ross, P. A. Adams, FEBS Lett. 352 (1994) 54-57.

[17] A. Dorn, S. R. Vippagunta, H. Matile, C. Jaquet, J. L. Vennerstrom, R. G. Ridley, Biochem. Pharmacol. 55 (1998) 727-736.

[18] M. V. Ignatushchenko, R. W. Winter, H. P. Bächinger, D. J. Hinrichs, M. K. Riscoe, FEBS Lett. 409 (1997) 67-73.

[19] W. Brown, J. Exp. Med. 13 (1911) 290.

[20] R. Lemberg, J. Legge in: Hematin Compounds and Bile Pigments, Interscience, New York, 1949, pp. 171-172.

[21] J. A. Sinton, B. N. Ghosh, Records of the Malaria Survey of India 4 (1934) 205-221.

[22] J. O. Ashong, I. P. Blench, D. C. Warhurst, Trans R. Soc. Trop. Med. Hyg. 83 (1989) 167-172.

[23] P. Goldie, E. F. Roth, J. Oppenheim, J. P. Vanderberg, Am. J. Trop. Med. Hyg. 43 (1990) 584-596.

[24] C. D. Fitch, P. Kanjananggulpan, J. Biol. Chem. 262 (1987) 15552-15555.

[25] A. Hamsik, Z. Physiol. Chem. 190 (1936) 199-215.

[26] D. S. Bohle, P. Debrunner, P. A. Jordan, S. K. Madsen, C. E. Schulz, J. Am. Chem. Soc. 120 (1998) 8255-8256.

[27] T. J. Egan, E. Hempelmann, W. W. Mavuso, J. Inorg. Biochem. 73 (1999) 101-107.

[28] D. S. Bohle, J. B. Helms, Biochem. Biophys. Res. Commun. 193 (1993) 504-508.

[29] D. S. Bohle, A. D. Kosar, P. W. Stephens, Acta Cryst. D58 (2002) 1752-1756.

[30] T. J. Egan, W. W. Mavuso, K. K. Ncokazi, Biochemistry 40 (2001) 204-213.

[31] B. R. Wood, S. J. Langford, B. M. Cooke, F. K. Glenister, J. Lim, D. McNaughton, FEBS Lett. 354 (2003) 247-252.

[32] D. S. Bohle, R. E. Dinnebier, S. K. Madsen, P. W. Stephens, J. Biol. Chem. 272 (1997) 713-716.

[33] S. Pagola, P. W. Stephens, D. S. Bohle, A. D. Kosar, S. K. Madsen, Nature 404 (2000) 307-310.

[34] B. R. Wood, S. J. Langford, B. M. Cooke, J. Lim, F. K. Glenister, M. Duriska, J. K. Unthank, D. McNaughton, J. Am. Chem. Soc. 126 (2004) 9233-9239.

[35] D. S. Bohle, A. D. Kosar, S. K. Madsen, Biochem. Biophys. Res. Commun. 294 (2002) 132-135.

[36] D. A. Skoog, in: Principles of Instrumental Analysis, Saunders College, 1980, pp. 270-271.

[37] H. B. Willard, L. L. Merritt, J. A. Dean, F. A. Settle in: Instrumental Methods of Analysis, Wadsworth, Belmont, 1988, pp. 195.

[38] W. Kaim, B. Schwederski in: Bioinorganic Chemistry: Inorganic Elements in the Chemistry of Life. An Introduction and Guide., Wiley, Chichester, 1994, p. 72.

[39] W. Kaim, B. Schwederski in: Bioinorganic Chemistry: Inorganic Elements in the Chemistry of Life. An Introduction and Guide., Wiley, Chichester, 1994, p. 44.

[40] G. D. Christian, J. E. O'Keilly in: Instrumental Analysis, Wells Avenue Newton, Massachusetts, 1986, p. 212.

[41] A. R. West, in: Solid State Chemistry and Its Applications, Wiley, 1984, p. 82-84.

[42] G. Schoffa, Nature (London) 203 (1964) 640-641.

[43] R. W. Hay in: Bio-Inorganic Chemistry, E. Howard Halsted, New York, 1987, p. 60.

[44] P. A. Adams, T. J. Egan, D. C. Ross, J. Silver, P. J. Marsh, Biochem. J. 318 (1996) 25-27.

[45] D. S. Bohle, B. J. Conklin, D. Cox, S. K. Madsen, S. Paulson, P. W. Stephens, G. T. Yee, ACS Symp. Ser. 572 (1994) 495-515.

[46] H. P. Klug, L. E. Alexander in: X-Ray Diffraction Procedures for Polycrystalline and Amorphous Materials, Wiley interscience, New York, 1974, p. 120.

[47] J. C. Walden, PhD thesis, University of Cape Town, 2003, 123.

[48] D. S. Bohle, A. D. Kosar, P. W. Stephens, Can. J. Chem. 81 (2003) 1285-1291.

[49] M. F. Oliveira, J. R. Silva, M. Dansa-Petretski, W. de Souza, U. Lins, C. M. S. Braga, H. Masuda, P. L. Oliveira, Nature 400 (1999) 517-518.

[50] M. F. Oliveira, J. R. Silva, M. Dansa-Petretski, W. de Souza, C. M. S. Braga, H. Masuda, P. L. Oliveira, FEBS Lett. 477 (2000) 95-98.

[51] C. M. Morel, Parasitol. Today 16 (2000) 522-525.

[52] G. A. Moore, C. A. Homewood, H. M. Gilles, Ann. Trop. Med. Parasitol. 69 (1975) 373-375.

[53] K. P. Dingemans, E. A. Elias, Ann. Trop. Med. Parasitol. 72 (1978) 231-242.

[54] E. C. Faust in: Human Helminthology, Lea and Febiger, Philadelphia, 1939, p. 133.

[55] N. R. Bergquist, Trends Parasitol. 18 (2002) 309-314.

[56] D. Engels, L. Chitsulo, A. Montresor, L. Savioli, Acta Tropica. 82 (2002) 139-146.

[57] J. Boissier, J. Jarkovsky, S. Morand, H. Mone, Theor. Popul. Biol. 66 (2004) 269-276.

[58] M. M. Chen, L. Shi, D. J. Sullivan, Mol. Biochem. Parasitol. 113 (2001) 1-8.

[59] G. S. Noland, N. Briones, D. J. J. Sullivan, Mol. Biochem. Parasitol. 130 (2003) 91-99.

[60] A. U. Orjih, Exp. Biol. 228 (2001) 746-752.

[61] A. Dorn, R. Stoffel, H. Matile, A. Bubendorf, R. G. Ridley, Nature 374 (1995) 269-271.

[62] A. Dorn, S. R. Vippagunta, H. Matile, A. Bubendorf, J. L. Vennerstrom, R. G. Ridley, Biochem. Pharmacol. 55 (1998) 737-747.

[63] C. D. Fitch, G. Z. Cai, Y. F. Chen, J. D. Shoemaker, Biochim. Biophys. Acta 1454 (1999) 31-37.

[64] D. J. Sullivan, I. Y. Gluzman, D. E. Goldberg, Science 271 (1996) 219-222.

[65] G. Blauer, M. Akkawi, Biochem. J. 346 (2000) 249-250.

[66] A. F. G. Slater, A. Cerami, Nature 355 (1992) 167-169.

[67] K. Bendrat, B. J. Berger, A. Cerami, Nature 378 (1995) 138-139.

[68] A. K. Tripathi, S. K. Garg, B. L. Tekwani, Biochem. Biophys. Res. Commun. 290 (2002) 595-601.

[69] V. Papalexis, M. Siomos, N. Campanale, X. Guo, G. Kocak, M. Foley, L. Tilley, Mol. Biochem. Parasitol. 115 (2001) 77-86.

[70] J. Ziegler, R. T. Chang, D. W. Wright, J. Am. Chem. Soc. 121 (1999) 2395-2400.

[71] W. Yu, R. A. Farrell, D. J. Stillman, D. R. Winge, Mol. Cell. Biol. 16 (1996) 2464-2472.

[72] A. V. Pandey, V. K. Babbarwal, J. N. Okoyeh, R. M. Joshi, S. K. Puri, R. L. Singh, V. S. Chauhan, Biochem. Biophys. Res. Commun. 308 (2003) 736-743.

[73] R. Buller, M. L. Peterson, Ö. Almarsson, L. Leiserowitz, Cryst. Growth Des. 2 (2002) 553-562.

[74] I. Weissbuch, L. Addadi, M. Lahav, L. Leiserowitz, Science 253 (1991) 637-645.

[75] I. Weissbuch, R. Popovitz-Biro, M. Lahav, L. Leiserowitz, Acta Crystallogr. B 51 (1995) 115-148.

[76] E. Hempelmann, C. Motta, R. Hughes, S. A. Ward, P. G. Bray, Trends Parasitol. 19 (2002) 23-26.

[77] J. Williams, G. S. Gill, W. Trager, Parasitol. Int. 47 (1998) 107-119.

[78] H. Ginsburg, Trends Parasitol. 19 (2003) 198-199.

[79] A. K. Tripathi, S. I. Khan, L. A. Walker, B. L. Tekwani, Anal. Biochem. 325 (2004) 85-91.

[80] A. K. Tripathi, A. Gupta, S. K. Garg, B. L. Tekwani, Life Sci. 69 (2001) 2725-2733.

[81] S. Parapini, N. Basilico, E. Pasini, T. J. Egan, P. Olliaro, D. Taramelli, D. Monti, Exp. Parasitol. 96 (2000) 249-256.

[82] G. Blauer, M. Akkawi, J. Inorg. Biochem. 66 (1997) 145-152.

[83] N. Basilico, E. Pagani, D. Monti, P. Olliaro, D. Taramelli, J. Antimicr. Chemother. 42 (1998) 55-60.

[84] B. J. Berger, K. Bendrat, A. Cerami, Anal. Biochem. 231 (1995) 151-156.

[85] M. Avrami, J. Chem. Phys 7 (1939) 1103-1112.

[86] A. Sharples in: Introduction to Polymer Crystallization, Edward Arnold, London, 1966, p. 50.

[87] W. Kaim, B. Schwederski in: Bioinorganic Chemistry: Inorganic Elements in the Chemistry of Life. An Introduction and Guide., Wiley, Chichester, 1994, p. 304.

[88] J. Aizenberg, G. Lambert, S. Weiner, L. Addadi, J. Am. Chem. Soc. 124 (2001) 32-39.

[89] L. G. Benning, V. R. Phoenix, N. Yee, K. O. Konhauser, Geochim. Cosmochim. Ac. 68 (2004) 743-757.

[90] D. A. Bazylinski, Internatl. Microbiol. 2 (1999) 71-80.

[91] N. B. Chapman, T. Shorter in: Correlation Analysis in Chemistry. Recent Advances, Plenum Press, London, 1978, p. 2.

[92] L. P. Hammett, Chem. Rev. 17 (1935) 125-136.

[93] C. Hansch, A. Leo in: Substituent Constants for Correlation Analysis in Chemistry and Biology., Wiley, New York, 1979, pp. 1-4.

[94] M. Charton, Prog. Phys. Org. Chem. 8 (1971) 235-317.

[95] T. Fujita, Prog. Phys. Org. Chem. 12 (1976) 49-89.

[96] K. K. Ncokazi, T. J. Egan, Anal. Biochem. 338 (2005) 306-319.

[97] W. W. Mavuso, PhD Thesis, University of Cape Town, 2001, 159.

[98] B. Gompertz, Phil. Trans. R. Soc. London 115 (1825) 513-585.

[99] H. R. Hirsch, J. Theor. Biol. 98 (1982) 32346.

[100] L. Norton, Cancer Res. 49 (1989) 6443-6444.

[101] M. A. A. Castro, F. Klamt, V. A. Grieneisen , I. Grivicich, J. C. F. Moreira, Cell Prolif. 36 (2003) 65-73.

[102] J. W. Mullin, K. D. Raven, Nature 195 (1962) 4836-4837.

[103] R. K. Lowry, P. Henderson, J. Nolan, Contr. Mineral. Petrol. 80 (1982) 254-261.

[104] C. M. Scarfe, Canad. Mineral. 15 (1977) 185-189.

[105] L. Higashi, Kinetics of crystallisation, phase transformation, and microstructure analysis of Corning 9608 glass.

[106] J. J. Thomas, H. M. Jennings, Chem. Mater. 11 (1999) 1907-1914.

[107] D. V. Jahagirdar, J. Inorg. Nucl. Chem. 36 (1974) 2390-2392.

[108] A. E. Martell, R. M. Smith in Critical Stability Constants, Volume 3, Plenum Press, New York.

[109] C. A. Hunter, J. K. M. Sanders, J. Am. Chem. Soc. 112 (1990) 5525-5534.